Doctoral Dissertation (Shinshu University)

Design of sol-gel chemistry-derived dispersants for SWCNT and its application

March 2017

Radovan Kukobat

Acknowledgment

*I am very grateful to **Prof. Katsumi Kaneko** and **Prof. Takuya Hayashi** for giving me the opportunity to study at Shinshu University in Nagano. I thank to both professors for the excellent guidance, valuable suggestions, support during the experimental work, and help with writing the articles that are included in this thesis.*

*I thank to **Dr. Daiki Minami** for introducing me to the laboratory and helping with the experiments at the beginning of my PhD work.*

*I thank to **Prof. Kiyotaka Asakura** for the EXAFS measurements of Zn atom and data analysis which gave understanding of the structure of Zn/Al complex dispersant.*

*I thank to **Prof. Yoshiyuki Hattori** for the fruitful discussion of EXAFS data which helped to understand the structure of Zn/Al complex dispersant.*

*I thank to **Ms. Manami Hoya** for her help with the administration work and ordering the stuff necessary for the laboratory experiments.*

*I am thankful to the **New Energy and Industrial Technology Development Organization (NEDO)** of Japan for the financial support of this research.*

*I am grateful to **Takagi Company** for the three-year scholarship which supported my life during the studies.*

*Finally, I am thankful to my **parents** for their patience and support in my life. Also, I am thankful to my wife **Dragana** for her support during writing this thesis.*

Radovan Kukobat

Nagano, 17.09.2016

Table of Contents

Chapter 1

1. General Introduction

1.1. Sol-gel Chemistry in the Material Processing: Transparent and Conductive Films

Sol-gel chemistry is a branch of chemistry applicable in the synthesis and processing of the organic and inorganic substances in particular metal oxides which are essential components of the glass and ceramics. Sol-gel method involves the synthesis of sol that is composed of the dispersed particles of various shapes and sizes in the range of ~ 0.1-1μm.[1] The particles are stabilized by the electrostatic repulsive interaction, allowing the Brownian motion in the dispersion system and maintaining stability of the sols that is crucial in the material fabrication. Gelation is facilitated by evaporation of the solvent, leading to the formation of complex network of colloidal particles, i.e. gel. During this process viscosity of gel increases as the solvent evaporates, forming a solid thin film eventually. In this manner transparent and conductive films (TCFs) are obtained which are essential parts of the electronic devices.

The extent of sol-gel processing depends on the type of material used in the TCF fabrication. The most promising materials for the TCF fabrication are nanomaterials including metal oxides, graphene, and carbon nanotubes (CNT). Those nanomaterials give the films with high electrical conductivity and optical transmittance on the transparent substrate. The metal oxide transparent conductors appeared in 1930s during the investigation of the transparent conducting oxides. This work was continued in 1940s, when the indium thin oxide (ITO) mixtures were discovered.[2] The discovery of ITO contributed significantly to the development of the transparent electronics. The discoveries of carbon nanotubes[3] in 1991 by S. Ijima and graphene[4] in 2004 by A. Geim and K. Novoselov opened up new possibilities in the TCF fabrication technologies. Despite the

excellent properties of CNTs and graphene, the commercialization of those materials for the TCF fabrication is still challenging.

The sol-gel processing in the synthesis of metal oxide based films is well known. The sol of metal hydroxides is deposited on the substrate and annealed to give oxide based thin films.[5] On the other hand, the preparation of sol or gel of graphene or CNTs with the metal oxides or hydroxides as the stable dispersion has not been succeed as the best to our knowledge. Therefore, it still remains a challenge to prepare the stable dispersion of graphene or CNTs by so called sol-gel dispersants.

1.2. Materials for the Transparent and Conductive Film Fabrication

This section gives a survey of materials for the application in TCF fabrication. The most common materials for the transparent conductor fabrication are as follows:

- Indium thin oxide (ITO);
- Graphene;
- Carbon nanotubes (CNTs).

The ITO film is currently used material for the transparent electronics, whereas Graphene and CNTs-based films are still in the development stage.

1.2.1. Indium Thin Oxide

The ITO is an attractive sol-gel material for the fabrication of transparent and conductive films. The ITO has high electrical conductivity and optical transparency in comparison with the other metal oxides. The bulk structure of ITO is similar to In_2O_3 with the slightly increased lattice constant in the range of 10.118 Å < a < 10.31 Å. The ITO film has strong orientation of (100) and (111) crystal planes when deposited on the substrate. However, the electrical conductivity and optical transmittance is not dependent on the orientation effects.[6]

The electrical conductivity of ITO film is a function of *Sn* concentration; as the *Sn* concentration increases electrical conductivity increases exhibiting the maximum at 6 at.% and then decreasing. This tendency is associated with the donation of free electrons of Sn^{4+} to the In_2O_3 crystal lattice.[7] The *Sn* atoms are replaced with *In* atoms in the crystal structure of In_2O_3 as shown in ***Figure 1-1***. Thus, the ITO film has a high carrier concentration of 10^{21} cm^{-3} and hole mobility of 15-40 $cm^2V^{-1}s^{-1}$, which leads to the resistance in the range from $7 \cdot 10^{-5}$ to $5 \cdot 10^{-4}$ $\Omega \cdot cm$.[6]

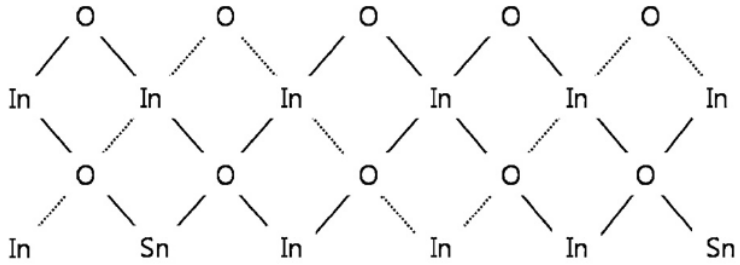

Figure 1-1. The crystal structure of In_2O_3 doped with *Sn* atoms.[8]

The ITO is prepared by coprecipitation from an aqueous solution of $InCl_3$ and $SnCl_4$ at the atomic ratio of $Sn/(Sn+In)$ of 0-10 %.[9] The aqueous solution of $InCl_3$ and $SnCl_4$ was diluted with the ammonia solution and precipitated. The supernatant was decanted and the resulting precipitate, containing the mixed hydroxides of In and Sn was washed with water to remove ammonia solution. The mixture of hydroxides was dispersed by stirring and water soluble polymer was added to maintain the stability of the dispersion system. The pH was adjusted by addition of HNO_3 to be between 2 and 3 to prevent aggregation.

The amount of polymer as well as the type of polymer affects the thickness of film by dip coating method. The resistivity and optical transmittance of the films is shown in Table 1-1.

Table 1-1. The resistivity and optical transmittance of ITO film on the glass substrate after treatment at 550 and 900 °C in air for 1h. The film treated at 900 °C was post treated at 350 °C in nitrogen for 30 min.[9]

Addition of polymer		ITO thin film			
Added polymer	Conc. (wt.%)	Thickness (Å)	ρ_s(Ω·cm), 550 °C	ρ_s(Ω·cm), 900 °C	T (%),550 nm
Poly(vinyl alcohol) ($2.5\cdot10^4$)	4.0	900	$2.8\cdot10^{-2}$	$3.7\cdot10^{-3}$	95
Poly(vinyl alcohol) ($3\cdot10^5$)	1.5	800	$2.0\cdot10^{-2}$	$1.8\cdot10^{-3}$	97
(Hydroxipropyl) cellulose ($1\cdot10^6$)	0.075	700	$1.6\cdot10^{-2}$	$1.3\cdot10^{-3}$	97
Poly(2-vinylpyrrolidone) ($3.6\cdot10^5$)	3.0	800	$2.1\cdot10^{-2}$	$2.8\cdot10^{-3}$	88

The poly(vinyl alcohol) of the molecular weight of $3\cdot10^5$ and hydroxypropyl cellulose of the molecular weight of $1\cdot10^6$ give the dispersion stability of the In and Sn hydroxide mixtures in aqueous media. This suggests that those polymers prevent the aggregation process of the metal hydroxides during the drying process, giving the uniform coatings. The amount of polymer in the film should be reduced to the minimum. The exceed of polymers gives the volatile moieties, causing inhomogeneous film formation after the thermal treatment.

Therefore, the ITO is highly transparent and conductive oxide which is widely used as an electrode in the transparent electronics.

1.2.2. Graphene

Graphene is 2D material whose thickness corresponds to the diameter of carbon atom as shown in ***Figure 1-2***. It is highly conductive in a direction parallel to the graphene layers because of the metallic character. On the other hand, it has poor conductivity in the direction perpendicular to the graphene layers due to the weak van der Waals interactions between the layers. The *s* orbitals of carbon atoms overlap, forming σ bonds, whereas p_z orbitals overlap and create π bonds of sp^2 hybridized carbon atoms. The filled π orbitals form a valence band and empty π^* orbitals form a conduction band, being responsible for the *in-plane* conductivity.[10]

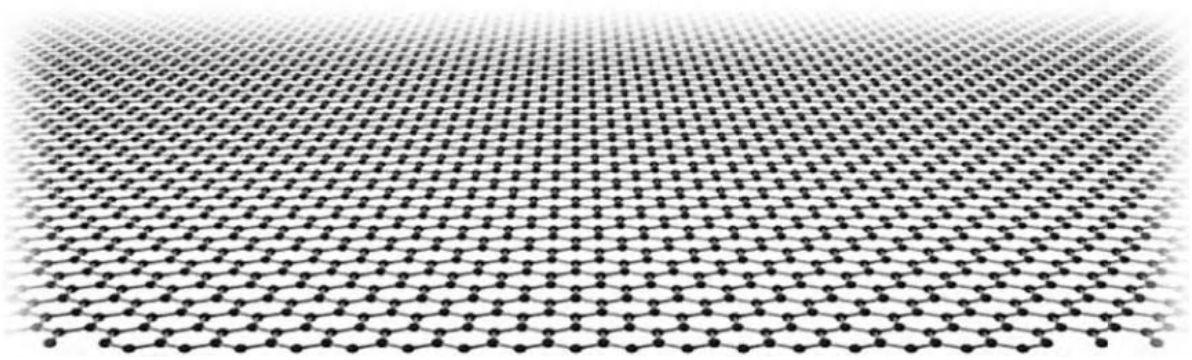

Figure 1-2. The structure of graphene.[11]

The simple route for the graphene preparation is exfoliation of graphite by Hummers method.[12] The graphite is exfoliated by oxidation with a mixture of $KMnO_4$ and H_2SO_4 from which the Graphene Oxide (GO) sheets are obtained. The GO sheets have the carboxyl, hydroxyl, and epoxy functional groups, inducing hydrophilicity to the surface.[13] However, the electrical conductivity of such graphene sheets is low because the carbon atoms are mainly sp^3 hybridized with plenty of defects.

The reduction of surface functional groups can give graphene. This reduction can be conducted chemically and thermally. The chemical reduction uses various chemical reagents among which hydrazine,[14] sodium borohydride,[15]hydroiodic acid[16] are commonly used. The reduction is conducted by dipping of GO film in the solution of reducing reagents to give reduced GO. The thermal reduction is conducted by the heat treatment at 1100 ^oC in the absence of oxygen or any halogen.[17,18] The oxygen functional groups evolve from the graphene plane as CO or CO_2, resulting in increase of the electrical conductivity.[17] However, these methods still cannot give the single layer graphite sheets. The graphene layers are usually stacked in several layers, giving high electrical conductivity. The transmittance of such graphene films is very poor,[19] which is an obstacle toward high quality TCF preparation.

1.2.3. Carbon Nanotubes

The carbon nanotubes (CNT) are promising 1D materials which attract a great attention in the TCF fabrication. The term CNT include the single wall carbon nanotube (SWCNT), double wall carbon nanotube (DWCNT), and multi wall carbon nanotube (MWCNT). However, the

SWCNTs are the most commonly used in the TCF fabrication. The carbon atoms of carbon nanotubes are sp^2 hybridized with a lone pair electrons of p_z orbital that is responsible for the high electrical conductivity.[20] The electronic structure of SWCNT with the free p_z orbitales is shown in ***Figure 1-3***. The electrons of p_z orbital are responsible for the strong van der Waals interactions present between nanotubes.

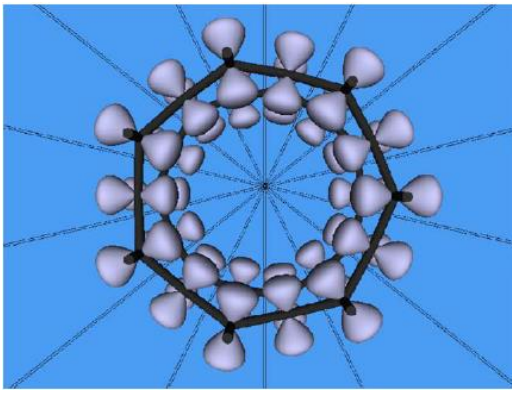

Figure 1-3. The schematic representation of the electronic structure of (7,7) SWCNT with the free p_z orbitals.[21]

The CNT can be synthesized by various techniques such as chemical vapor deposition (CVD), laser ablation, and arc discharge.[22] The CVD method gives slightly pure and crystalline CNT suitable for versatile applications. The production conditions determine quality of CNT including purity, crystallinity, and weather they are SWCNT, DWCNT, or MWCNT. The SWCNTs are composed of one graphitic layer, DWCNTs of two graphitic layers, and MWCNTs of several graphitic layers as shown in ***Figure 1-4***. The number of walls in CNTs depends on the catalyst. In the presence of catalyst they are single walled and in the absence of catalyst they are multi walled.

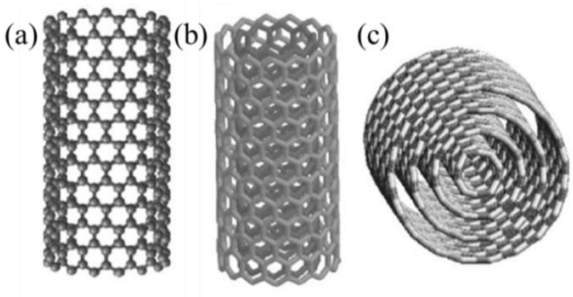

Figure 1-4. (a) Structural models of SWCNT, (b) DWCNT, and (b) MWCNT.[23]

The conduction properties of SWCNT have stimulated their large scale production. The electrical and thermal conductivity of SWCNT are higher than those of graphite. An individual SWCNT has small band gap of the order of magnitude of 10 meV,[24] indicating high electrical conductivity. The thermal *in-plane* conductivity of graphite is 1000 W/m·K, whereas the thermal conductivity of individual SWCNT and DWCNT is 2400 and 1980 W/m·K, respectively.[25,26] However, the SWCNTs are normally produced in bundle form of several hundreds of nanotubes which significantly reduce their excellent conduction properties. It is still challenging to make use of this excellent material for versatile applications.

1.3. Selecting the Suitable Material for the Application in Transparent Electronics

In order to choose the suitable material for transparent electronics we need to take into account physical properties, chemical properties, mechanical properties as well as the cost and availability of the materials. Here, we consider the suitability of ITO, graphene, and CNTs for the fabrication of TCFs.

The ITO is a ceramic material which has very high electrical conductivity and optical transmittance. The sheet resistance is measured to be 15 ohm/sq at the optical transmittance of 80 % at 550 nm. However, the ITO has disadvantages that can cause serious obstacles toward its efficient use in the electronic devices. The ITO is very fragile, forming the cracks at the low strains of 2-3 %.[27] These micro-cracks can cause the decrease of the electrical conductivity of films. The crack formation also places the durability and lifetime issues in the electronic devices. The index of refraction of ITO films is relatively high (nearly 2.0), which leads to unwanted reflection when coupled with the materials or substances with lower refraction index.[28] This issue can be solved by coatings which reduce the refraction index of ITO films; however, these materials can be expensive. The corrosion issue of the ITO films is very important as well.[29] The small amount of acids or salts in the environment or the device adhesives can cause the damage of ITO electrode and significantly reduce the device lifetime. The price of ITO is very high, which is the most serious obstacle in the industrial application of ITO films. The dominant metal of ITO is *In* which takes about 75 % of the mass. The price of ITO depends on the price of *In*

that increases with time. The price of *In* was about 200 $/kg in 1990s in order to increase to 720 $/kg in 2015. This indicates the price increasing tendency of ITO film in the global market.

On the other hand, graphene and CNTs in particular SWCNTs are very promising materials in the TCF fabrication due to the extraordinary electrical, optical, and mechanical properties. These materials possess numerous advantages, being superior to the ITO in TCF fabrication. The individual SWCNT has extremely high hole mobility of >100 000 $cm^2/V{\cdot}s$,[30] while graphene has the hole mobility between 3000 and 10 000 $cm^2/V{\cdot}s$[4]. The SWCNTs and graphene are flexible materials. The tensile strength of individual SWCNT was measured to be 22.2 ± 2.2 GPa[31] and the tensile strength of graphene was reported to be 130 GPa,[32] being one of the strongest materials known today. The price of CNTs and graphene decreases as the technologies for their production improving.

The graphene and CNTs are promising materials for the commercial applications in the transparent electronics. A lot of efforts have been made to make use of graphene and CNTs in the real application. The various products containing graphene and CNT such as touch screens, tennis rackets, skis, bicycle wheels, helmets, automobile components, and cycling shoes have already begun to appear commercially.[33,34] However, there is still room to improve the properties of these materials in order to have better performances and functionality of their final products. Here, we will concentrate our attention on the development of the SWCNT films for the application in transparent electronics.

1.3.1. The SWCNTs in Transparent and Conductive Film Fabrication

The quality of SWCNT depends on the technique applied for their synthesis. Here, we show the most commonly used SWCNT in the TCF fabrication, ***Figure 1-5***.

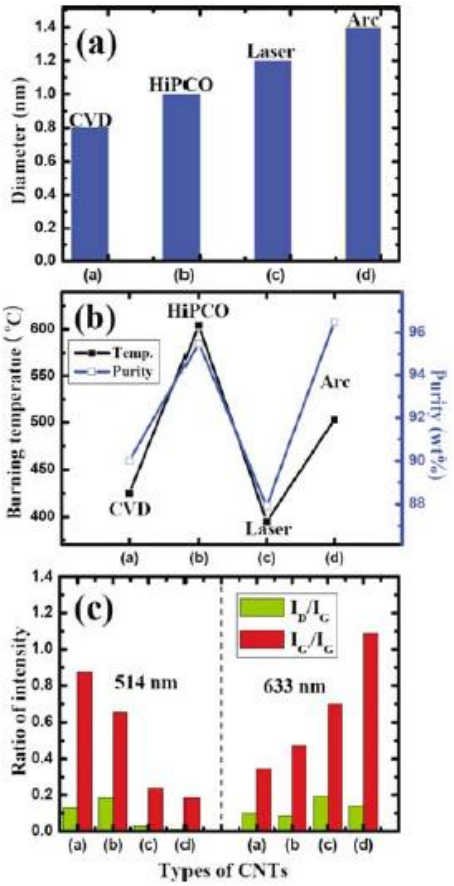

Figure 1-5. Characteristics of SWCNT synthetized by different techniques. (a) Diameter of SWCNT versus the type of SWCNT, (b) burning temperature and purity dependence on SWCNT type, and (c) the ratio of I_D/I_G and $I_{G'}/I_G$ intensities on the SWCNT type.[35]

The Arc method gives the SWCNT with the largest diameter of SWCNT of 1.4 nm, while the smallest diameter of 0.8 nm has the SWCNT obtained from CVD method. The HiPCO and Laser SWCNT have diameter of 1.1 and 1.2 nm, respectively as shown in ***Figure 1-5a***. The burning temperature changes with the content of impurities of SWCNT, ***Figure 1-5b***. ***Figure 1-5c*** shows the ratio of I_D/I_G and $I_{G'}/I_G$ bands at 514 and 633 nm for semiconducting and metallic SWCNT, respectively. The impurity content and the ratio of I_D/I_G bands influence the electrical conductivity of nanotubes. The larger I_D/I_G ratio the lower electrical conductivity. This indicates the lower electrical conductivity of metallic than semiconducting nanotubes. The presence of metallic components is represented by the $I_{G'}/I_G$ ratio. As this ratio is larger the amount of metallic components is larger. The presence of large quantity of metallic SWCNT gives a high electrical conductivity to the materials.

The band gap of semiconducting nanotubes depends on their diameter according to following expression:[36]

$$E_g = \frac{2a_{C-C}\gamma_0}{D}\ (eV) \tag{1.1}$$

Where $a_{C\text{-}C}$ is 0.142 nm and γ_0 is an empirical parameter taken as 2.9 eV. The conductivity of SWCNT can be expressed by the following equation:

$$\sigma = ne\mu_n + pe\mu_p \tag{1.2}$$

where *n* and *p* correspond to electron and hole type carrier concentrations, while μ_n and μ_p are the electron and hole motilities, respectively. The mobility is governed by the random scattering with lattice atoms, impurity atoms, and the other scattering centers. The intrinsic carrier concentration decreases exponentially with the band gap as described by the equation:

$$n_i = n_0 exp(-E_g/2k_bT) \tag{1.3}$$

where k_b and T are the Boltzmann constant and temperature of the system. The concentrations of carriers of *p* and *n*-type carriers can be expressed by the equations as follows:

$$p = n_i\, exp\big[(E_i - E_f)/k_bT\big] \tag{1.4}$$

$$n = n_i exp\big[(E_i - E_f)/k_bT\big] \tag{1.5}$$

where E_i and E_f are intrinsic Fermi level used as a reference level and extrinsic Fermi level of the given semiconductors, respectively. The electrical conductivity is proportional to carrier concentration for the semiconducting nanotubes:

$$\sigma \sim exp(-E_g/2k_bT)exp\big[(E_i - E_f)/k_bT\big] \tag{1.6}$$

The intrinsic semiconducting nanotubes have equal E_i and E_f value and the conductivity depends on the exponential factor, $exp(-E_g/2k_bT)$. In case of metallic nanotubes, the π and π^* orbitals overlap at the Fermi level. However, it was suggested by Denaley et al. (1998) that metallic nanotubes have a pseudo band gap of ~ 0.1 eV originated from the tube-tube interaction in the bundles.[37] The pseudo band gap of metallic nanotubes is small in comparison with the direct band gap of semiconducting nanotubes. The band gap of semiconducting nanotubes with

diameter of 1 ~ 1.4 nm was estimated to be in the range of 0.7 ~ 1.0 eV. The pseudo band gap depends on the tube diameter as denoted by the following expression[35]:

$$E_{pg} \approx \frac{0.105}{D}(eV) \tag{1.7}$$

Then, the electrical conductivity of the semiconducting nanotubes is expressed as follows:

$$\sigma \sim exp(-\frac{E_{pg}}{2k_bT}) \tag{1.8}$$

The Raman spectroscopy is a useful technique in the characterization of CNT samples. There are two excitation energies at which we observe semiconducting and metallic CNT; one is at 514 nm (2.41 eV) and another one at 633 nm (1.96 eV) as shown in ***Figure 1-6***. The Raman signal is generated when the transitions between van Hove singularities correspond to the excitation energies of nanotubes. The energy of van Hove singularities depends on the diameter and chirality of nanotubes, suggesting that the metallicity can be determined thoroughly.[35]

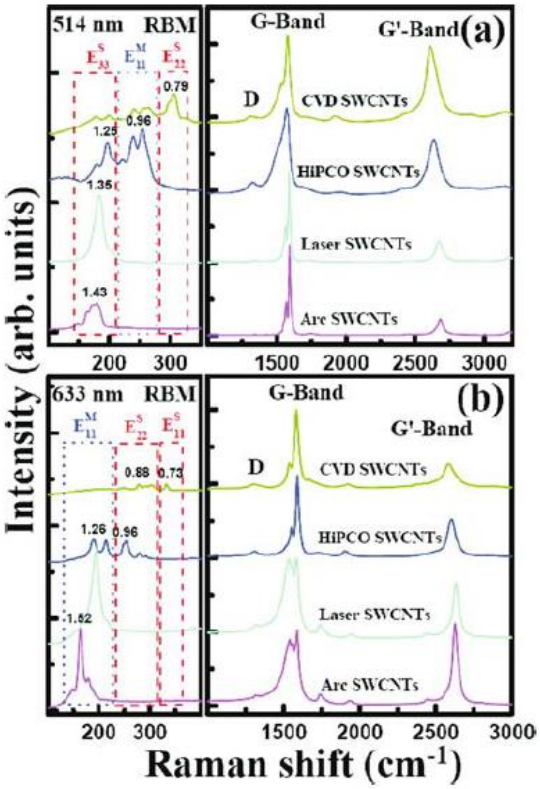

Figure 1-6. The semiconducting SWCNT excited at 514 nm and metallic ones excited at 633 nm.[35]

The semiconducting nanotubes are observed at the excitation wavelength of 514 nm as can be seen in ***Figure 1-6a***. However, the CVD and HiPCO is composed of the semiconducting and metallic nanotubes. The contribution of metallic nanotubes is observed as the long tail of G-band at the lower energy side which corresponds to the Fano line.[38] Arc and laser nanotubes are mostly metallic, the HiPCO nanotubes contain metallic, and CVD nanotubes are mostly semiconducting as observed in ***Figure 1-6b***. The metallicity of nanotubes can be observed in the RBM-band. The presence of D-band shows the defectivity of nanotubes. The higher intensity of D-band the more defective nanotubes. The G'-band is the second order Raman signal and indicates the metallicity of nanotubes. The intensity of G'-band is directly proportional to the metallic component of nanotubes.[39] At 514 nm the Arc and Laser SWCNT exhibit a small G'-band, indicating that those nanotubes are mostly semiconducting. The CVD and HiPCO nanotubes contain a certain amount of metallic nanotubes and G'-band has higher intensity. At 633 nm similar tendency can be observed. The intensity of G'-band increases with increasing metallic component.

Therefore, the G'-band is a measure of metallicity of CNTs. As the intensity of G'-band is increasing the concentration of metallic component increases as well. The intensity of G'-band is in agreement with the intensity of RBM band. Despite the presence of the metallic nanotubes, the electrical conductivity decreases as the intensity of D-band increases due to the increase of the scattering centers which degrade electrical conductivity. Therefore, the nanotubes will have a high electrical conductivity if the intensity ratio of G'-band/D-band is large. The nanotubes with high metallicity without or with very small amount of defects are highly conductive.

The parameters such as purity, defectivity, metallicity, and diameter affect the quality of nanotubes. The combination of these parameters into equation that represent the relationship between the parameters gives the quality factor. The defects reduce the mean free path and decrease the electron and hole mobility of carriers. Thus, the conductivity is proportional to the metallicity and inversely proportional to the defectivity of nanotubes. Therefore, the quality factor of SWCNT is given by an expression as follows:[35]

$$Q_m = P \times \left(\exp\left(-\frac{E_g}{2k_bT}\right) \times \exp\left(E_i - E_f\right) \times \overline{\sum I_S} + \exp(-E_{pq}/2k_BT \times \overline{\sum I_M}\right) \qquad (1.9)$$

where E_g and E_{pq} are the band gap of semiconducting and metallic nanotubes described by equation (1) and (7), respectively. P is the purity of nanotubes, $\overline{\sum I_S}$ and $\overline{\sum I_M}$ are the average intensity ratios of G'/D bands for semiconducting and metallic nanotubes, respectively. The intensities $I_S(I_M)$ are defined as follows:

$$I_S(I_M) = I_{G'/D} \times \frac{A_S(A_M)}{A_S + A_M} \tag{1.10}$$

where the A_S/A_M is the area of semiconducting (metallic) bands of RBM from ***Figure 1-6***. The first exponential term in Equation 9 represents the carrier concentration and the second exponential term represents the mobility which changes with doping effect in semiconducting nanotubes. The third term shows the contribution from metallic nanotubes. The abundance of metallic nanotubes described with the $I_{G'/D}$ ratio. The metallic SWCNTs affects electrical conductivity much more than semiconducting ones, the exponential factor of semiconducting SWCNT with diameter of 1~2 nm is negligible for intrinsic SWCNT when $E_i \approx E_f$. In case of doping, the Fermi level is shifted, meaning that $E_i \neq E_f$ and the first term is not negligible. Also the pseudo band gap of metallic nanotubes can be shifted by doping effect; the Equation (9) does not take it into account because it is negligible in comparison with the semiconducting nanotubes.[40] Therefore, the material quality factor Q_m was calculated with the assumption that $E_i \approx E_f$ for four types of SWCNT as shown in ***Figure 1-7***.

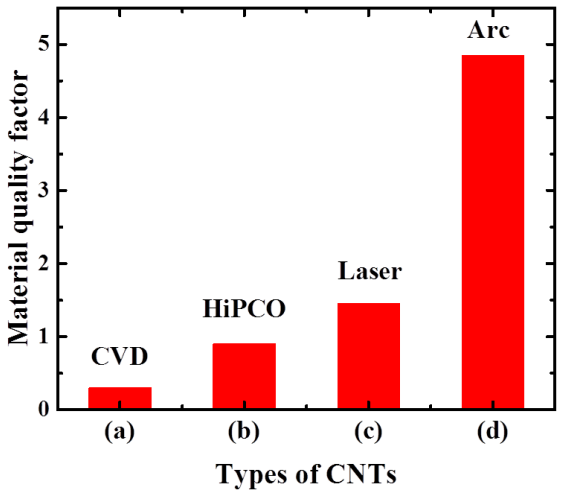

Figure 1-7. The material quality factor Q_m of different types of CNT estimated from Eq. (9).

According to this evaluation method, the Arc SWCNT has the highest electrical conductivity. This indicates that Arc SWCNT give the films with the highest quality in terms of electrical conductivity and optical transparency.

1.4. The SWCNT Inks

The Single Wall Carbon Nanotubes (SWCNTs) are present in the bundles of several hundreds of nanotubes as shown in ***Figure 1-8***. The excellent optical and electrical properties of the intrinsic SWCNTs are hindered when they are in the bundles. The easiest way to isolate SWCNTs from the bundles and exhibit their excellent optical and electrical properties is to disperse them by suitable dispersant, i.e., the SWCNT ink preparation. However, the dispersing SWCNTs into individual tubes is not straightforward. The SWCNTs are hold together by van der Waals attractive interactions. The van der Waals attractive energy estimated to be 500 eV/μm[41] is responsible for the aggregation of SWCNTs. The surface of SWCNTs should be modified to lower this energy and prevent the aggregation. The modification involves dispersing SWCNTs with the aid of surfactants,[42] polymers,[43] organic solvents,[44] superacids,[45] and chemical functionalization.[46] This modification lowers the attractive energy between SWCNTs due to the change of the surface properties from hydrophobic to hydrophilic ones. Thus, the SWCNTs become hydrophilic water like, yielding the stable dispersion.

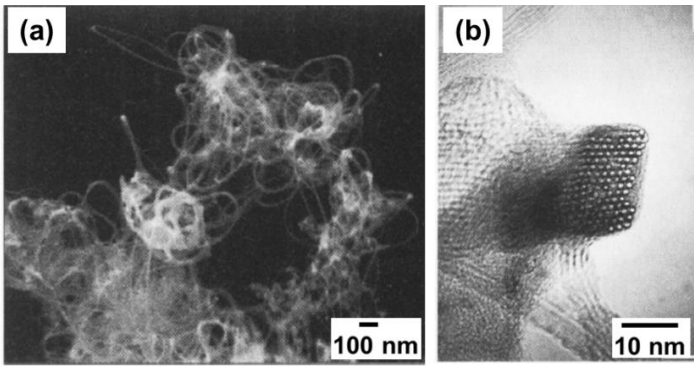

Figure 1-8. The SWCNT bundles. (a) The SEM image of SWCNT bundles in diameter of 10 ~ 20 nm and several tenths of microns in length. (b) The HRTEM image of SWCNT bundle of nearly 100 SWCNTs.[47]

The process of dispersing SWCNTs is followed by ultrasonication, which takes place in the ultrasonicator. There are two types of the ultrasonicators for dispersing SWCNTs. One is the "bath ultrasonicator" and another one is the "tip ultrasonicator". The "tip ultrasonicator" is more powerful and gives more homogeneous dispersion with the larger quantity of isolated SWCNTs. The mechanism of dispersing SWCNTs by ultrasonication is shown in ***Figure 1-9***. During the ultrasonication process, the small cavities in the liquid are being formed as microbubbles that penetrate into the intertubular space and disrupt the SWCNT bundles.[48] This is followed by adsorption of dispersant on SWCNTs from the edge of bundle (ii) and its penetration along SWCNTs (iii), leading to the isolation of SWCNT (iv).[42,49]

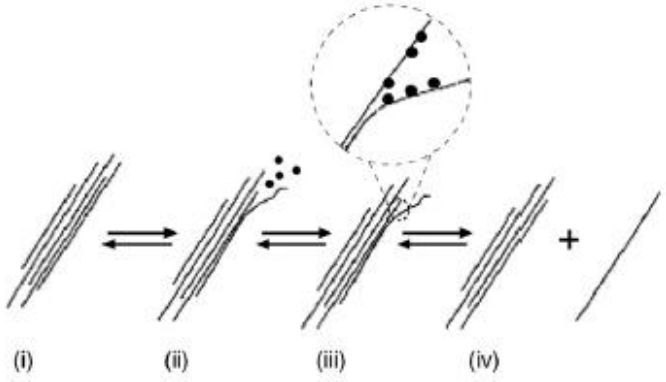

Figure 1-9. The possible mechanism for dispersing SWCNTs with surfactants by aid of ultrasonication treatment. The SWCNT bundle (i) disrupted by ultrasonication at the edge (ii) followed by penetration of surfactants along SWCNT (iii), giving isolated SWCNT (iv).[49]

The quantity of isolated SWCNTs in the dispersion state is the key point for the application of SWCNTs. The large quantity of highly dispersed SWCNTs is preferable in the fabrication of TCF for transparent electronics. The dispersibility depends on the type of dispersant used for SWCNT ink preparation. Since the dispersibility of SWCNTs is very important in the TCF fabrication, here will be briefly reviewed the dispersants for SWCNT inks.

1.4.1. The Surfactant Based SWCNT Inks

There are variety of surfactants that have been used for the SWCNT ink preparation. Here we will mention some of the most commonly used surfactants in the TCF fabrication: Sodium Dodecyl Sulfate (SDS), Sodium Dodecyl Benzene Sulfonate (SDBS), Lithium Dodecyl Sulfate

(LDS), Tetradecyl Trimethyl Ammonium Bromide (TTAB), and Sodium Cholate (SC).[50] The possible mechanism of the adsorption of surfactants on SWCNT surface is shown in ***Figure 1-10***.

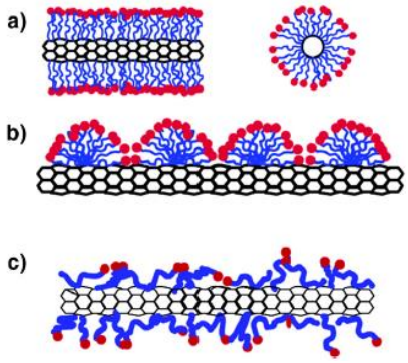

Figure 1-10. The possible mechanisms by which surfactants stabilize SWCNT in the aqueous solution. The adsorption of surfactants on SWCNT can be in the following forms: (a) cylindrical micelles, (b) hemimicelles, and (c) random adsorption.[51]

The surfactants have both hydrophilic and hydrophobic parts. The hydrophilic parts composed of functional groups are polar, interacting with the dispersion media (water), while the hydrophobic parts composed of the long hydrophobic chains adsorb on the hydrophobic surface of SWCNT. The surface charge of SWCNT is changed from slightly negative that corresponds to the bare SWCNT[52] to highly positive or negative depending on the kind of surfactants. The cationic surfactants give positive charge and anionic ones give negative charge to the SWCNTs. This surface charge is determined by Zeta potential and expressed in the units of voltage (mV). If the zeta potential is higher than +30 mV or lower than -30 mV, the SWCNT dispersion is highly stable.[52] Therefore, the SWCNTs are stabilized by the electrostatic repulsive interactions.

1.4.2. The Polymer Based SWCNT Inks

Variety of polymers have been used for dispersing SWCNT in aqueous and non-aqueous media: Polyvinylpyrrolidone (PVP),[53] polyvinyl alcohol (PVA),[54] polystyrene sulfonate (PSS),[53] poly(9,9-dioctylfluorenyl-2,7-diyl) (PFO)[43], Poly(diallyldimethylammonium chloride) (PDDA),[55] and Poly(allylamine hydrochloride).[56] The biopolymers such as deoxyribonucleic acid (DNA)[57], chitosan,[58] gelatin,[59] amylose,[60] β-1,3-glucans,[61] carboxymetyl cellulose sodium

salt (CMC)[62] can be used for SWCNT inks as well. The block copolymers such as polystyrene-b-poly(4-vinyl piridine) (P4VP) also give the stable dispersions of SWCNTs.[63]

There are two possible mechanisms for stabilization of SWCNTs with polymers. One is the wrapping mechanism, where the SWCNTs are wrapped in the polymer matrix and another one is the long ranged entropic repulsion between the polymers surrounding SWCNTs and preventing their aggregation.[42] An example of stabilization of SWCNT by wrapping mechanism is shown in ***Figure 1-11***.

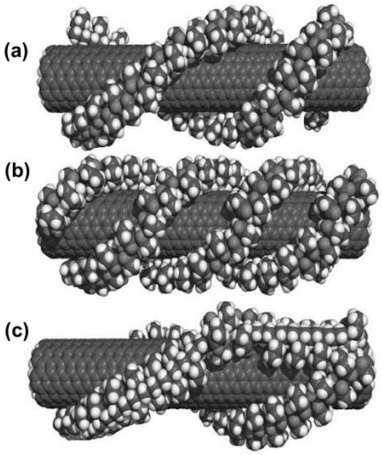

Figure 1-11. The possible wrapping mechanism of (8,8) SWCNT with PVP. (a) Double helix wrapping, (b) triple helix wrapping, and (c) backbone bond rotation which introduced switch-backs, allowing double parallel wrapping with the same polymer chain.[53]

The wrapping process is driven thermodynamically so that the hydrophobic interface between SWCNT and water is eliminated. The outer surface of SWCNT is helically wrapped with the polymer, maintaining dispersion stability.[53]

1.4.3. The Organic Solvent Based SWCNT Inks

The solubilization of SWCNT in organic solvents is probably the easiest route for dispersing SWCNTs. The best solvents for solubilization of SWCNTs are following: N,N-Dimethylformamide (DMF), N-methylpyrrolidone (NMP), hexamethylphosphoramide, cyclopentanone, tetramethylene sulfoxide, and ε-caprolactone.[44] Among the organic solvents for SWCNT, the DMF and NMP appear as the best solvents for the SWCNT ink preparation. The

TEM images of SWCNT dispersed by DMF, mixed DMF:NMP with increasing NMP concentration, and NMP are shown in ***Figure 1-12***.

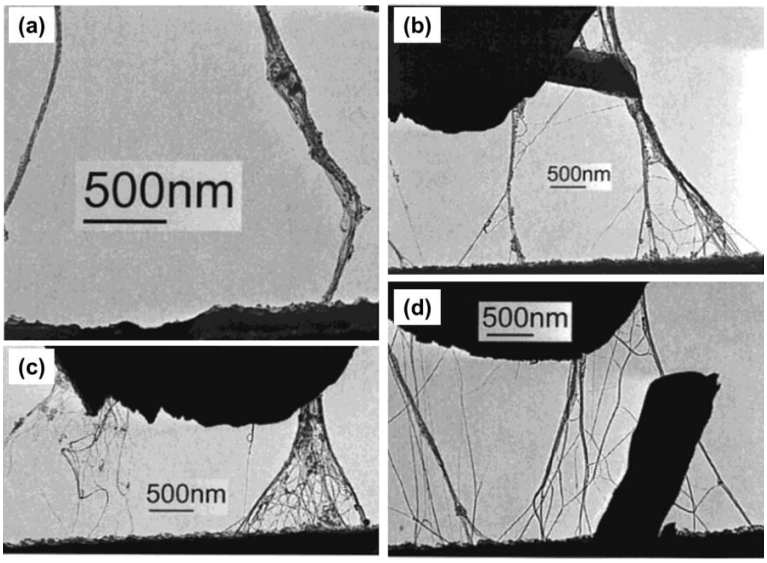

Figure 1-12. The TEM images of SWCNT dispersion by organic solvents. (a) The SWCNT dispersed with DMF. (b) The SWCNT dispersed with saturated NMP and diluted with DMF by 1:9. (c) Dispersed by saturated NMP and diluted with DMF, 1:8. (d) Dispersed with saturated NMP and diluted with 1:9 NMP.[44]

The dispersibility of SWCNT increases with the concentration of NMP in the dispersion system. This suggests that NMP is better dispersing agent than DMF. The dispersion phenomena with organic solvents can be explained by solubility parameters. Those solvents have negligible value of hydrogen bond donation[64] (HBD) parameter α, high value of hydrogen bond acceptance[64] (HBA) basicity parameter β, and high value of solvochromic parameter π*. This means that the Lewis basicity without hydrogen donors is a key property for dissolution of SWCNTs in the organic solvents.[44] The solvochromic parameter should be responsible for the surface charge and Colomb repulsive interactions between the SWCNTs.

Also, the evaluation of dispersibility of SWCNTs in organic solvents can be conducted with the *Hildebrand* and *Hansen* solubility parameters. The *Hildebrand* solubility parameter (δ) considers the cohesive energy density of the material according to following expression:[65]

$$\delta = \frac{(\Delta H - RT)}{V_m} \tag{1.11}$$

where the parameters are as follows: ΔH-heat of vaporization, R-gas constant, and V_m-molar volume. The attractive forces between nanotubes should be overcome in order to obtain the stable SWCNT dispersion. This cohesive energy arises from the dispersive forces (δ_D), the forces between permanent dipoles (δ_P), and hydrogen bonding (δ_H). These parameters are called the *Hansen* solubility parameters. The relationship between the *Hildebrand* and *Hansen* parameters is given by the following expression:[65]

$$\delta = \delta_D + \delta_P + \delta_H \tag{1.12}$$

The *Hansen* solubility parameters involve the type of interactions between the solvent and solute. The solute is SWCNT in this system. Sometimes is possible that two solvents have the same values of *Hildebrand* parameters and different values of *Hansen* parameters. Therefore, it is necessary to evaluate both parameters to know the origin of the interactions between solvent and SWCNT in the dispersion system. The interaction type depends on the organic solvent. The most of organic solvents give the stable SWCNT inks when the *Hildebrand* parameters are in the range of ~ 22-24 $MPa^{1/2}$ and *Hansen* polarity component in the range of ~ 12-14 $MPa^{1/2}$. This correlation between *Hildebrand* and *Hansen* parameters is correct for most of the examined organic solvents in the preceding literature.[65]

1.4.4. The Superacid Based SWCNT inks

The superacids have an ability to highly disperse SWCNTs. Here are listed the superacids which can disperse SWCNTs: 100 % sulfuric acid (H_2SO_4), oleum (20 % of free SO_3), methanesulfonic acid (CH_3SO_3H+$S_2O_8^{2-}$), trifluoromethanesulfonic acid (trifilic acid) (CF_3SO_3H), and chlorosulfonic acid ($ClSO_3H$).[45] Among the various superacids, the $ClSO_3H$ is the most efficient for dispersing SWCNTs. It can disperse 45 g/L of SWCNT, being the most efficient dispersing medium. The dispersion of SWCNTs by $ClSO_3H$ is shown in Cryo-TEM image in ***Figure 1-13***. This was the first TEM image that reports the isolated pristine SWCNTs and the first Cryo-TEM of the superacid solution.[66]

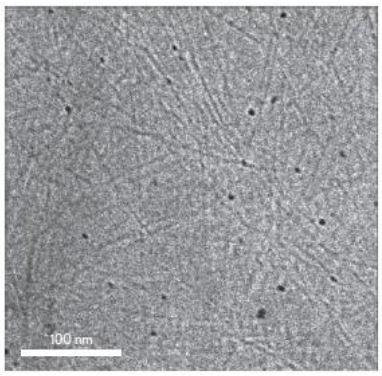

Figure 1-13. The Cryo-TEM image of SWCNTs dispersed in $ClSO_3H$. The SWCNTs are individually dispersed and the black points come from the catalyst.[66]

The SWCNTs have amorphous nature, suggesting that they will behave as a weak base during the dissolution in the acids. Thus, the SWCNTs are being protonated directly with the acid, leading to the delocalization of the positive charge of the entire SWCNTs. This process is described by following reaction:[45]

$$C_X + yAH \rightarrow \left[C_x^{\delta+} H_y^{(1-k\delta)+}\right] + yA^-$$

where k is the ratio of the number of carbon atoms (x) and the number of anions (y), δ is the fractional positive charge of each carbon atom of SWCNTs. The formation and stability of carbocation depends on the stability of conjugate base anion, A^-. The absence evolution of hydrogen during the dispersing SWCNTs by superacids suggests the polarization of the carbon atoms as denoted with $C{:}H^+$. The system superacid-SWCNT can be expressed by $\left[C_x^{\delta+} H_y^{(1-k\delta)+}\right] A_y^{-1}$.[45] Thus, the SWCNTs are stabilized by electrostatic repulsive interactions, giving the highly dispersed SWCNTs.

1.4.5. The SWCNT Inks Stabilized with Chemical Functionalization

The chemical functionalization involves the attachment of functional groups on SWCNT surface. The functional groups induce the hydrophilicity to the nanotubes, reducing the intertubular van der Waals interactions. Thus, the SWCNTs are charged positively or negatively, leading to the electrostatic stabilization of the SWCNT inks. This charge depends on the type of moieties attached to the SWCNT surface. The species with the electronegative atoms give the

negative charge to the SWCNTs and vice versa. Thus, the following functionalities give the negative charge to the SWCNTs: -COO, -C=O, -OH, C-O-C, Cl^-, and F^-. On the other hand, the functionalities based on nitrogen give the positive charge to SWCNTs. The SWCNTs with the variety of functionalities are shown in the ***Figure 1-14***.

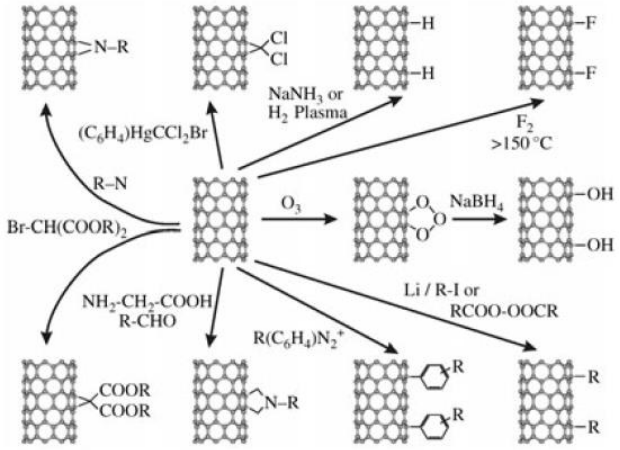

Figure 1-14. The SWCNTs functionalized with the addition reactions.[67]

The functionalization of SWCNTs can be conducted by the thermal oxidation process in the presence of HNO_3 or H_2SO_4. This process yields the SWCNTs with carboxyl and hydroxyl functionalities.[46,67] The future reactions of addition or substitution can give various functional groups to SWCNTs. Here the carbon atoms are mostly sp^3 hybridized,[20] suggesting the low electrical conductivity of nanotubes. Therefore, this method gives stable dispersion of SWCNT, but the inks based on this SWCNTs is not desirable in the fabrication of the TCF due to the low electrical conductivity.

1.5. The Techniques for TCF Fabrication

The variety of techniques has been employed in the TCF fabrication. The films can be prepared by dry and wet deposition techniques. Since the main topic of this work is the TCF fabrication from SWCNT inks, here we will focus on the wet techniques. The most commonly used methods for the fabrication of TCFs are following: Bar coating, spray coating, dip coating, spin coating, vacuum filtration, and Langmuir-Blodgett.

1.5.1. Bar coating

Bar coating is a well-known technique for the preparation of liquid thin films in a very controlled manner.[68–70] This technique is scalable and convenient for the industrial fabrication of TCFs. The scheme of bar coating is shown in ***Figure 1-15***.

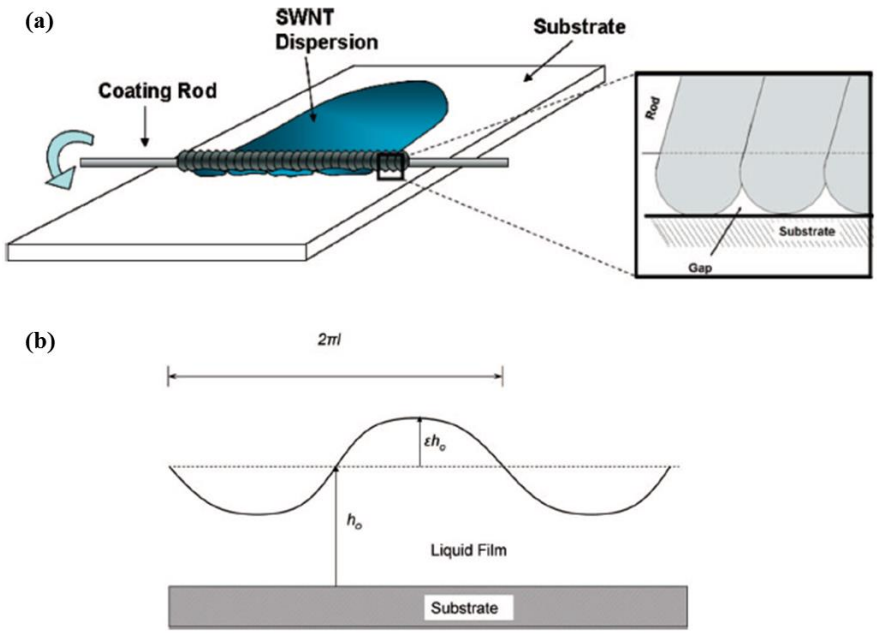

Figure 1-15. (a) Schematic representation of bar coating technique. (b) The sinusoidal surface profile of liquid film immediately after bar coating.[70]

The bar of stainless steel wound with the wire of stainless steel of the certain diameter is scanned over the substrate. The SWCNT ink spreads on the substrate during the scanning process, forming a liquid thin film as shown in ***Figure 1-15a***. Since the part of the ink flows in the grooves of bar, the liquid film whose surface has the shape of sinusoidal wave is formed, ***Figure 1-15b***. The properties of SWCNT inks play a role in the bar coating process. The surface tension of SWCNT ink should be low to suppress dewetting process and allow the uniform coating formation. After the coating process the viscosity of liquid film should be high enough to slow down the local flows of film and allow the homogeneous drying. The role of viscosity and surface tension in the process of film formation can be understood from the Capillary (*Ca*) and Reynolds (*Re*) number:[70]

$$Ca \equiv \frac{\mu v}{\sigma} \tag{1.13}$$

$$Re = \frac{\rho v l}{\mu} \tag{1.14}$$

where μ is viscosity, v is velocity, σ is surface tension, ρ is density, and 2πl wavelength of sinusoidal disturbance. After the coating, the liquid film has a wavy configuration which must flatten before the drying process. The flattening is driven by the capillary forces and gravity. The average thickness of liquid film h_0 is significantly lower than capillary length ($\kappa^{-1} \infty (\sigma/\rho g)$), suggesting that the gravitational effects are negligible in comparison with the capillary effects. The capillary flattening is driven by the electrostatic pressure difference between the convex and concave regions in the liquid film. The velocity of flattening depends on the viscosity of SWCNT inks. The high viscosity inks flatten slowly and oppositely. The slow flattening is desirable because it gives the uniformly distributed thickness of the liquid film. This is ensured by the low value of *Reynolds* number. The low *Capillary* number means the high surface tension and quick spreading of the ink on the substrate. The compromise between those numbers is necessary for the uniform film formation.[70] If the viscosity is too low, the flattening process would occur quickly. This often leads to the inhomogeneous film formation. Therefore, the SWCNT inks of sufficient surface tension and viscosity are required for the homogeneous film formation.

1.5.2. Spray coating

The spray coating method is used for the deposition of the liquids on the hot plate where the substrate is placed.[71] The temperature of hot plate depends on the boiling point of liquid and melting point of the substrate. For example the heating temperature of the poly ethylene terephthalate (PET) film should not exceed 120 ^{o}C due to the melting issue.[72] The schema of spray coating process is shown in ***Figure 1-16***.

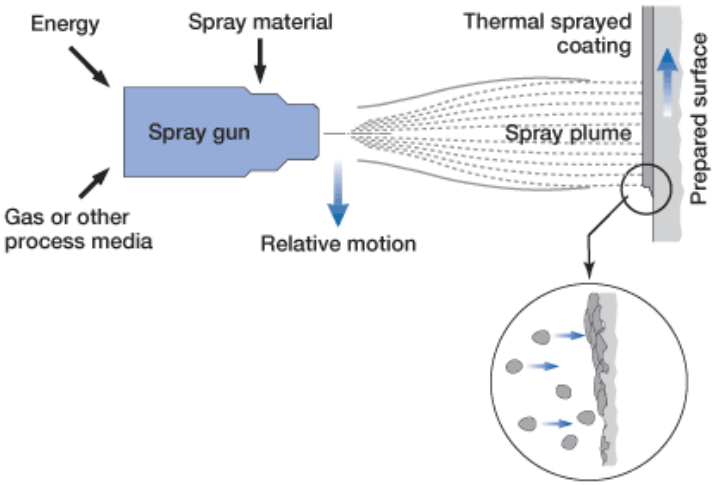

Figure 1-16. The schema of spray gun for coatings.[73]

The liquid carried by inert gas spreads onto the hot plate in the form of small droplets which immediately evaporate at the hot plate. The droplets are formed by passing the liquid through the nozzle in the spray gun. The thickness of the film is controlled manually so that the operator needs to be careful during this process. The homogeneity of the film depends on the SWCNT ink stability as well.

1.5.3. Dip coating

Dip coating is a convenient method for the preparation of SWCNT films without any sophisticated equipment. The process of the film formation is depicted in ***Figure 1-17***. It consists of the three steps: dipping the substrate into SWCNT ink, staying in the SWCNT ink, and lifting up by certain speed.

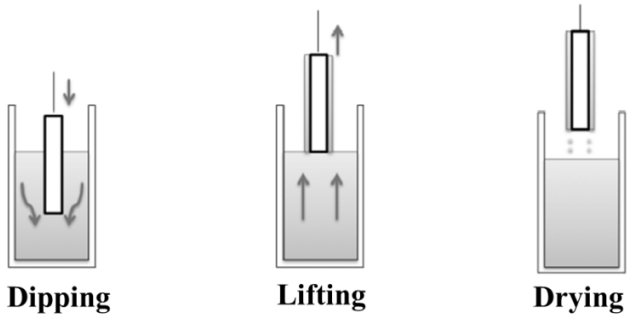

Figure 1-17. The schematic diagram of the dip coating process.[74]

During the lifting some amount of SWCNT ink is adsorbed on the substrate. The amount of adsorbed SWCNT ink depends on the viscosity, immersion time, lifting speed, and interactions between SWCNT ink and substrate. The drying process affects the quality of film as well. The only drawback of this process is coting of both sides of the substrate. However, the dip coating method is promising for the scalable fabrication of TCFs for the electronic devices.[75]

1.5.4. Spin Coating

The spin coating method involves rotation of the substrate where the droplet of SWCNT ink is placed. During rotation the droplet is spread from the center to the periphery by the centrifugal force. The process of film formation is shown in ***Figure 1-18***.

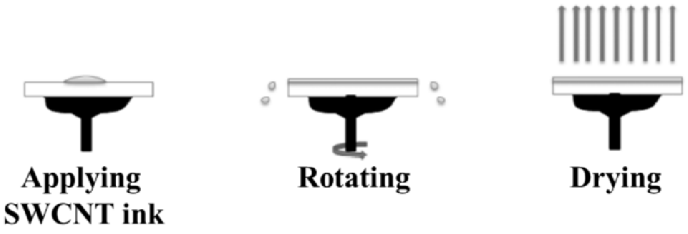

Figure 1-18. The SWCNT film formation by spin coating method.[74]

The thickness of SWCNT film depends on the viscosity of inks, angular velocity, spinning time, and the substrate-ink interactions.

1.5.5. Vacuum filtration

Vacuum filtration is a simple method for the preparation of SWCNT films. This method involves filtration of diluted SWCNT ink through the filtration membrane[76] as shown in ***Figure 1-19***. The film thickness is determined by the concentration and amount of ink passed through the membrane.

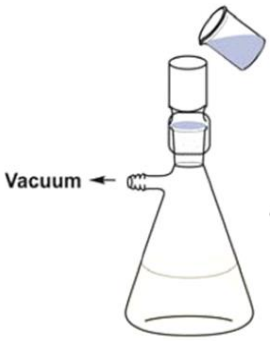

Figure 1-19. The SWCNT film fabrication by vacuum filtration method.[77]

After filtration the film needs to be transferred from the membrane onto the substrate such as flexible PET, glass substrate or some other substrate depending on the application. Also, in this manner can be prepared self-standing SWCNT film by pilling off from the membrane as reported in the preceding article.[76]

1.5.6. Langmuir-Blodgett

The Langmuir-Blodgett film deposition is based on the affinity of the substrate for solute; in this case solute is SWCNT coated with the dispersant, i.e., the SWCNT inks. The process of film deposition is shown in ***Figure 1-20***.

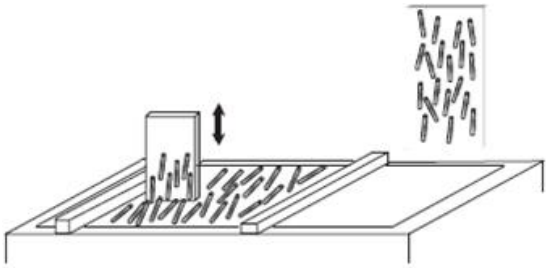

Figure 1-20. The Langmuir-Blodgett deposition of SWCNT onto the substrate.[78]

At the deposition process, the crucial role plays the surface chemistry of the substrate and SWCNTs. The SWCNTs are hydrophilic in the dispersion state that is ensured by the stability of dispersion system. Also, the substrate needs to be hydrophilic to allow the uniform adsorption of the SWCNT to the substrate. The hydrophilicity of substrate is created by washing with acids or by plasma treatment.[79] Then the SWCNT ink driven by the capillary forces penetrate to the substrate forming a monolayer film. By the repetition of this process the multilayer SWCNT film can be produced.

1.6. Requirements of the Transparent Electrodes for the Electronic Device Fabrication

The TCFs are widely used as electrodes in the electronic devices such as touch panels, displays, solar cells, and light emitting diodes.[2]The functionality of those devices depends on the electrical conductivity and optical transmittance of the transparent electrodes. Various devices have different electrode requirements in terms of the sheet resistance and optical transmittance as shown in ***Table 1-2***.

Table 1-2. The requirements of electronic devices in terms of the sheet resistance and optical transmittance.[2]

Transparent Electrode Type	Device Type	% Range	R_S Range (ohm/sq)
Touch side	Resistive touch panel	86-90	300-500
Device side	Resistive touch panel	88-90	200-500
Top or Bottom	Projected Capacitive touch panel	88-92	100-300
Primary	Surface Capacitive touch panel	88-90	900-1500
Pixel	LCD	87-90	100-300
Common	LCD	87-90	30-80

Each type of the electronic device requires the certain range of the sheet resistance and optical transmittance for the proper functionality. The sheet resistance should be minimized and optical transmittance maximized to obtain an electronic device with good performances such as the response time, touch representation accuracy, and activation force. The electronic devices are composed of the two electrodes faced toward each other. The current flow between the two electrodes allows the controller to identify the location of the touch position and forwards the signal to the computer software to process the action.[2]

The contact resistance between the electrodes is determined by the interfaces, roughness, film porosity, and uniformity.[28] Thus, the film needs to be smooth at the atomic level in order to ensure the contact between the touch side and device side. Also, the optical and electrical uniformity play a role in the efficient functionality of the electronic devices in particular touch screens. The color neutrality of the transparent films is important as well. The neutral color of the transparent electrodes is desirable because it will not distort the image color affected by the device side. The mechanical properties of transparent electrodes are important as well. If the mechanical properties are not high enough the electrode can crack, causing a serious damage of the electronic device. The environmental and chemical stability of the transparent electrodes determine the durability of the electronic device. It is critical that touch screen can function normally after 2-3 years of the everyday use. The conditions for this evaluation are high and low temperature as well as humidity. The chemical stability of the electrodes to various acids and chemical compounds is desirable to preserve electrode during the processing steps.[28,80]

Therefore, the TCFs are of the crucial importance for the assembly of the electronic devices. The electrical conductivity and optical transmittance of TCF determines the quality of the electronic devices.

1.7. Purpose of the Present Study

The development of highly transparent and conducting films of SWCNTs is still challenging. The theory predicts that the electrical conductivity and optical transmittance of SWCNT films should go beyond ITO film. However, the industrially applicable SWCNT film comparable to ITO film has not been fabricated as the best to our knowledge. There are two stages in the fabrication of SWCNT films: The preparation of SWCNT ink and removal of the dispersant from the film. The dispersant is a desirable component in the dispersion state because it gives a raise to the dispersion stability. On the other hand, it is not desirable component on the film due to the suppression of electrical conductivity of SWCNTs. This work deals with the synthesis of sol-gel dispersants which give high dispersibility and stability to SWCNTs in aqueous media. Also, the dispersant should be easily removed from the SWCNT film, increasing the electrical conductivity and optical transmittance. Therefore, we use sol-gel method to synthesize dispersants for SWCNTs with high capability of dispersing SWCNTs and high level of solubility in the film form.

1.8. Scope of the Thesis

This thesis is consisted of three papers published during the period of PhD program of three years. The thesis is divided into five chapters that are briefly summarized in the text below.

The first chapter is general introduction which should introduce the rider to the area of sol-gel chemistry and materials for the preparation of TCFs. It deals with the SWCNT inks prepared by various dispersants and the techniques for preparation of TCFs as well. The aim of this work is explained at the end of chapter.

The second chapter describes the sol-gel synthesis of the Zn/Al complex dispersant for the SWCNT inks. The structure of the dispersant is explained with the aid of EXAFS, XPS, FTIR, and XRD. The dispersion mechanism of Zn/Al complex-SWCNTs inks is also explained in details. The dispersion stability of SWCNT inks stabilized with Zn/Al complex is similar to the surfactants such as SDS and CTAB.

The third chapter deals with the TCFs fabrication from the Zn/Al complex-SWCNT inks by bar coating method. Here are discussed the electrical conductivity and optical transparency change after HNO_3 treatment. The effect of removal of SWCNT film was characterized by XPS analysis. The complete removal of Zn/Al complex was evidenced and the significant increase of the electrical conductivity.

The fourth chapter is about homogeneity of SWCNT films in terms of the sheet resistance and optical transmittance by bar coating method. Here is revealed the importance of viscosity, surface tension, and contact angle of SWCNT inks on the film homogeneity. This phenomenon was examined on the SWCNT inks stabilized with Zn/Al complex, Silica, SDS, and SDBS. The Zn/Al complex and silica based SWCNT give homogeneous films, while SDS and SDBS give inhomogeneous films.

The fifth chapter is the summery and conclusion of this work. It summarizes the progress in the area of SWCNT ink research and the TCF fabrication.

Literature

(1) Kumar, A.; Yadav, N.; Bhatt, M.; Mishra, N. K.; Chaudhary, P.; Singh, R. *Res. J. Chem. Sci.* **2015**, *5*, 98.

(2) Hecht, D. S.; Hu, L.; Irvin, G. *Adv. Mater.* **2011**, *23*, 1482.

(3) Ijima, S. *Nature* **1991,** *354*, 56.

(4) Novoselov, K. S.; Geim, a. K.; Morozov, S. V.; Jiang, D.; Zhang, Y.; Dubonos, S. V.; Grigorieva, I. V.; Firsov, A.A. *Science* **2004**, *306*, 666.

(5) Brinker, C.J.; Scherer, G.W. *Sol-gel science: the physics and chemistry of sol-gel processing*; Academic Press, **1990**, p. 907.

(6) Chopra, K. L.; Major, S.; Pandya, D. K. *Thin Solid Films* **1983**, *102*, 1.

(7) Nadaud, N.; Lequeux, N.; Nanot, M.; Jové, J.; Roisnel, T. *J. Solid State Chem.* **1998**, *135*, 140.

(8) Kang, J. H.; Uthirakumar, P.; Katharria, Y. S.; Ryu, J. H.; Kim, H. K.; Kim, H. Y.; Han, N.; Park, Y. J.; Beak, Y. S.; Kim, S. M.; Hong, C. H. *Appl. Surf. Sci.* **2012**, *258*, 8996.

(9) Kanbara, T.; Nagasaka, M.; Yamamoto, T. *Chem. Mater.* **1990**, *2*, 643.

(10) Inagaki, M.; Kang, F. *Matherial Science and Engineering of Carbon: Fundamentals*, 2-nd Edition, Tsinghua University Press **2014**, p. 542.

(11) Geim, A.; Novoselov, K. S. *Nat. Mater.* **2007**, *6*, 183.

(12) Hummers, W. S.; Offeman, R. E. *J. Am. Chem. Soc.* **1958**, *80*, 1339.

(13) Luo, J.; Cote, L. J.; Tung, V. C.; Tan, A. T. L.; Goins, P. E.; Wu, J.; Huang, J. *J. Am. Chem. Soc.* **2010**, *132*, 17667.

(14) Stankovich, S.; Dikin, D. A.; Piner, R. D.; Kohlhaas, K. A.; Kleinhammes, A.; Jia, Y.; Wu, Y.; Nguyen, S. T.; Ruoff, R. S. *Carbon* **2007**, *45*, 1558.

(15) Shin, H. J.; Kim, K. K.; Benayad, A.; Yoon, S. M.; Park, H. K.; Jung, I. S.; Jin, M. H.; Jeong, H. K.; Kim, J. M.; Choi, J. Y.; Lee, Y. H. *Adv. Funct. Mater.* **2009**, *19*, 1987.

(16) Pei, S.; Zhao, J.; Du, J.; Ren, W.; Cheng, H. M. *Carbon* **2010**, *48*, 4466.

(17) Wang, X.; Linjie Zhi; Müllen, K. *Nano Lett.* **2007**, *8*, 323.

(18) Pei, S.; Cheng, H.M. *Carbon* **2012**, *50*, 3210.

(19) Zheng, Q.; Li. Z.; Yang, J.; Kim, J. K. *Prog. Mater. Sci.* **2014**, *64*, 200.

(20) Niyogi, S.; Hamon, M. A.; Hu H.; Zhao, B.; Bhowmik, P.; Sen, R.; Itkins, M. E.; Haddon, R. C. *Acc. Chem. Res.* **2002**, *35*, 1105.

(21) Kuzmany, H.; Kukovecz, A.; Simon, F.; Holzweber, M.; Kramberger, C.; Pichler, T. *Synth. Met.* **2004**, *141*, 113.

(22) Paradise, M.; Goswami, T. *Mater. Des.* **2007**, *28*, 1477.

(23) Dresselhaus, M. S.; Lin, Y. M.; Rabin, O.; Jorio, A.; Souza Filho, A. G.; Pimenta, M. A.; Saito, R.; Samsonidze, G.; Dresselhaus, G. *Mater. Sci. Eng. C* **2003**, *23*, 129.

(24) Zhou, C.; Zhou, C.; Kong, J.; Kong, J.; Dai, H.; Dai, H. *Phys. Rev. Lett.* **2000**, *84*, 3.

(25) Che, J.; Cagin, T.; Goddard, W. *Nanotechnology* **2000**, *11*, 65.

(26) Berber, S.; Kwon, Y.K.; Tomanek, D. *Phys. Rev. Lett.* **2000**, *84*, 4613.

(27) Cairns, D. R.; Witte II, R. P.; Sparacin, D. K.; Sachsman, S. M.; Paine, D. C.; Crawford, G. P.; Newton, R. R. *Appl. Phys. Lett.* **2000**, *76*, 1425.

(28) Hecht, D. S.; Thomas, D.; Hu, L.; Ladous, C.; Lam, T.; Park, Y.; Irvin, G.; Drzaic, P. *J. SID* **2009**, *17*, 941.

(29) Sierros, K. A.; Morris, N. J.; Ramji, K.; Cairns, D. R. *Thin Solid Films* **2009**, *517*, 2590.

(30) Dürkop, T.; Getty, S. A.; Cobas, E.; Fuhrer, M. S. *Nano Lett.* **2004**, *4*, 35.

(31) Li, F.; Cheng, H. M.; Bai, S.; Su, G. *Appl. Phys. Lett.* **2000**, *77*, 3161.

(32) Xu, Z.; Gao, C. *Mater. Today* **2015**, *18*, 480.

(33) Online Source: Carbon nanotube products. Mesothelioma 2015, http://www.mesothelioma.com/.

(34) Online Source: Graphenea. Graphene Products. *Graphenea*, 2014. http://www.graphenea.com/

(35) Geng, H.Z.;Lee, Y. H. *Nanoscale phenomena: basic science to device applications*; Springer: New York, **2008**; pp. 15–28.

(36) Dresselhaus, M. S.; Dresselhaus, G.; Saito, R.; Jorio, a. *Phys. Rep.* **2005**, *409*, 47.

(37) Delaney, P.; Joon Choi, H.; Ihm, J.; Louie, S.; Cohen, M. *Nature* **1998**, *391*, 466.

(38) Brown, S.; Jorio, a.; Corio, P.; Dresselhaus, M.; Dresselhaus, G.; Saito, R.; Kneipp, K. *Phys. Rev. B* **2001**, *63*, 1.

(39) Geng, H.-Z.; Kim, K. K.; So, K. P.; Lee, Y. S.; Chang, Y.; Lee, Y. H. *J. Am. Chem. Soc.* **2007**, *129*, 7758.

(40) Kwon, Y.-K.; Saito, S.; Tománek, D. *Phys. Rev. B* **1998**, *58*, R13314.

(41) Girifalco, L. A.; Hodak, M.; Lee, R. S. *Phys. Rev. B* **2000**, *62*, 104.

(42) Vaisman, L.; Wagner, H. D.; Marom, G. *Adv. Colloid Interface Sci.* **2006**, *128-130*, 37.

(43) Nish, A.; Hwang, J.-Y.; Doig, J.; Nicholas, R. J. *Nat. Nanotechnol.* **2007**, *2*, 640.

(44) Ausman, K. D.; Piner, R.; Lourie, O.; Ruoff, R. S. *J. Phys. Chem. B* **2000**, *104,* 8911.

(45) Ramesh, S.; Ericson, L. M.; Davis, V. a.; Saini, R. K.; Kittrell, C.; Pasquali, M.; Billups, W. E.; Adams, W. W.; Hauge, R. H.; Smalley, R. E. *J. Phys. Chem. B* **2004**, *108*, 8794.

(46) Wang, Y.; Iqbal, Z.; Mitra, S. *J. Am. Chem. Soc.* **2006**, *128*, 95.

(47) Thess, A.; Lee, R.; Nikolaev, P.; Dai, H.; Petit, P.; Obert, J.; Xu, C.; Lee, Y. H.; Kim, S. G.; Rinzler, A. G.; Colbert, D. T.; Scuseria, G. E.; Tomanek, D.; Fischer, J. E.; Smalley, R. E. *Science* **1996**, *273*, 483.

(48) Lu, K. L.; Lago, R. M.; Chen, Y. K.; Green, M. L. H.; Harris, P. J. F.; Tsang, S. C. *Carbon* **1996**, *34*, 814.

(49) Strano, M. S.; Moore, V. C.; Moller, M. K.; Allen, M. J.; Haroz, E. H.; Kittell, C.; Hauge, R. H.; Smalley, R. E. *J. Nanosci. Nanotechnol.* **2003**, *3*, 81.

(50) Sun, Z.; Nicolosi, V.; Rickard, D.; Bergin, S. D.; Aherne, D.; Coleman, J. N. *J. Phys. Chem. C* **2008**, *112*, 10692.

(51) Yurekli, K.; Mitchell, C. a; Krishnamoorti, R. *J. Am. Chem. Soc.* **2004**, *126*, 9902.

(52) White, B.; Banerjee, S.; O'Brien, S.; Turro, N. J.; Herman, I. P. *J. Phys. Chem. C* **2007**, *111*, 13684.

(53) Connell, M. J. O.; Boul, P.; Ericson, L. M.; Hu, C.; Wang, Y.; Haroz, E.; Kuper, C.; Tour, J.; Ausman, K. D.; Smalley, R. E.*Chem. Phys. Lett.* **2001**, *342*, 265.

(54) Zhang, X.; Liu, T.; Sreekumar, T. V; Kumar, S.; Moore, V. C.; Hauge, R. H.; Smalley, R. E. *Nano Lett.* **2003**, *3*, 1285.

(55) Yang, D.; Rochette, J.; Sacher, E. *J. Phys. Chem. B* **2005**, *109*, 4481.

(56) Yan, X.; Han, Z.; Yang, Y.; Tay, B. *J. Phys. Chem. C* **2007**, *111*, 4125.

(57) Zheng, M.; Jagota, A.; Semke, E. D.; Diner, B. a.; McLean, R. S.; Lustig, S. R.; Richardson, R. E.; Tassi, N. G. *Nat. Mater.* **2003**, *2*, 338.

(58) Takahashi, T.; Luculescu, C. R.; Uchida, K.; Ishii, T.; Yajima, H. *Chem. Lett.* **2005**, *34*, 1516.

(59) Maria, K. H.; Mieno, T. *Jpn. J. Appl. Phys.***2016,** *55*, 01AE04.

(60) Star, A.; Steuerman, D. W.; Heath, J. R.; Stoddart, J. F. *Angew. Chem. Int. Ed.* **2002**, *41*, 2508.

(61) Numata, M.; Asai, M.; Kaneko, K.; Bae, A. H.; Hasegawa, T.; Sakurai, K.; Shinkai, S. *J. Am. Chem. Soc.* **2005**, *127*, 5875.

(62) Minami, N.; Kim, Y.; Miyashita, K.; Kazaoui, S.; Nalini, B. *Appl. Phys. Lett.* **2006**, *88*, 3.

(63) Shin, H.; Min, B. G.; Jeong, W.; Park, C. *Macromol. Rapid Commun.* **2005**, *26*, 1451.

(64) Marcus, Y. *J. Solution Chem.* **1991**, *20*, 929.

(65) Cheng, Q.; Debnath, S.; O'Neill, L.; Hedderman, T. G.; Gregan, E.; Byrne, H. J. *J. Phys. Chem. C* **2010**, *114*, 4857.

(66) Davis, V. A; Parra-Vasquez, A. N. G.; Green, M. J.; Rai, P. K.; Behabtu, N.; Prieto, V.; Booker, R. D.; Schmidt, J.; Kesselman, E.; Zhou, W.; Fan, H.; Adams, W. W.; Hauge, R. H.; Fischer, J. E.; Cohen, Y.; Talmon, Y.; Smalley, R. E.; Pasquali, M. *Nat. Nanotechnol.* **2009**, *4*, 830.

(67) Balasubramanian, K.; Burghard, M. *Small* **2005**, *1*, 180.

(68) Khim, D.; Han, H.; Baeg, K.-J.; Kim, J.; Kwak, S.-W.; Kim, D.-Y.; Noh, Y.-Y. *Adv. Mater.* **2013**, *25*, 4302.

(69) Kitano, T.; Maeda, Y.; Akasaka, T. *Carbon* **2009**, *47*, 3559.

(70) Dan, B.; Irvin, G. C.; Pasquali, M. *ACS Nano* **2009**, *3*, 835.

(71) Tucker, R. C. *ASM Handbook* **1994,** *5*, 497-509.

(72) Park, C.; Kim, S. W.; Lee, Y.S.; Lee, S. H.; Song, K. H.; Park, L. S. *J. Nanosci. Nanotechnol.* **2012**, *12*, 5351.

(73) Online source: Engineering, Coating Services Information, 2016. http://www.globalspec.com/

(74) Fu, L.; Yu, A. M. *Rev. Adv. Mater. Sci* **2014**, *36*, 40.

(75) Mirri, F.; Ma, A. W. K.; Hsu, T. T.; Behabtu, N.; Eichmann, S. L.; Young, C. C.; Tsentalovich, D. E.; Pasquali, M. *ACS Nano* **2012**, *6*, 9737.

(76) Wu, Z.; Chen, Z.; Du, X.; Logan, J. M.; Sippel, J.; Nikolou, M.; Kamaras, K.; Reynolds, J. R.; Tanner, D. B.; Hebard, A. F.; Rinzler, A. G. *Science* **2004**, *305*, 1273.

(77) Guntupalli, B.; Liang, P.; Lee, J. H.; Yang, Y.; Yu, H.; Canoura, J.; He, J.; Li, W.; Weizmann, Y.; Xiao, Y. *ACS Appl. Mater. Interfaces* **2015**, *7*, 27049.

(78) Kim, Y.; Minami, N.; Zhu, W.; Kazaoui, S.; Azumi, R.; Matsumoto, M. *Jpn. J. Appl. Phys.* **2003**, *42*, 7629.

(79) Junkar, I.; Vesel, A.; Cvelbar, U.; Mozetič, M.; Strnad, S. *Vacuum* **2009**, *84*, 83.

(80) Peltola, J.; Weeks, C.; Levitsky, I. A.; Britz, D. A.; Glatkowski, P.; Trottier, M.; Huang, T. *Inf. Disp. (1975)*. **2007**, *23*, 20.

Chapter 2

2. Sol-gel chemistry mediated Zn/Al-based complex dispersant for SWCNT in aqueous media[1]

2.1. Introduction

Single-wall carbon nanotubes[1] (SWCNT) are known to possess outstanding physical and chemical properties such as high electrical and thermal conductivities, photo luminescence, and mechanical properties.[2–5] However, pure SWCNT form firm bundles,[6] which hampers their application to various technologies. Hence, it is indispensable to dissociate the bundles to make use of the outstanding properties of SWCNT. Non-covalent methods using surfactants,[7,8] polymers,[9,10] and covalent chemical functionalization [11] have been widely used to disrupt the bundle structures in aqueous media. One of the major drawbacks of using surfactants and polymers is foam formation, which is not environmentally friendly, causing serious hurdles in industrial application.[12,13] Chemical functionalization, which is quite efficient for dispersing SWCNT, affects their electronic properties due to sp^3 hybridization of C-atoms,[14] diminishing electrical conductivity, which is a disadvantage of this method. Recent super-molecular chemistry approaches have offered a powerful route for the reversible and controllable dispersion of SWCNT.[15,16] However, there has been little research on inorganic dispersants for SWCNT; our preceding study showed that nanosilica can disperse SWCNT, but loses its dispersibility over time.[17] Thus, the inorganic SWCNT dispersant of sufficient stability should offer a new application field of SWCNT.

[1] Adapted from (R. Kukobat et al. *Carbon* 94, **2015**, pp. 518-523).

Sol-gel chemistry has been used in energy-saving ceramics processing. The sol-gel method enables us to prepare powders, thin films, and fibers of metal oxides and/or hydroxides.[18,19] This suggests that sol-gel agents can form intermediate self-assembly oxophilic structures, depending on the precursors of the process. We hypothesized that the self-assembly structures in sol-gel chemistry[20,21] can play a role as dispersants for SWCNT. The dispersion stability arises from electrostatic repulsive interactions between charged SWCNT.[22] Bimetallic sol-gel agents of mixed valence should be promising for the dispersion of SWCNT. A systematic study of bimetallic sol-gel agents lead to a Zn/Al complex as an outstanding dispersant for SWCNT. Here will be revealed the dispersion mechanism of highly dispersed SWCNT in water by Zn/Al complex dispersant.

2.2. Experimental Section

2.2.1. Preparation of the Materials

We used highly pure and crystalline SWCNT (Meijo) prepared by arc method [23] as delivered without any future purification; the SWCNTs samples were used for the dispersion experiments without any pre-treatment. The Zn/Al complex was prepared by the sol-gel method using $Zn(CH_3COO)_2$ and $Al(NO_3)_3$. 1 g of the reaction mixture with a molar fraction of Zn of 0.66 and Al of 0.34 was dissolved in distilled water of 20 g, and the reaction was conducted in an oil bath with reflux at 373 K for 2 h. After the reaction, the solvent was evaporated using a rotary evaporator, and a viscous colorless liquid was obtained. The obtained product was dried in a vacuum oven for 3 h at 373 K to yield the solidified Zn/Al complex.

We chose $Zn(CH_3COO)_2$ and $Al(NO_3)_3$ for the best bimetallic complex through qualitative dispersion testing of different combinations of nitrates of Al, Fe, Co, Ag, Gd, Cu, Ni, Mg, Ca, Li, and K with $Zn(CH_3COO)_2$ at certain molar ratios.

2.2.2. Evaluation of Dispersibility

The SWCNTs of 0.50 mg were dispersed in 25 g of aqueous solution containing dispersants of the different concentration, from 0.001 to 1.000 wt.%, with ultrasonic treatment for 20 min using a homogenizer tip (SONIC, VS 505) of 150 W and 20 kHz. The dispersibility was

evaluated using a calibration curve against the SWCNT concentration with an optical absorption spectrometer (JASCO, V 670); the standard calibration curve was obtained using cetyltrimethylammonium bromide (CTAB) as shown in ***Figure 2-1***.

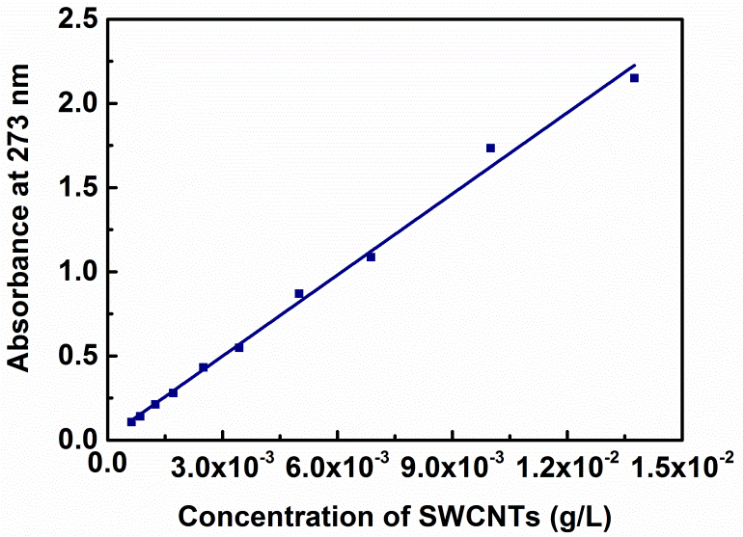

Figure 2-1. Calibration curve of SWCNT obtained using CTAB as a well-known surfactant for SWCNT.

The concentration of CTAB was 0.05 wt.% at wt.% of SWCNT from 6.25×10^{-4} to 1.38×10^{-2} g/L. Optical absorbance was measured at 273 nm, because at this wavelength SWCNTs were excited.[24] The linearity of the calibration curve is expressed by an equation as follow: $y = 160.63\ x + 0.0172$. It is important to note that the dispersibility was expressed as relative wt.% of dispersed SWCNT, having values from 0 to 100 wt.%. Relative wt.% of dispersed SWCNT is a ratio of the amount of SWCNT in the supernatant determined from the calibration curve and the total amount of SWCNTs in the system.

2.2.3. Characterization of the Structure of Zn/Al Complex Dispersant

The solid complex was characterized with X-ray diffraction (XRD) using a Bruker X-ray diffractometer with CuKα, X-ray photoelectron spectroscopy (JPS-9200, JEOL, Mg Kα), Fourier transform infrared spectroscopy (FTIR; Nicolet 6700), and thermal gravimetric mass spectrometry (TGMS; Rigaku). The local structure of the complex in aqueous solution was studied with extended X-ray absorption fine structure (EXAFS; Aichi Synchrotron center).

2.2.4. Analysis of the SWCNT Dispersion

The Zeta potential changes of the SWCNT dispersions at different concentrations of Zn/Al complex, from 0.001 to 1.000 wt.%, and at constant SWCNT concentration of 0.002 wt.% were measured with a Nicomp 380 ZLS at a laser intensity of 300 kHz. Raman spectra were recorded using an inVia Raman microscope (IAB 8303) at an excitation wavelength of 735 nm and 532 nm. The nanotubes were observed by a High-Resolution Transmission Electron Microscope (HRTEM), JEOL JEM 2100.

2.3. Results and Discussion

2.3.1. The SWCNT Inks Stabilized with Zn/Al Complex and Surfactants

Dispersion of SWCNT obtained using the Zn/Al complex is similar to the dispersion of SWCNT dispersed with surfactants. The Zn/Al complex does not form any foam after shaking, while the surfactants generate a stable foam as shown in ***Figure 2-2***.

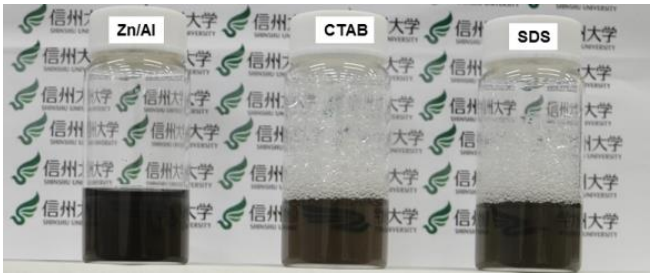

Figure 2-2. SWCNT dispersed in water with Zn/Al complex and the two types of surfactants, CTAB and SDS, after shaking.

The Zn/Al complex induces incredibly high stability to SWCNTs, giving a stable dispersion for hours, days, months, or up to one year as we have examined so far ***Figure 2-3***.

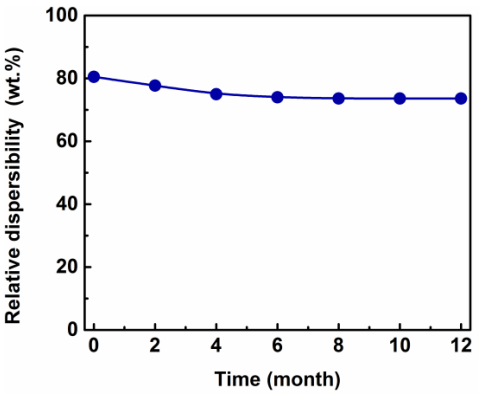

Figure 2-3. The relative dispersibility of SWCNT against time. The relative dispersibility diminishes about 6 wt.% after three months and does not change thereafter for nine months.

Figure 2-4a shows the relative dispersibility of SWCNT dispersed with Zn/Al complex, cetyl trimethylammonium bromide (CTAB), and sodium dodecyl sulfate (SDS). The relative dispersibility maximum of SWCNT dispersed with the surfactants is more than five times larger than the relative dispersibility maximum of SWCNT dispersed with the Zn/Al complex. This suggests that the Zn/Al complex is highly efficient at dispersing SWCNT in comparison with surfactants. Dispersibility of SWCNT in aqueous solution sensitively depends on the composition of Zn/Al complex as shown in ***Figure 2-4b***. Pure components of $Zn(CH_3COO)_2$ and $Al(NO_3)_3$ cannot act as dispersants for SWCNT in aqueous media, while a bimetallic Zn/Al complex shows remarkable dispersibility at a molar fraction of Zn in the range of 0.5~0.9. The composition of Zn/Al of 0.66 gives the highest dispersibility of SWCNTs in aqueous media.

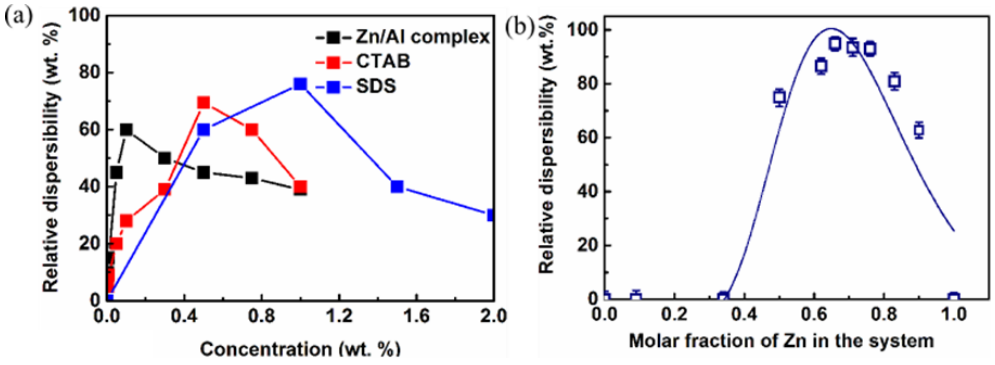

Figure 2-4. (a) Comparative study of the relative dispersibility of SWCNT against concentration of Zn/Al complex, CTAB, and SDS. (b) Relative dispersibility of SWCNT as function of the molar fraction of Zn in Zn/Al complex

The molar ratio of Zn/Al which gives the highest dispersibility corresponds to the stoichiometric ratio of Zn/Al for the synthesis of Zn/Al complex as depicted by following reaction:

$$3Zn(CH_3COO)_2 + 2Al(NO_3)_3 \rightarrow 3Zn(NO_3)_2 + 2Al(CH_3COO)_3$$

This indicates that a Zn/Al complex of a definite structure gives a stable dispersion of SWCNTs in aqueous media. Dispersibility of SWCNT strongly depends on the concentration of the Zn/Al complex as shown in ***Figure 2-5a***. Relative wt.% of dispersed SWCNT gradually increases with the concentration up to 0.10 wt.% and then decreases. ***Figure 2-5b*** shows the dependence of the zeta potential on the concentration of the Zn/Al complex.

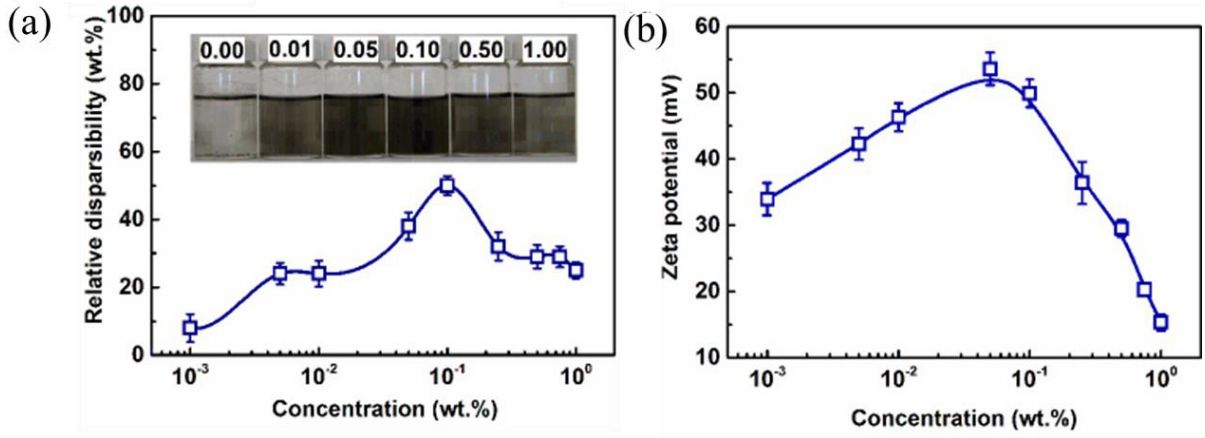

Figure 2-5. The dispersibility and stability of SWCNTs in aqueous media. (a) Relative dispersibility of SWCNTs against concentration of Zn/Al complex. (b) The zeta potential of SWCNTs as a function of concentration of Zn/Al complex.

Importantly, the zeta potential dependence briefly agrees with the dispersibility vs. concentration of the Zn/Al complex. The dispersibility is maximized at 0.10 wt.%, which can be assigned to the uniform adsorption of Zn/Al complex per unit surface area of SWCNT, exhibiting a positive charge of +55 mV. A highly positive zeta potential value indicates that SWCNT is stabilized due to electrostatic repulsive interactions [22]. Below 0.10 wt.%, the amount of Zn/Al complex is insufficient to coat the surface of SWCNT completely, exhibiting lower dispersibility. Above

0.10 wt.%, SWCNT precipitate due to high loading of Zn/Al complex onto their surface, leading to destabilization and partial precipitation.

2.3.2. The Structure of Zn/Al Complex dispersant

In order to better understand the mechanism of SWCNT dispersion, structural determination of the Zn/Al complex is of crucial importance. The amorphous nature of the Zn/Al complex was confirmed by XRD, ***Figure 2-6***. XRD pattern of the Zn/Al complex shows very broad peaks, being completely different from $Al(NO_3)_3$ and $Zn(CH_3COO)_2$ crystals.

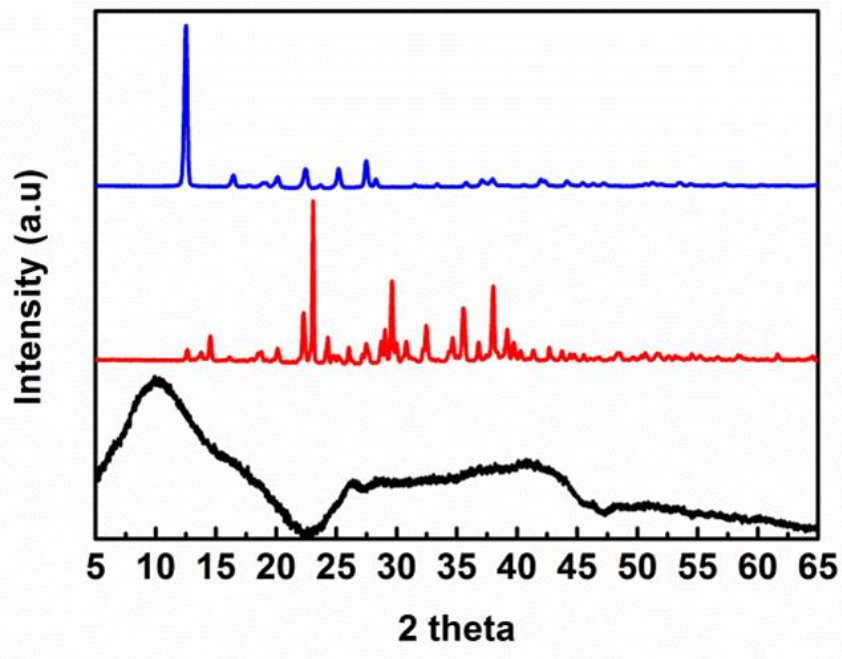

Figure 2-6. The XRD patterns of Zn/Al complex (black line), $Al(NO_3)_3$ (red line), and $Zn(CH_3COO)_2$ (blue line).

The local structure around Zn was examined with EXAFS, while the structure around Al was investigated with XPS. ***Figure 2-7a and b*** show the Fourier transform (FT) and k^3-weighted EXAFS signals for Zn of the Zn/Al complex in solid and liquid phases and $Zn(CH_3COO)_2$ as a reference as well. The intense signal in FT corresponds to the Zn-O first shell distance, suggesting that Zn is coordinated with O.

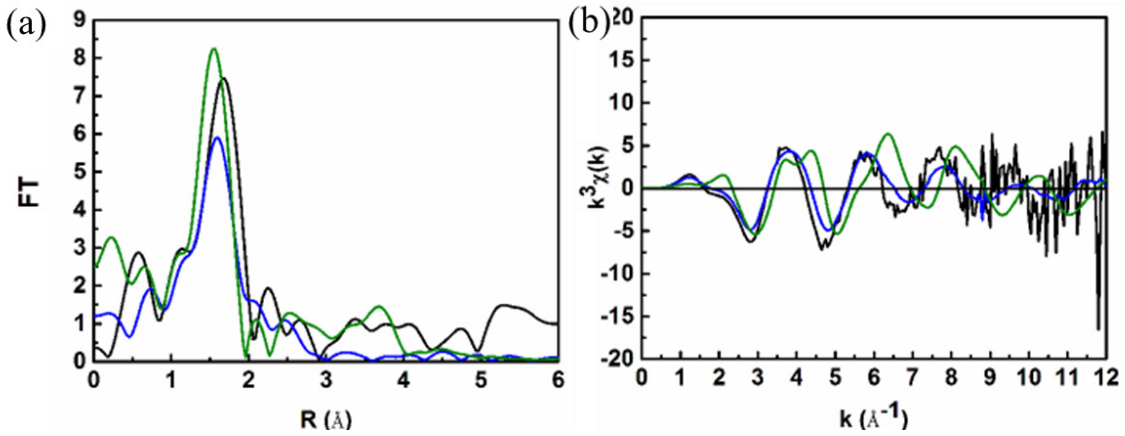

Figure 2-7. The EXAFS of Zn atom. (a) Fourier transform (FT) and (b) k^3-weighted EXAFS signals of Zn/Al complex aqueous solution with a concentration of 0.05 wt.% (green line), solid Zn/Al complex (blue line), and $Zn(CH_3COO)_2$ (black line).

The coordination number of Zn and the bond length between Zn and O, obtained by fitting EXAFS data, are shown in ***Table 2-1***.

Table 2-1. Table S1. Coordination number and Zn-O distance (Å) for the first hydration shell of $Zn(CH_3COO)_2$, $Zn(NO_3)_2$, and Zn/Al complex.

Sample	Coordination number	Bond lengths of Zn-O
$Zn(CH_3COO)_2 \cdot H_2O$ (solid)	4	1.96
Zn/Al complex (solid)	5.3	2.03
Zn/Al complex (0.05 wt %, liquid)	5.8	2.09

The coordination number of Zn increased up to 5.8 upon formation of the Zn/Al complex in aqueous solution. Thus, Zn was presented in the form of a Zn^{2+} ion hydrated with 6 molecules of H_2O, where the distance of Zn-O was determined to be 2.07 Å, corresponding to the literature value [25] of Zn^{2+} hydrated ions obtained by XRD analysis.

Figure 2-8 shows XPS spectra of the Zn/Al complex for Al 2p, O 1s and C1s. The peak at 75.37 eV suggests the presence of oxidized Al, while the peak at 533.35 eV indicates the presence of O covalently bound with Al as suggested by Bournel et al.[26] Accordingly, the Al and O atoms were bound in the sequence Al-O-C, which can be assigned to the frame structure of $Al(CH_3COO)_3$.

The peaks of C1s at 285.73 eV and 289.07 eV are attributed to the CH_3^- group and COO^- group, respectively.[27] Therefore, the C atoms indicate the presence of the CH_3COO^- group.

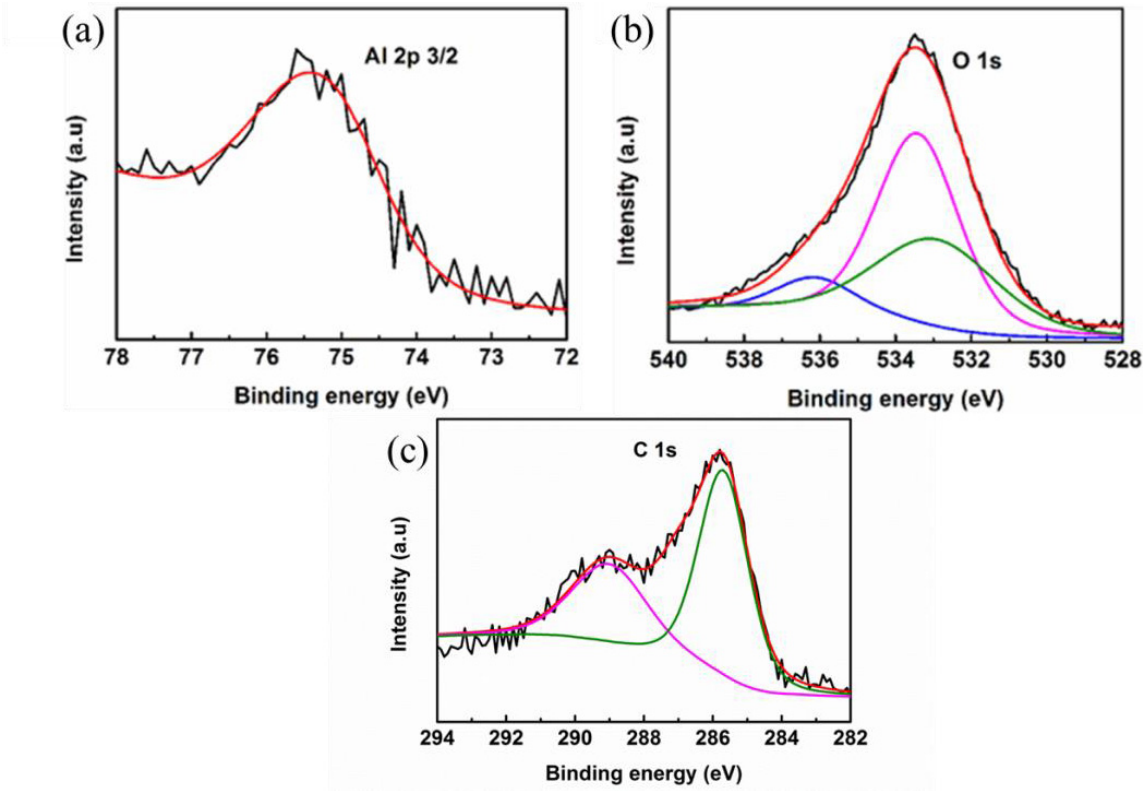

Figure 2-8. The XPS spectra of Zn/Al complex for (a) Al 2p, (b) O 1s, and (c) C 1s.

The structural analysis of Zn/Al complex dispersant was carried out using FTIR and TG-mass spectroscopy as shown in ***Figure 2-9***. These structural data confirm that the Zn/Al complex is composed of $Zn(NO_3)_2$ and $Al(CH_3COO)_3$ obtained by a stoichiometric reaction.

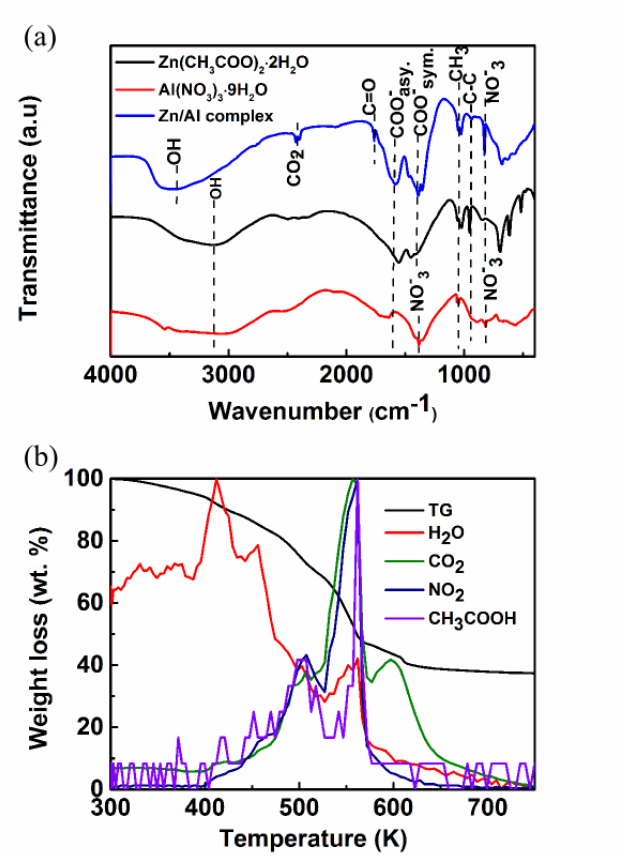

Figure 2-9. (a) The FTIR and (b) TG-mass spectra of Zn/Al complex and its precursors.

The vibration at 3500 cm^{-1} and 3200 cm^{-1} can be attributed to OH stretching in H_2O molecules. The stretching at 1765 cm^{-1} is assigned to C=O bonding in the COO^- group. The peak at 1580 cm^{-1} can be assigned to antisymmetric stretching vibrations of the COO^- group; the stretching at 1390 cm^{-1} can be attributed to the symmetric stretching in the COO^- group and stretching in the NO_3^- group as well. The band at 1035 cm^{-1} was assigned to the rocking and bending in the CH_3^- group; a small band at 950 cm^{-1} can be attributed to C-C bonding in the CH_3COO^- group. The band at 829 cm^{-1} originates from the stretching of the NO_3^- group.[28,29]

The TG-mass spectra of the Zn/Al complex indicates the presence of 62 wt.% of organic and 38 wt.% of inorganic species. Hence, the Zn/Al complex contains H_2O molecules, C atoms that are assigned to CH_3COOH, and N atoms assigned to the NO_3^- group. The TG curve suggests that dispersant was decomposed completely at 620 K.

2.3.3. The Interactions between Zn/Al complex and SWCNT in the dispersion system

The Zn/Al complex consists of $Al(CH_3COO)_3$ acting as the amphiphilic carrier and a complex of Zn^{2+} and NO_3^- ions acting as the hydrophilicity carrier. Therefore, the Zn/Al complex is amphiphilic. Relative dispersibility of SWCNTs stabilized with Zn/Al complex and that of $Zn(NO_3)_2$ and $Al(CH_3COO)_3$ is shown in ***Figure 2-10***. Since $Zn(NO_3)_2$ cannot disperse SWCNT in water, and $Al(CH_3COO)_3$ gives rise to an extremely poor dispersion of SWCNT, the Zn/Al complex, which bridges $Al(CH_3COO)_3$ with Zn^{2+} and NO_3^- ions, gives a raise to the excellent dispersion of SWCNTs.

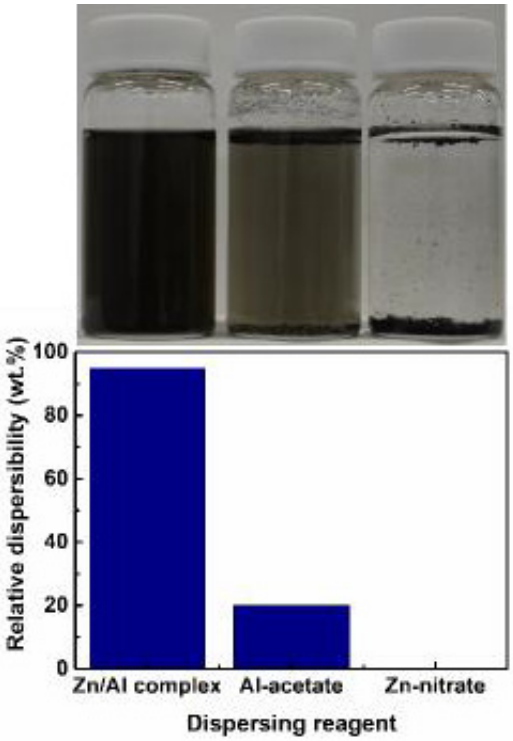

Figure 2-10. Relative dispersibility of SWCNT dispersed using Zn/Al complex, $Al(CH_3COO)_3$, and $Zn(NO_3)$ in aqueous solution. The Zn/Al complex yields high dispersion of SWCNTs, while $Al(CH_3COO)_3$ shows very poor dispersibility and $Zn(NO_3)_2$ none. The concentration of dispersant and SWCNT was 0.1 wt.% and 0.001 wt.%, respectively.

Therefore, in the dispersion system, SWCNT can be embedded into the amorphous Zn/Al complex, inducing dissociation of SWCNT bundles in water as we observed by HRTEM, ***Figure 2-11.***

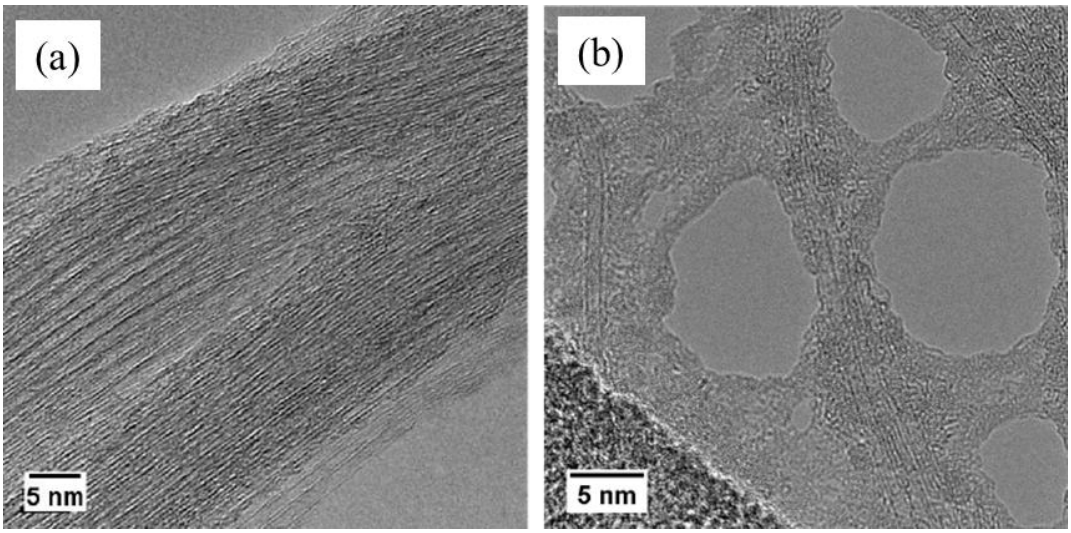

Figure 2-11. The HR-TEM images of SWCNT dispersion (a) without Zn/Al complex and (b) with Zn/Al complex

Highly stable dispersion of SWCNTs indicates high affinity of the Zn/Al complex for SWCNTs, whose interactions were studied by optical absorption and Raman spectroscopy. Direct evidence of a charge transfer interaction between Zn/Al complexes and SWCNT can be observed in ***Figure 2-12***. For pristine SWCNT, we observed three characteristic peaks at 0.63 eV, 1.18 eV, and 1.62 eV, corresponding to S11, S22, and M11 transitions, respectively.[14,30] However, in the presence of the Zn/Al complex, the peak at 0.63 eV corresponding to the S11 transition cannot be observed, suggesting that valence electrons are depleted from SWCNT;[14] the Zn/Al complex acts as an electron acceptor. The S22 and M11 bands are slightly shifted, suggesting a charge transfer interaction as well.

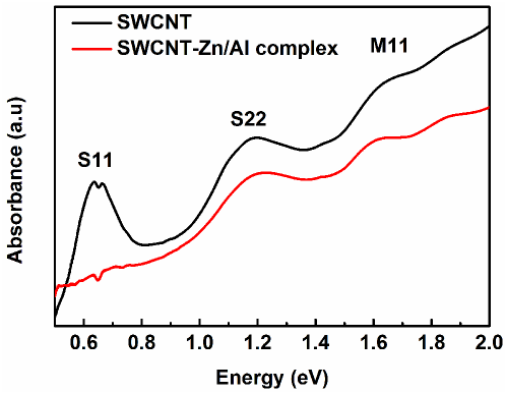

Figure 2-12. Optical absorption spectra of SWCNT and SWCNT-Zn/Al complex recorded in the film form.

Raman spectroscopic examination also supports the presence of a charge transfer interaction at the metallic and semiconducting SWCNTs. Metallic SWCNTs were excited at 785 nm, showing interesting features of RBM and G-band, ***Figure 2-13a and b***. The intensity of RBM band decreases markedly with the increase concentration of Zn/Al complex. In particular, the depression of the band at 172.6 cm^{-1} is more remarkable than that at 161.5 cm^{-1}. The intensity depression should come from the severe suppression of the RBM vibration due to the adherence of the dispersant on the SWCNT surface. On the other hand, the G-band change is more drastic. The SWCNTs without dispersant have a distinct doublet structure consisting of G^- at 1568.3 cm^{-1} and G^+ at 1591.1 cm^{-1}. The G-band is blue-shifted by 16 cm^{-1}, suggesting a charge transfer from SWCNTs to Zn/Al complex.[31,32] Semiconducting nanotubes were excited at 532 nm, ***Figure 2-13b and d***. The tendency of the depression of RBM band and shift of G-band with the increase of the concentration of Zn/Al complex is similar to the metallic nanotubes. However, the intensity change of the RBM and blue-shift of the G-band is less significant, indicating that semiconducting SWCNTs have smaller affinity for Zn/Al complex than metallic SWCNT.

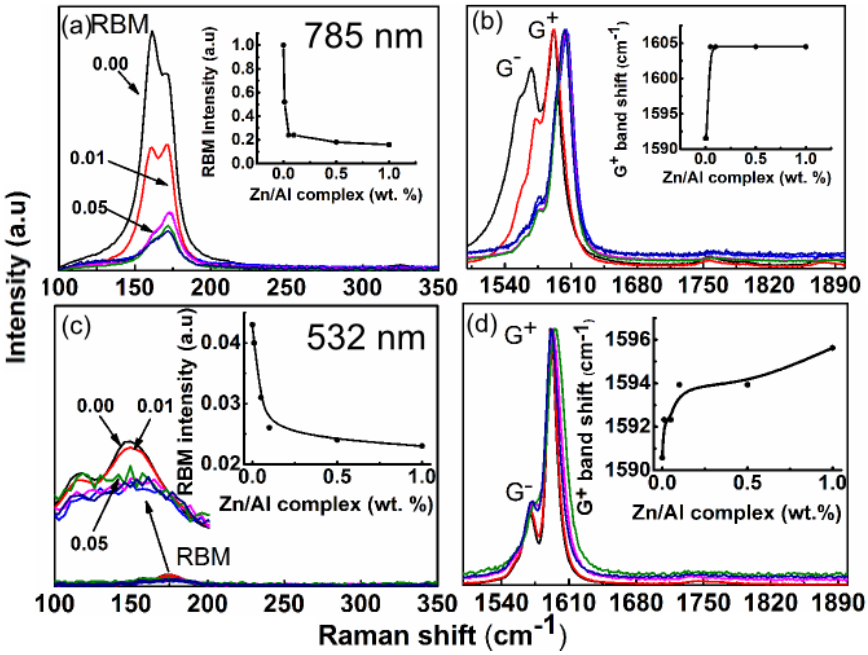

Figure 2-13. Raman spectra of the metallic and semiconducting SWCNT dispersed using Zn/Al complex. (a) The RBM and (b) G-band of the metallic SWCNT was recorded at the laser wavelength of 785 nm; (c) the RBM and (d) G-band of the semiconducting SWCNT was recorded at the laser wavelength of 532 nm.

The charge transfer interaction can be attributed to the presence of Al atoms whose species have a tendency to act as electron acceptors.[33] Hence, the molecules of $Al(CH_3COO)_3$ are strongly adsorbed onto the SWCNT surface via Al atoms, which possess hydrophobicity as shown in ***Figure 2-14***.

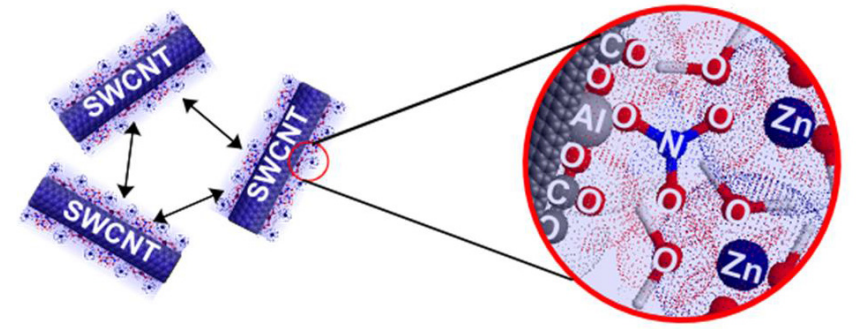

Figure 2-14. The mechanism of SWCNT dispersion stabilized by Zn/Al complexes. The surface of the nanotube is coated with $Al(CH_3COO)_3$ via Al atoms in the first layer, while the second layer is composed of Zn^{2+} and NO_3^- ions.

Since a positive charge is detected, we assume that Zn^{2+} ions are present in the outer layer of SWCNTs, inducing a highly positive charge to the SWCNTs. Zeta potential was measured to be +55 mV. A higher zeta potential value indicates a greater stability of the SWCNT dispersion; the magnitude of zeta potential should be greater than ±15 mV for the electrostatic stabilization of the colloidal dispersions. Conventional surfactants such as Dowfax 3B2, SDS, CTAB, and NaDBS have large magnitudes of the zeta potential of -97,3; -79,3; +61,5; and -60,4 mV; respectively.[22] Such a large magnitudes of zeta potential arise from the high degree of packing of SWCNT surface with the surfactant molecules; the higher degree of packing, the more difficult to remove the surfactant from the SWCNT surface in a dry state. This feature is important in the transparent and conducting film fabrication, where it is necessary to remove dispersants from the surface of film in order to improve the opto-electronic properties. Therefore, the Zn/Al complex has relatively large zeta potential, which is slightly lower in comparison with the surfactants, guaranteeing a high stability of SWCNT aqueous dispersion and easy removal from the SWCNTs as well.

Literature

(1) Ijima, S. *Nature* **1991**, 354, 56.

(2) Bandaru, P.R. *J. Nanosci. Nanotechnol.* **2007**, *7*, 1239.

(3) Salvetat, J.P.; Bonard, J.M.; Thomson, N.H.; Kulik, A.J.; Forro, L.; Benoit, W.; Zuppiroli, W. *Appl. Phys. A* **1999**, *69*, 255.

(4) Ruoff, R.S.; Lorents, D.C. *Carbon* **1995**, *33*, 925.

(5) O'Connell, M.J.; Bachilo, S.M.; Huffman, C.B.; Moore, V.C.; Strano, M.S.; Haroz, E.H.; Rialon, K.L.; Boul, P.J.; Noon, W.H.; Kittrell, C.; Ma, J.; Hauge, R.H.; Weisman, R.B.;Smalley, R.E. *Science* **2002**, *297*, 593.

(6) Dumlich, H.; Gegg, M.; Hennrich, F.; Reich, S.; *Phys. Status Solidi Basic Res.* **2011**, *248*, 2589.

(7) Vaisman, L.; Wagner, H. D.; Marom, G. *Adv. Colloid Interface Sci.* **2006**, *128-130*, 37.

(8) Shin, J.Y.; Premkumar, T.; Geckeler, K. E. *Chem. Eur. J.* **2008**, *14*, 6044.

(9) Park, C.; Ounaies, Z.; Watson, K.A.; Crooks, R.E.; Smith, J.; Lowther, S.E.; Connell, J.W.; Siochi, E.J.; Harrison, J.S.; Clair, T.L.S. *Chem. Phys. Lett.* **2002**, *364*, 303.

(10) Shvartzman-Cohen, R.; Nativ-Roth, E.; Baskaran, E.; Levi-Kalisman, Y.; Szleifer, I.; Yerushalmi-Rozen, R. *J. Am. Chem. Soc.* **2004**, *126*, 14850.

(11) Wang, Y.; Iqbal, Z.; Mitra, S. *J. Am. Chem. Soc.* **2006**, *128*, 95.

(12) Chaisalee, R.; Soontravanich, S.; Yanumet, N.; Scamehorn, J. F. *J. Surfactants Deterg.* **2003**, *6*, 345.

(13) Denkov, N. D. *Langmuir* **2004**, *20*, 9463.

(14) Niyogi, S.; Hamon, M.A.; Hu, H.; Zhao, B.; Bhowmik, P.; Sen, R.; Itkins, M.E.; Haddon, R.C. *Acc. Chem. Res.* **2002**, *35*, 1105.

(15) Chichak, K. S.; Star, A.; Altoé, M. V. P.; Stoddart, J. F. *Small* **2005**, *1*, 452.

(16) Prevoteau, A.; Soulie, C.; Leibler, L. *J. Am. Chem. Soc.* **2012**, *134*, 19961.

(17) Matsuda, T.;Minami, D.;Khoerunnisa, F.;Sunaga, M.;Nakamura, M.;Utsumi, S.;Itoh, T.;Fujimori, T.;Hayashi, T.;Hattori, Y.;Endo, M.;Isobe, H.;Onodera, H.;Kaneko, K. *Langmuir* **2015**, *31*, 3194.

(18) Brinker, C.J.; Scherer, G.W. *Sol-gel science: the physics and chemistry of sol-gel processing*; Academic Press, **1990**, p. 907.

(19) Livage, J.; Henry, M.; Sanchez, M. *Prog. Solid St. Chem.* **1988**.

(20) Uekawa, N.; Kaneko, K. *J. Phys. Chem.* **1996**, *100*, 4193.

(21) Uekawa, N.; Kaneko, K. *Adv. Mater.* **1995**, *7*, 312.

(22) White, B.; Banerjee, S.; O'Brien, S.; Turro, N. J.; Herman, I. P. *J. Phys. Chem. C* **2007**, *111*, 13684.

(23) Szabó, A.; Perri, C.; Csato, A.; Giordano, G.; Vuono, D.; Nagy, J.B. *Materials* **2010**, *3*, 3092.

(24) Attal, S.; Thiruvengadathan, R.; Regev, O. *Anal. Chem.* **2006**, *78*, 8098.

(25) Marcus, Y. *J. Solution Chem.* **1983**, *12*, 271.

(26) Bournel, F.; Laffon, C.; Parent, P.; Tourillon, G. *Surf. Sci.* **1996**, *352-354*, 228.

(27) Mar, L. G.; Timbrell, P.Y.; Lamb, R.N. *Thin Solid Films* **1993**, *223*, 341.

(28) Zhang, Y.; Zhu, F.; Zhang, J.; Xia, L. *Nanoscale Res. Lett.* **2008**, *3*, 201.

(29) Stählin, W.; Oswald, H. R. *J. Solid State Chem.* **1971**, *3*, 252.

(30) Hamon, M. A.; Itkins, M.E.; Niyogi, S.; Alvaraez, T.; Kuper, C.; Menon, M.; Haddon, R.C. *J. Am. Chem. Soc.* **2001**, *123*, 11292.

(31) Rao, A. M.; Richter, E.; Bandow, S.; Chase, B.; Eklund, P.C.; Williams, K.A.; Fang, S.; Subbaswamy, K.R.; Menon, M.; Thess, A.; Smalley, R.E.; Dresselhaus, G.; Dresselhaus, M.S. *Science* **1997**, *275*, 187.

(32) Geng, H.Z.; Kim, K.K.; So, K.P.; Lee, Y.S.; Chang, Y.; Lee, Y.H. *J. Am. Chem. Soc.* **2007**, *129*, 7758.

(33) Burova, M.V.; Fionov, A.V.; Tveritinova, E.A.; Kharlanov, A.N.; Lunin, L.L. *Russ. J. Phys. Chem. A* **2007**, *81*, 164.

Chapter 3

3. Zn/Al complex-SWCNT ink for transparent and conducting homogeneous films by scalable bar coating method[2]

3.1. Introduction

Rapid development of the transparent electronics, including touch panel displays and transparent electrodes requires new materials for the transparent and conducting film (TCF) fabrication. So far, Indium Tin Oxide (ITO) film has been widely used as an electrode for the fabrication of transparent conductors.[1,2] However, ITO has several obstacles for this application: Limited resources, high cost and non-flexibility.[3,4] Thus, Single Wall Carbon Nanotube (SWCNT), having excellent opto-electrical and mechanical properties,[5,6] which is superior to ITO, have attracted attention of scientists and engineers to make use of this unique material in the TCF fabrication.[7–11]

Despite many attempts for the application of SWCNT in the transparent electronics, preparation of high quality TCF is still challenging. Thus, Y. Zhou et al. reported the stable doping of SWCNT film by CuI with the sheet resistance of 55-65 ohm/sq at the transmittance of 80%.[12] Also the films prepared by dry printing of SWCNTs on the substrate with the sheet resistance of 86 ohm/sq at 90%[13] and 53 ohm/sq at 80%[14] have been reported. The free self-standing films of SWCNT with the sheet resistance of 84 ohm/sq and transmittance 90 % have

[2] Adapted from (R. Kukobat, et al. *Chem. Phys. Lett.* 650, **2016**, pp. 113-118).

been developed as well.[15] Although these techniques give highly transparent and conductive films, easy and scalable methods for the TCF fabrication are still required.

The film fabrication with the SWCNT inks is a promising route for the SWCNT films on a large scale, if we have an excellent dispersant for SWCNTs. The efficient debundling of the SWCNTs is requested for the TCF fabrication technology.[16] Organic dispersants such as surfactants have been widely used to disperse SWCNTs in aqueous media; Sodium Dodecylbenzene Sulfonate (SDBS) and Sodium Dodecyl Sulfate (SDS) have been used for the film fabrication up to date.[7,17–19] However, the application of surfactants is not suitable for the TCF fabrication because of its non-transparency and non-conductivity in a dry state. This implicates that the surfactants need to be removed from the SWCNT film in order to maintain the high electrical conductivity and optical transparency of the SWCNT film. Several studies have shown that the surfactants are removable with concentrated HNO_3 treatment for 30 or 60 min.[7,17–19] Indeed, the film with sheet resistance of 70 ohm/sq at the transmittance of 80% has been obtained after removal of SDS.[17] Reducing of the removal time as well as concentration of HNO_3 for the film treatment should improve efficiency in the scalable TCF fabrication technology. Thus we have an intensive demand for the new type of SWCNT dispersant which can overcome these drawbacks of the surfactants.

Variety of techniques have been employed for the fabrication of homogeneous TCF such as spray coating,[20] spin coating,[20] vacuum filtration,[21] Langmuir-Blodgett[22] and bar coating[23,24] methods. Bar coating method can be applied to the scalable film fabrication, because it is easy and practical to be used for this purpose. Thus, we have chosen bar coating technique as the most efficient technique for the preparation of the uniform TCF.[24] The films prepared using SWCNT ink stabilized with surfactants such as SDS and SDBS have poor homogeneity due to the low viscosity, which is not fit for the production of homogeneous film.[24,25] The additive such as nonionic surfactant, TX-100, needs to be added to increase viscosity of the surfactant-based SWCNT inks for better homogeneity of the TCF.[24,25] However, the additives suppress electrical conductivity of the film, which is an obstacle toward efficient TCF fabrication.

We have found that nanosilica can be used as an efficient dispersant for carbon nanotubes.[26] However, its dispersibility changes with aging time, which is not desirable for the TCF fabrication. Then, we developed a quite stable Zn/Al complex dispersant for the fabrication of

SWCNT based film.[27] The Zn/Al complex is amphiphilic, containing amorphous Al-acetate and Zn-nitrate. Here, the Al-acetate can be adsorbed on the hydrophobic surface of SWCNTs and Zn-nitrates have affinity to water phase.[27] Thus, the SWCNTs are stabilized in an aqueous media for at least one year. The Zn/Al complex dispersant has two merits of an easy removal of the dispersant from the film by simple washing treatment with 1M HNO_3 during 10 min and of an appropriate viscosity for the production of uniform SWCNT films with bar coating method.

As the homogeneity and opto-electrical properties of the SWCNT film depend on the viscosity of SWCNT ink and substrate for the film fabrication, we must examine the optimum conditions for the high quality SWCNT films. This paper reports that Zn/Al complex aided SWCNT ink of an optimum viscosity is an excellent candidate for homogeneous TCF fabrication with bar coating method.

3.2. Experimental section

3.2.1. Materials and ink for TCF preparation

The SWCNT (eDIPS) for the ink preparation was synthesized by Chemical Vapor Deposition (CVD) method after the established procedures.[28] The Zn/Al complex dispersant was prepared by sol-gel technique. The salts $Zn(CH_3COO)_2$ and $Al(NO_3)_3$ for the synthesis of Zn/Al complex dispersant were purchased from Sigma Aldrich. $Zn(CH_3COO)_2$ and $Al(NO_3)_3$ of 1.00 g at the 1:1 weight ratio were dissolved in 40 g of ethanol and mixed for 2 h to produce the Zn/Al complex dispersant. The obtained Zn/Al complex was dried in vacuum at 303 K after evaporation of ethanol. We prepared Zn/Al complex-SWCNT inks with the concentration of SWCNT from 0.01 to 0.05 wt.%. to examine the concentration effect on the film homogeneity. The concentration of Zn/Al complex dispersant of 1.00 wt.% was used for the preparation of SWCNT ink. The inks were prepared by sonication for 20 min using the homogenizer tip (SONIC, VS 505) with power of 100 W at the frequency of 20 kHz. Commercial polyethylene terephthalate (PET) was used as a transparent substrate for the SWCNT film preparation (OHP, A450). The SWCNT dispersion was coated onto the PET substrate by use of a bar coater (Kobayashi Engineering Works).

3.2.2. Characterization of SWCNT ink and TCF

The wettability of the SWCNT ink was examined using a contact angle measuring instrument (DMC-MC3). The viscosity of the SWCNT inks was measured using an Ostwald viscometer at 298 K. The sheet resistance was measured using four point probe method (LORESTA-GP, MCP-T610). Optical absorption spectra and the transmittance at 550 nm were measured using a UV-vis spectrophotometer (JASCO, V-670). The SWCNT bundles before and after dispersion-treatment were observed using a High-Resolution Transmission Electron Microscope (HRTEM, JEOL JEM 2100). Atomic force microscope (AFM, Agilent Technologies) was used for the observation of the SWCNT films on the PET and WSxM software[29] was used for the image processing. Effect of the removal of dispersants from the SWCNT film was examined by X-ray Photoelectron Spectroscopy (XPS; AXIS-ULTRA, DLD, Al Kα). The Raman spectral change of SWCNT films on the PET with HNO_3-treatment was examined using a Raman microscope (Renishaw, inVia) with the excitation using lasers of 532 and 785 nm.

3.3. Results and discussion

3.3.1. Homogeneity of the SWCNT film

Homogeneity of the SWCNT film prepared using bar coating method is closely related with the concentration of SWCNT ink. ***Figure 3-1*** shows the sheet resistance and optical transmittance versus the coordinates of the film (x, y), whose unit is cm; the film size is 23 cm x 17 cm. The variation of sheet resistance and transmittance at different coordinates is ascribed to the inhomogeneity of SWCNT film. The SWCNT ink of 0.005 wt.% gives the highly transparent film, whose transmittance is 99 %, as shown in ***Figure 3-1a and a_0***. Extremely high transmittance suggests that the film is thin with randomly distributed SWCNT network. The sheet resistance of SWCNT film markedly varies from 10^5 to 10^7 ohm/sq, indicating that the SWCNT film is non-conductive and inhomogeneous. In case of 0.02 wt.% SWCNT transmittance of the film slightly decreases to 98 %, while the sheet resistance lies in the range from 10^3 to 10^5 ohm/sq, showing presence of inhomogeneously distributed SWCNTs on the PET substrate (***Figure 3-1b and b_0***). The ink of 0.05 wt.% SWCNTs provides quite homogeneous

SWCNT film with the uniform transmittance of 90 % and the sheet resistance of 307 ± 35 ohm/sq, as shown in ***Figure 3-1c and c_0***.

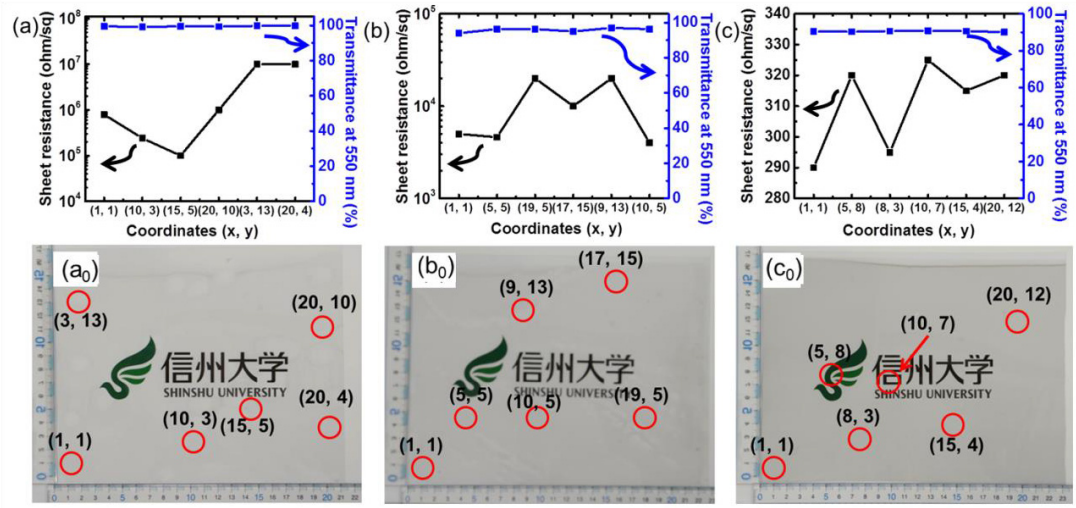

Figure 3-1. Variations of the sheet resistance and transmittance with the coordinates (x, y) in cm of SWCNT film, at the constant concentration of the Zn/Al complex of 1.00 wt.%. The SWCNT concentration of ink: 0.005 wt. % (a) and (a_0), 0.02 wt.% (b) and (b_0), 0.05 wt.% (c) and (c_0).

The surface tension and viscosity of SWCNT inks play a key role in the production of homogenous films.[24,25] The surface tension of SWCNT inks of 70.50 mN/m does not change with the concentration of SWCNTs, allowing uniform spreading of the ink onto the PET substrate. ***Figure 3-2*** shows a briefly proportional increase of viscosity with the concentration of SWCNTs which can be explained by more entangled network formation at the higher concentration of SWCNTs.[25] This viscosity change directly governs the film homogeneity with the relevance to local flow of the SWCNT ink on the PET substrate. An evident irregularity in the thickness of the coated SWCNT film is formed immediately after coating. Flattening of the SWCNT film occurs spontaneously in a wet state by the local flow of the SWCNT ink. Thus, the local flow is controlled by the viscosity of SWCNT ink. The local flow is significant at viscosity below 1.30 mPa·s, leading to local thinning and inhomogeneous film formation. However, the rapid and local flow is suppressed at viscosity above 1.30 mPa·s, allowing a uniform SWCNT film formation.

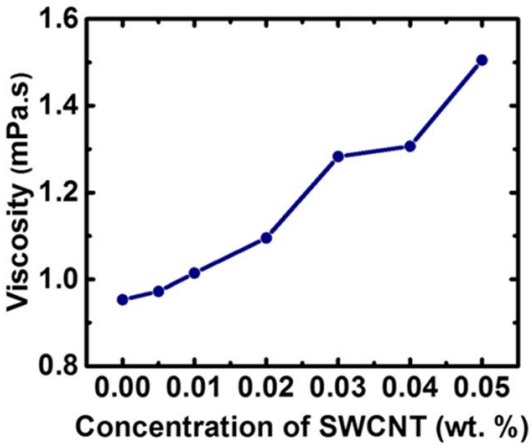

Figure 3-2. Viscosity of Zn/Al complex-SWCNT ink against the concentration of SWCNT (a) and contact angle of SWCNT ink on the PET substrate (b). Here the concentration of Zn/Al complex dispersant is kept at 1.00 wt.% for all dispersion systems.

The surface coating quality is also strongly influenced by affinity of the substrate against the SWCNT ink. ***Figure 3-3*** shows hydrophilicity/hydrophobicity of the PET substrate determined by contact angle measurements. The contact angle of SWCNT ink against PET substrate is 77.5^{o}, indicating a sufficient wettability.

Figure 3-3. Contact angle of SWCNT ink on the PET substrate.

The wettability of PET substrate is associated with the hydrophilicity and surface roughness. The hydrophilicity can be attributed to the presence of hydrophilic functionalities such as C-O, O=C-O and C=O, inducing negative charges to the surface.[30] The zeta potential measurement in the preceding study[27] showed that SWCNTs coated with Zn/Al complex were positively charged. Thus, the stable SWCNT deposition should be guaranteed by the electrostatic attractive interactions between SWCNTs and PET substrate in the presence of Zn/Al complex. The surface roughness of the PET substrate additionally supports the deposition of the SWCNTs onto the substrate. ***Figure 3-4*** shows the AFM image of the PET substrate.

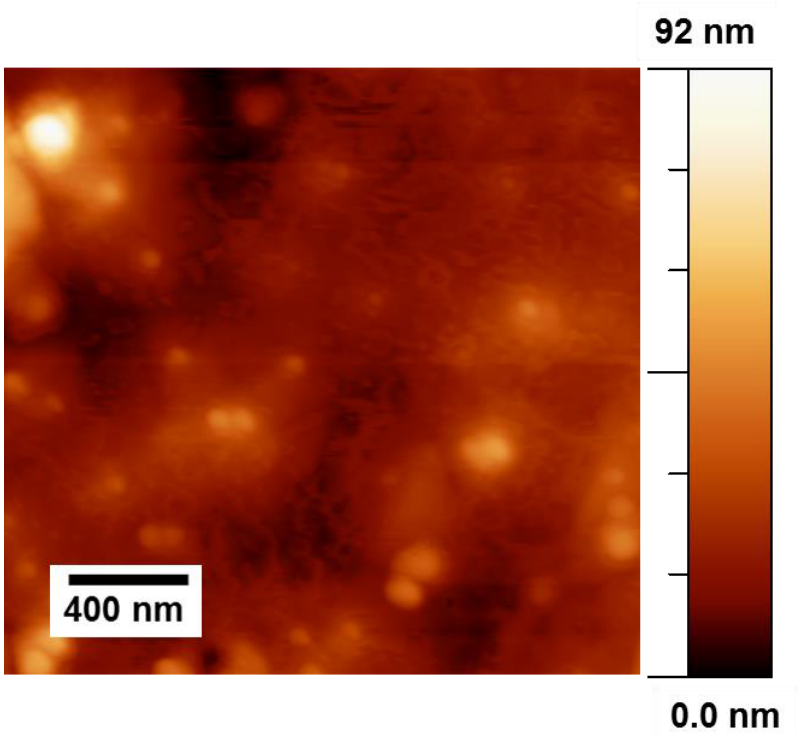

Figure 3-4. The AFM image of PET substrate.

The roughness average of the substrate is estimated to be 6.4 nm. This roughness of the PET substrate facilitates the deposition of SWCNTs as the surface is scanned by a bar coater. During this process SWCNTs are being trapped on the surface of the rough substrate and the uniformly coated film can be obtained.

3.3.2. Factors for high quality TCF on PET substrate

The sheet resistance of SWCNT film depends on the wire-wound diameter of bar used for coating as shown in ***Figure 3-5a***. By increasing the wire diameter from 0.025 to 0.20 mm the size of groove increases, suggesting that capacity of bar increases as well.[24] The smaller capacity of bar indicates that adhesion of SWCNT on the substrate is limited, giving the film with high sheet resistance. On the other hand, large capacity of bar implicates that adhesion of SWCNT on the substrate is enhanced, resulting the film with low sheet resistance.

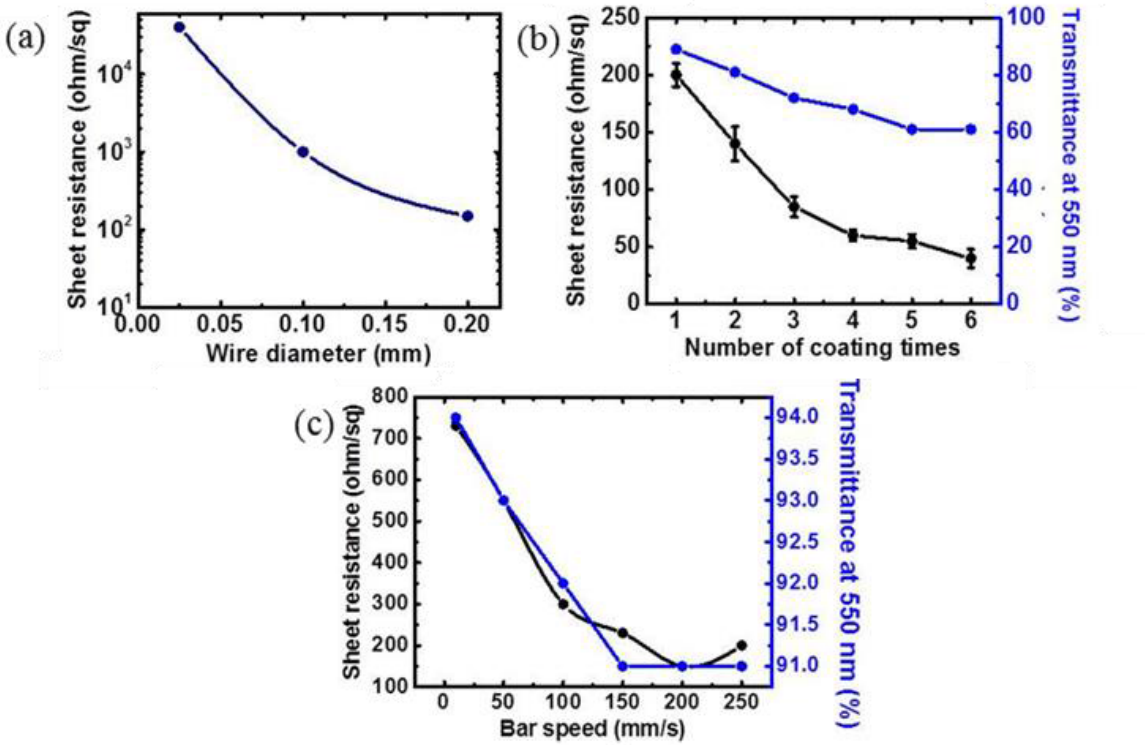

Figure 3-5. The effect of the bar coating conditions on sheet resistance and transmittance at 550 nm of SWCNT film. (a) Sheet resistance against wound wire diameter of the bar for coating of SWCNT on PET substrate. (b) Effect of number of coating times on sheet resistance and transmittance of the film and (c) dependence of bar speed on sheet resistance and transmittance of the film.

Opto-electrical properties of the film can be controlled by the number of coating times as shown in ***Figure 3-5b.*** The repeated coating decreases sheet resistance, giving the conducting path network of SWCNTs. Transmittance of the film follows the tendency of sheet resistance; the thicker the film, the greater the light absorption.[16] Thus, at six times coating, the film has sheet resistance of 50 ohm/sq and transmittance 60 %. The scanning speed of bar also affects the sheet resistance as shown in ***Figure 3-5c***. When the speed is lower than 100 mm/s, adhesion of SWCNT is followed with adsorption of the Zn/Al complex from the bulk phase, giving the film with higher sheet resistance. On the contrary, the speed over 100 mm/s leads to an optimum adhesion of SWCNT with less Zn/Al complex , giving the film with lower sheet resistance.

3.3.3. Change in opto-electrical properties of the film with acid treatment

Removal of the Zn/Al complex from the SWCNT surface with the HNO_3 solution lowers the sheet resistance; the HNO_3 concentration affects intensively the removal of the Zn/Al complex from SWCNTs, as shown in ***Figure 3-6a***. The minimum sheet resistance of 150 ohm/sq at 1M HNO_3 indicates that even diluted acid can remove the Zn/Al complex efficiently without deterioration of the SWCNT film. The sheet resistance against the treatment time shows the minimum, as shown in ***Figure 3-6b***. The minimum sheet resistance comes from two contrary effects: 1.) dissolution of the Zn/Al complex from the film surface, decreasing the sheet resistance and 2.) detachment of SWCNT from the film surface, increasing the sheet resistance. The most conducting film is obtained by the washing treatment with 1M HNO_3 for 10 min, being derived from the compromising condition of the opposite effects. Then, we adopted this washing condition as a standard procedure for the removal of Zn/Al complex dispersant.

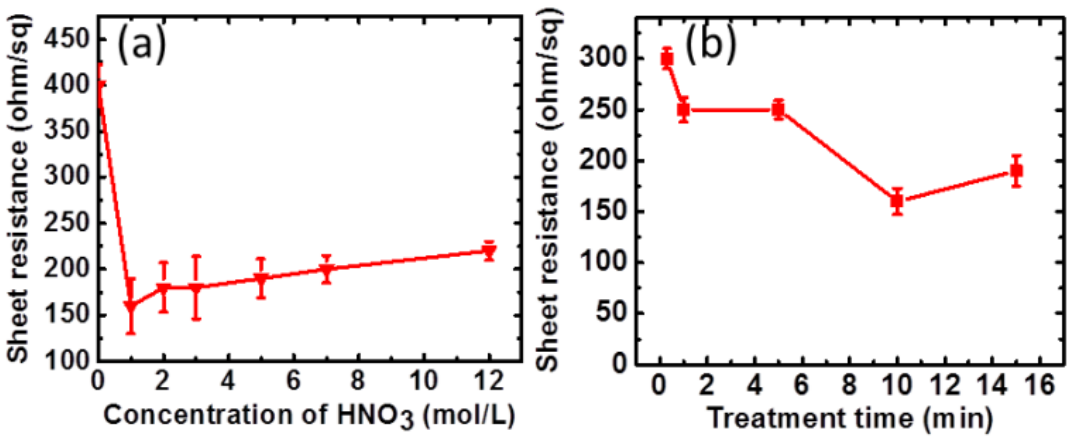

Figure 3-6. Sheet resistance against the concentration of HNO_3 used for the washing treatment (a) and sheet resistance versus the treatment time by 1M HNO_3 (b).

We need to understand the arrangement of SWCNTs coated on the PET substrate. The HR-TEM observation of SWCNTs shows that SWCNTs form an ordered bundle structure which is partially de-bundled by dispersion treatment with Zn/Al complex as shown in ***Figure 3-7***.

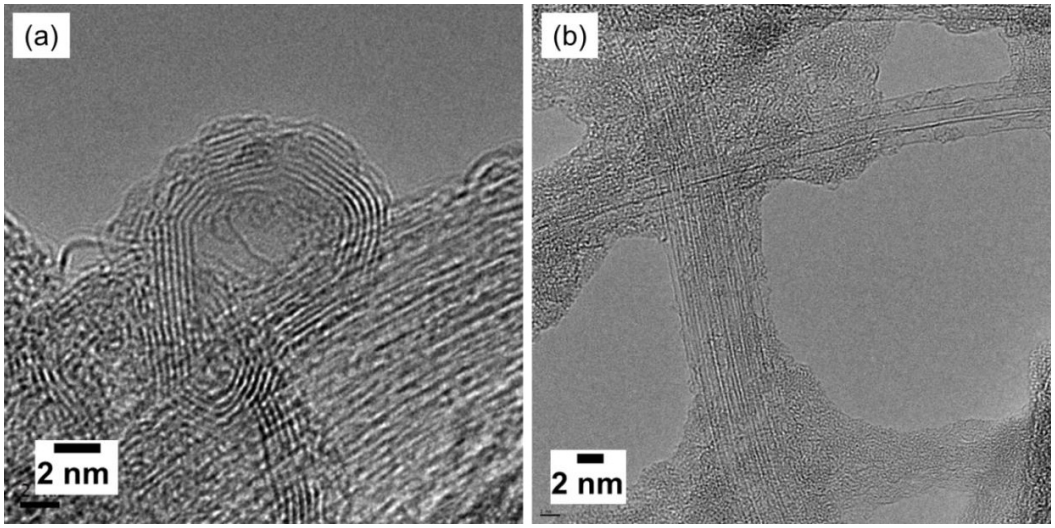

Figure 3-7. The HR-TEM images of (a) SWCNTs and (b) dispersed SWCNTs with Zn/Al complex.

Here, these HR-TEM images on the Cu grid are shown, because we cannot observe directly SWCNT on the PET substrate. The Zn/Al complex dispersants are adhered on the fine SWCNT bundles to separate the bold bundles. The SWCNT bundles on the PET substrate after the dispersion treatment are assumed to be finer than those on the Cu grid, because SWCNT interacts more strongly with the PET than with the Cu grid. The HR-TEM observation of the SWCNT with Zn/Al complex dispersant on the Cu grid with the acid treatment should be challenged in the future. Instead of HR-TEM observation, AFM gives important information on the SWCNT structure coated on the PET substrate before and after HNO_3 treatment.

Figure 3-8 shows the AFM micrographs and the size distribution histograms of the SWCNT on PET before and after HNO_3 treatment. The average size of SWCNT bundles with Zn/Al complex is evaluated to be 310 nm, whereas the acid treatment decreases this value to 48 nm in size.

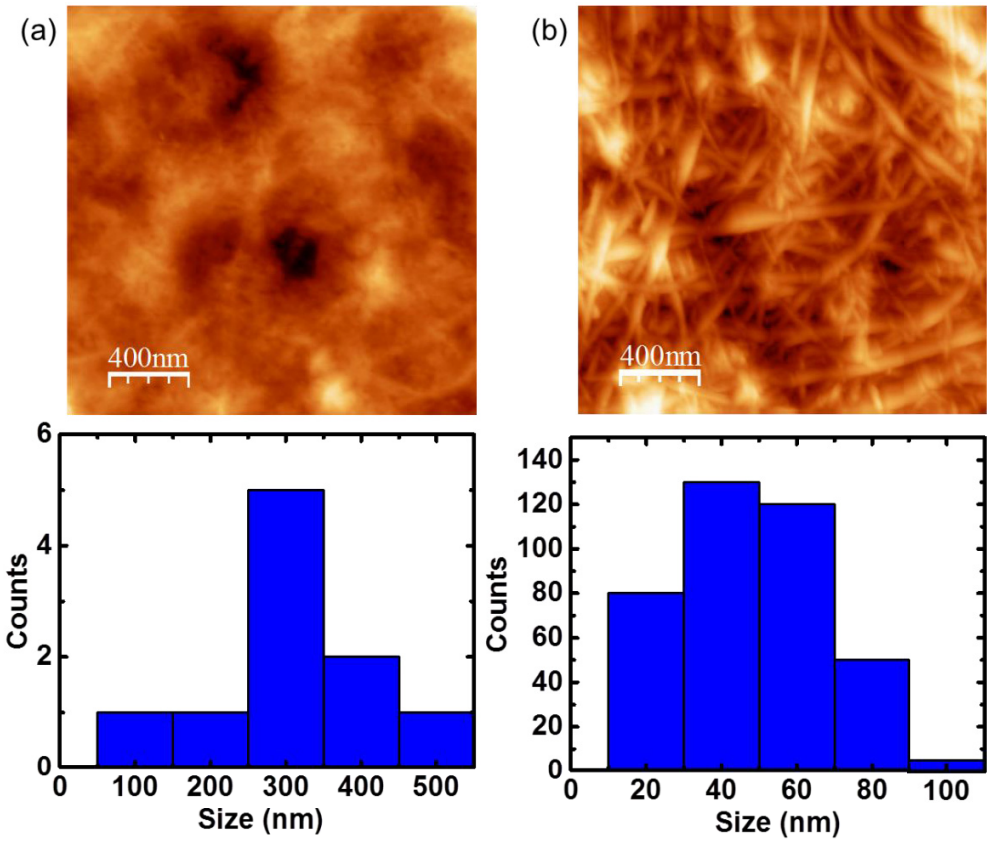

Figure 3-8. The AFM micrographs of SWCNT film on PET substrate (a) before and (b) after acid treatment and size-distribution histograms of bundles corresponding to the above micrographs.

The AFM studies clearly show the effectiveness of the removal treatment of Zn/Al complex with diluted HNO_3. The efficient removal of Zn/Al complex improves the electrical contact between fine SWCNT bundles, lowering the electrical resistivity as observed.

3.3.4. Changes in surface chemistry and electrical properties of SWCNT on HNO_3 treatment

The XPS examination clearly evidences the effectiveness of removal of the Zn/Al complex from SWCNT film, as shown in ***Figure 3-9a***. The Zn 2p peaks in the range from 1050 to 1020 eV and peaks of Al 2s, 2p, Zn 3p, 3s in the range from 140 to 70 eV disappear after acid treatment, indicating SWCNT film free of Zn/Al complex. The atomic percentages of the elements before and after acid treatment are shown in ***Table 3-1***. The C content becomes almost twice, while the O content almost triples after acid treatment. The resultant XPS data clearly

indicate an effective removal of Zn/Al complex from the SWCNT film. ***Figures 3-9b, c and d*** show the C1s XPS spectra of the bare PET, SWCNT film before and after acid treatment with their deconvoluted spectra, respectively. The bare PET has C1s peaks coming from the surface oxygen groups (C-O at 286.19 eV and O=C-O at 288.77 eV) in addition to the C1s peak from the C-C bonding at 284.36 eV.[30] The C1s XPS spectrum of the SWCNT film before acid treatment has a weak peak coming from sp^2 SWCNTs at 284.94 eV in addition to the C1s peak from the C-C bonding.[31] The C1s peaks of the surface oxygen groups are relatively weak in comparison with those of the bare PET. The Zn/Al complex dispersant should partially cover the PET surface. The acid treatment gives a distinct C1s peak having a strong sp^2 carbon peak at 285.02 eV and evident surface oxygen peaks due to removal of the Zn/Al complex. A slightly higher energy shift of the sp^2 carbon peak from 284.94 eV to 285.02 eV after HNO_3 treatment[32] must be noted. The literature[32] reported that the sp^2 carbon peak of SWCNTs gave the higher energy shift after doping with HNO_3. Also it is well known that simple treatment with HNO_3 decreases the electrical resistivity of SWCNTs due to creation of holes by doping effect.[33] Consequently the treatment of SWCNT-Zn/Al complex with the diluted HNO_3 for 10 min should induce the doping effect.

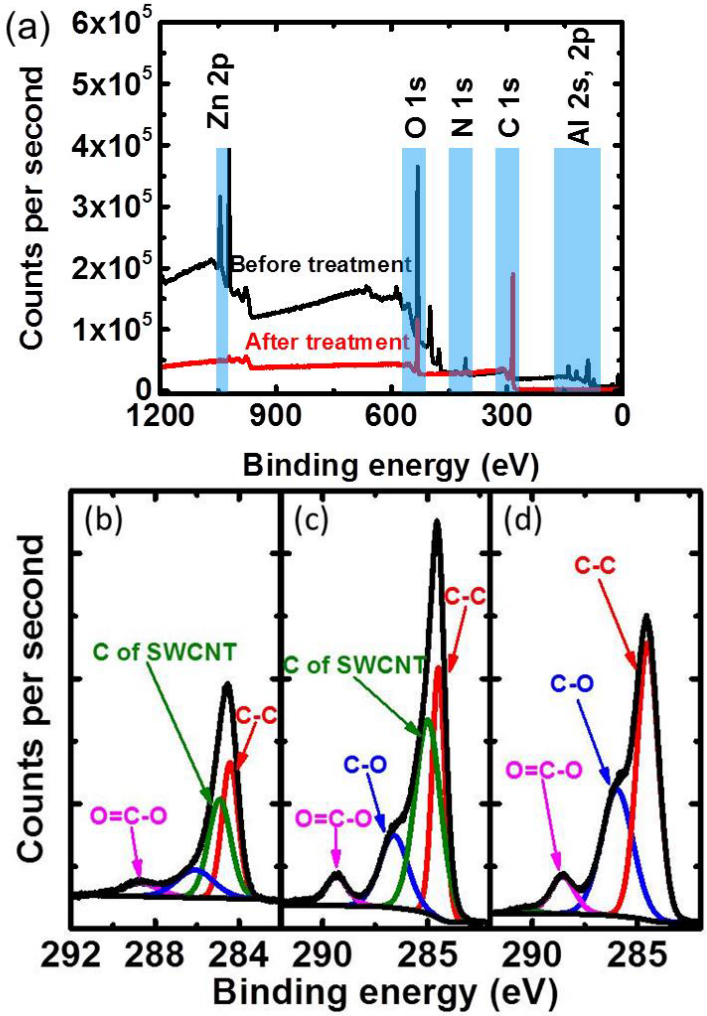

Figure 3-9. (a) XPS spectra of the film before and after acid treatment on the PET substrate. (b) Spectra of C 1s of PET substrate: Spectra of C 1s (c) after and (d) before the treatment with the deconvoluted spectra.

Table 3-1. Chemical composition change of the SWCNT film before and after acid treatment.

Element	Before treatment at. %	After treatment at. %
Zn	5.9	0.0
Al	5.5	0.0
C	43.8	83.4
O	43.3	15.9

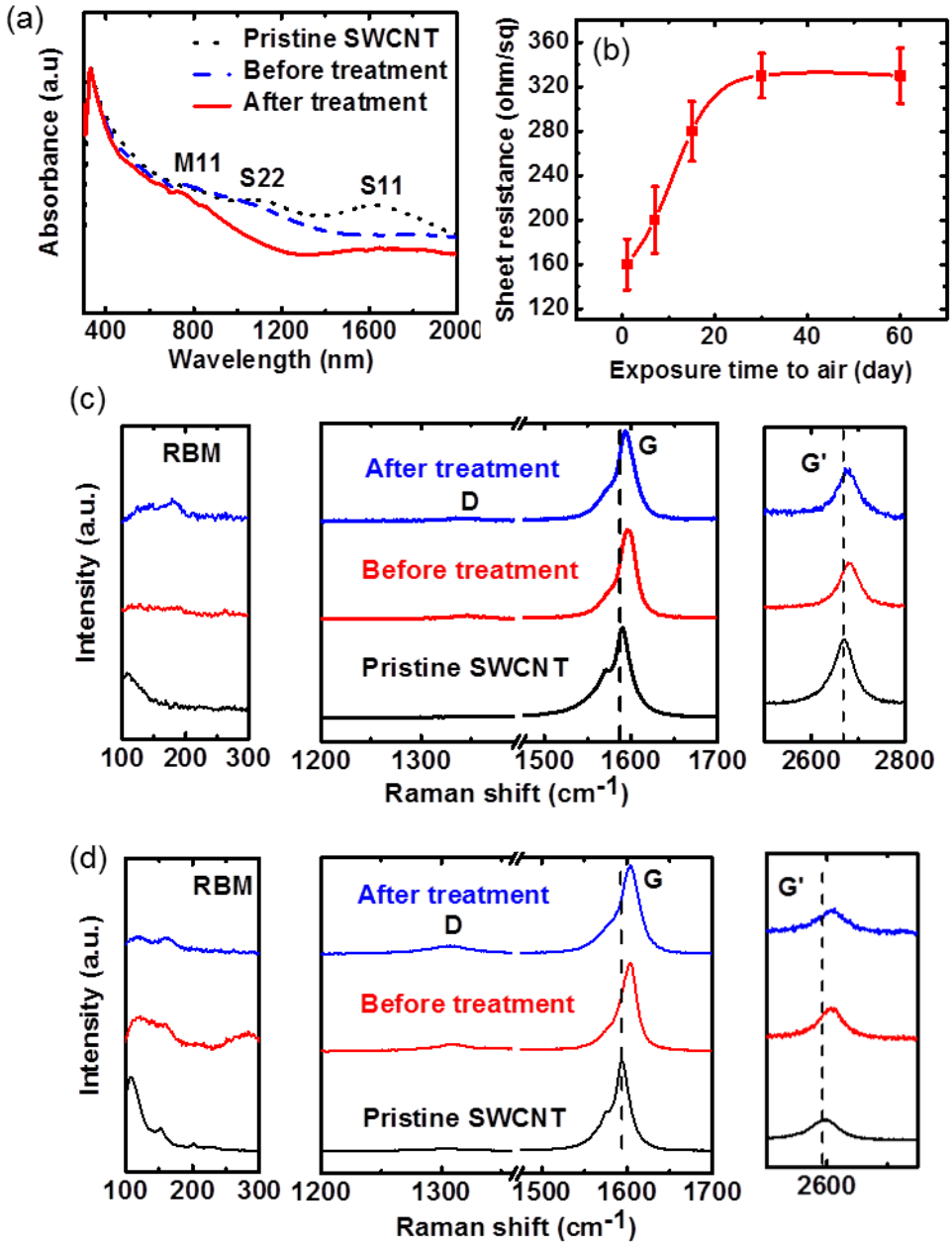

Figure 3-10. (a) Optical absorption spectra and (b) exposure time dependence of sheet resistance of SWCNT film after acid treatment. Raman spectra recorded at the laser wavelengths of (c) 785 and (d) 532 nm.

Doping effect is also evidenced by the optical absorption spectra, as shown in ***Figure 3-10a***. We clearly observe the S11 and S22 transitions of the semiconducting SWCNT and a weak M11

transition of metallic SWCNT. The dispersion treatment of SWCNT with Zn/Al complex decreases slightly the absorbance of these transitions. This can be explained by the charge transfer between SWCNT and Zn/Al complexes according to our preceding study.[27] We observe the pronounced depression of these transitions after the acid treatment even for only 10 min with diluted HNO_3, which evidences the doping of SWCNT with HNO_3 according to the literature.[33,34] Nevertheless, this doping effect is not stable under an ambient condition. The sheet resistance of the film increases with the exposure time to air, as shown in ***Figure 3-10b***. This indicates evolution of doped nitrogen species, losing doping effect; the sheet resistance becomes almost constant of 320 ohm/sq after 30 days.

The Raman spectroscopy using the excitation wavelengths of 532 nm and 785 nm gives the information inherent to semiconducting and metallic SWCNTs, respectively. ***Figure 3-10c and d*** shows Raman spectra of SWCNT film on the PET substrate before and after the acid treatment with excitation using 532 and 785 nm. The RBM peaks of semiconducting and metallic SWCNTs almost disappear after coating on the PET with Zn/Al complex dispersant. The acid treatment does not recover the RBM peak due to loss of the resonance enhancement induced by doping with NO_3^- ions.[33] The intensity ratio of the disordered peak (I_D) to graphite like band (I_G) is 0.1, indicating quite high crystallinity of this SWCNT. The preceding study[28] showed the blue-shift of both of G and G'-bands of SWCNT with Zn/Al complex due to the charge transfer interaction. The acid treatment also induces similar blue shift of G and G'-bands of SWCNT. This also indicates p-type doping of SWCNT on the HNO_3 treatment.

Literature

(1) Chopra, K. L.; Major, S.; Pandya, D. K. *Thin Solid Films* **1983**, *102*, 1.

(2) Hösel, M.; Angmo, D.; Søndergaard, R. R.; dos Reis Benatto, G. a.; Carlé, J. E.; Jørgensen, M.; Krebs, F. C. *Adv. Sci.* **2014**, *1*.

(3) Hecht, D. S.; Hu, L.; Irvin, G. *Adv. Mater.* **2011**, *23*, 1482.

(4) Geng, H.Z.;Lee, Y. H. *Nanoscale phenomena: basic science to device applications*; Springer: New York, 2008; pp. 15–28.

(5) Bandaru, P. R. *J. Nanosci. Nanotechnol.* **2007**, *7*, 1239.

(6) Salvetat, J.P.; Bonard, J.M.; Thomson, N.H.; Kulik, A.J.; Forro, L.; Benoit, W.; Zuppiroli, L. *Appl. Phys. A* **1999**, *69*, 255.

(7) Y. Wang, H.J. Yang, H.Z. Geng, Z.C. Zhang, E.X. Ding, Y. Meng, Z.J. Luo, J. Wang, X. M. S. and S. X. D. *J. Mater. Chem. C* **2015**, *3*, 3796.

(8) De, S.; Lyons, P. E.; Sorel, S.; Doherty, E. M.; King, P. J.; Blau, W. J.; Nirmalraj, P. N.; Boland, J. J.; Scardaci, V.; Joimel, J.; Coleman, J. N. *ACS Nano* **2009**, *3*, 714.

(9) Rowell, M. W.; Topinka, M. A.; McGehee, M. D.; Prall, H.J.; Dennler, G.; Sariciftci, N. S.; Hu, L.; Gruner, G. *Appl. Phys. Lett.* **2006**, *88*, 233506.

(10) Zhang, D.; Ryu, K.; Liu, X.; Polikarpov, E.; Ly, J.; Tompson, M. E.; Zhou, C. *Nano Lett.* **2006**, *6*, 1880.

(11) Hecht, D. S.; Heintz, A. M.; Lee, R.; Hu, L.; Moore, B.; Cucksey, C.; Risser, S. *Nanotechnology* **2011**, *22*, 075201.

(12) Zhou, Y.; Shimada, S.; Saito, T.; Azumi, R. *Carbon* **2015**, *87*, 61.

(13) Reynaud, O.; Nasibulin, A. G.; Anisimov, A. S.; Anoshkin, I. V.; Jiang, H.; Kauppinen, E. I. *Chem. Eng. J.* **2014**, *255*, 134.

(14) Fukaya, N.; Kim, D. Y.; Kishimoto, S.; Noda, S.; Ohno, Y. *ACS Nano* **2014**, *8*, 3285.

(15) Nasibulin, A. G.; Kaskela, A.; Mustonen, K.; Anisimov, A.S.; Ruiz, V.; Kivisto, S.; Rackauskas, S.; Timmermans, M.Y.; Pudas, M.; Aitchison, B.; Kauppinen, M.; Brown, D.P.; Okhotnikov, O.G.; Kauppinen, E.I. *ACS Nano* **2011**, *5*, 3214.

(16) Biswas, C.; Lee, Y. H. *Adv. Funct. Mater.* **2011**, *21*, 3806.

(17) Geng, H.-Z.; Kim, K. K.; So, K. P.; Lee, Y. S.; Chang, Y.; Lee, Y. H. *J. Am. Chem. Soc.* **2007**, *129*, 7758.

(18) Rösner, B.; Guldi, D. M.; Chen, J.; Minett, a I.; Fink, R. H. *Nanoscale* **2014**, *6*, 3695.
(19) Gao, J.; Wang, W. Y.; Cui, L. J.; Chen, L. T.; Hu, X. Y.; Li, H.; Geng, H. Z. *Adv. Mater. Res.* **2013**, *658*, 3.
(20) Kim, S.; Yim, J.; Wang, X.; Bradley, D. D. C.; Lee, S.; DeMello, J. C. *Adv. Funct. Mater.* **2010**, *20*, 2310.
(21) Wu, Z.; Chen, Z.; Du, X.; Logan, J. M.; Sippel, J.; Nikolou, M.; Kamaras, K.; Reynolds, J. R.; Tanner, D. B.; Hebard, A. F.; Rinzler, A. G. *Science* **2004**, *305*, 1273.
(22) Kim, Y.; Minami, N.; Zhu, W.; Kazaoui, S.; Azumi, R.; Matsumoto, M. *Jpn. J. Appl. Phys.* **2003**, *42*, 7629.
(23) Khim, D.; Han, H.; Baeg, K.-J.; Kim, J.; Kwak, S.-W.; Kim, D.-Y.; Noh, Y.Y. *Adv. Mater.* **2013**, *25*, 4302.
(24) Dan, B.; Irvin, G. C.; Pasquali, M. *ACS Nano* **2009**, *4*, 835.
(25) Maillaud, L.; Poulin, P.; Pasquali, M.; Zakri, C. *Langmuir* **2015**, *31*, 5928.
(26) Matsuda, T.;Minami, D.;Khoerunnisa, F.;Sunaga, M.;Nakamura, M.;Utsumi, S.;Itoh, T.;Fujimori, T.;Hayashi, T.;Hattori, Y.;Endo, M.;Isobe, H.;Onodera, H.;Kaneko, K. *Langmuir* **2015**, *31*, 3194.
(27) Kukobat, R.; Minami, D.; Hayashi, T.; Hattori, Y.; Matsuda, T.; Sunaga, M.; Bharti, B.; Asakura, K.; Kaneko, K. *Carbon* **2015**, *94*, 518.
(28) Saito, T; Ohshima, S.; Okazaki, T.; Ohmori, S.; Yumura, M.; Ijima, S. *J. Nanosci. Nanotechnol.* **2008**, *8*, 6153.
(29) Horcas, I.; Fernández, R.; Gómez-Rodríguez, J. M.; Colchero, J.; Gómez-Herrero, J.; Baro, a. M. *Rev. Sci. Instrum.* **2007**, *78*.
(30) Setsuhara, Y.; Cho, K.; Shiratani, M.; Sekine, M.; Hori, M. *Thin Solid Films* **2010**, *518*, 6492.
(31) Wang, J.; Sun, J.; Gao, L.; Wang, Y.; Zhang, J.; Kajiura, H.; Li, Y.; Noda, K. *J. Phys. Chem. C* **2009**, *113*, 17685.
(32) Morant, C.; Torres, R.; Jimenez, I.; Sanz, J. M.; Elizalde, E. *J. Nanosci. Nanotechnol.* **2008**, *8*, 1.
(33) Kaskela, A.; Nasibulin, A.G.; Timmermans, M.Y.; Aitchison, B.; Papadimitratos, A.; Tian, Y.; Zhu, Z.; Jiang, H.; Brown, D. P.; Zakhidov, A.; Kauppinen, E. I. *Nano Lett.* **2010**, *10*, 4349.

(34) Itkis, M.E.; Niyogi, S.; Meng, M.E.; Hamon, M.A.; Hu, H.; Haddon, R.C. *Nano Lett.* **2002**, *2*, 155.

Chapter 4

4. An essential role of viscosity of SWCNT inks in homogeneous conducting film formation[3]

4.1. Introduction

Single Wall Carbon Nanotube (SWCNT) attracts attention in the fabrication of Transparent and Conductive Film (TCF) due to the excellent opto-electrical properties.[1] However, the TCFs are often not homogeneous in terms of the electrical conductivity and optical transparency because of non-uniform distribution of SWCNT.[2–4] The parts with the thick layers of SWCNT are more conductive and less transparent and vice versa.[5] The uniformity of the electrical conductivity and optical transparency of SWCNT films is important for the proper functionality of touch panels,[6] displays,[7,8] solar cells,[9] and light emitting diodes.[10] The better performances of these devices can be achieved if we fundamentally understand the process for the scalable and homogeneous film formation.

The TCF can be prepared by the techniques as follows: Spray coating;[11] spin coating;[12] Langmuir-Blodgett;[13] vacuum filtration;[14] dip coating;[15] and bar coating.[2–4] The bar coating technique is the most promising for scalable and homogeneous film fabrication.[2,7,16,17] The SWCNT ink spreads on the transparent substrate by moving a metal bar wound with a wire of certain thickness, which controls the thickness of the film.[18] The viscosity and dispersibility of SWCNT are of the crucial importance for the uniform TCF formation.[18] If the viscosity is high

[3] This chapter is adapted with permission from (R. Kukobat et al. *Langmuir* 2016, 32 (27), pp. 6909–6916).

enough to suppress dewetting process, the homogenous film can be formed.[2] The dispersibility and viscosity depend on the dispersant for the SWCNT ink preparation. The SWCNT inks can be prepared with the aid of organic surfactants,[19–26] polymers,[19,27–29] organic solvents,[30,31] super acids,[32,33] chemical functionalization,[34–36] and inorganic dispersants recently developed by our group.[37,38] Sodium Dodecyl Sulfonate (SDS), Sodium Dodecyl Benzene Sulfonate (SDBS), lithium dodecyl sulfate, tetradecyl trimethyl ammonium bromide, and sodium cholate are widely used organic surfactants for SWCNT ink preparation.[39,40] In particular, SDS and SDBS are commonly used organic surfactants for the SWCNT film preparation. However, the surfactant based SWCNT inks have encountered several obstacles for the high performance SWCNT film fabrication such as deterioration of high electrical conductivity of SWCNT, foam formation during the dispersion process, and a serious difficulty in the uniform film production. Polymers, organic solvents, and super acid based SWCNT inks are poorly dispersed,[40] being non-compatible for the production of SWCNT film by bar coating method. The chemical functionalization method gives the stable dispersion of CNT in variety of solvents. Thus, the MWCNT functionalized with supermolecular polymers,[34] Eu (III) complex species,[35] and ureidopyrimidinone molecules[36] has the potential applications for the light emitting diodes, photo-electrochemical diodes, mechanically robust optical memories, and fuel cells. On the other hand, recently developed inorganic Zn/Al complex[37] and colloidal silica[38] dispersants exhibit better dispersion properties than commonly used dispersants for SWCNT.

Then, we need to elucidate the role of viscosity, surface tension, and wettability of the SWCNT ink to prepare the uniform SWCNT film with bar coating method. In particular, the uniformity of the SWCNT film must be elucidated quantitatively. We elucidate the position dependence of the sheet resistance and optical transmittance of the SWCNT film and show the relationship between the uniformity of SWCNT film and contact angle, surface tension, and viscosity of the SWCNT inks by use of Zn/Al complex, colloidal silica, SDS, and SDBS, showing superiority of Zn/Al complex and silica dispersants.

4.2. Experimental section

4.2.1. Materials and methods

The SWCNT inks were prepared using SDS, SDBS, Zn/Al complex, and silica dispersants. SWCNT was purchased from Meijo Nano Carbon with diameter of 2 nm, produced by CVD method.[41] SDS and SDBS purchased from Sigma Aldrich were used in this study. The Zn/Al complex dispersant was synthesized from Zn-acetate and Al-nitrate; those substances were mixed in ethanol to yield the solution of 3.00 wt.% and reacted at the molar fraction of Zn of 0.66 for 2 hours. After reaction ethanol was evaporated using rotary evaporator and dried at 100 ^{o}C in vacuum for 3 hours.[37] The silica dispersant was synthesized from sodium silicate. The sodium ions were exchanged with the hydrogen ions of HCl and silica dispersant was obtained.[38]

The SWCNT inks were prepared using homogenizer tip (SONIC VS 505) by sonication at very mild conditions: sonication time of 20 min, frequency of 20 kHz, and power of 100 W. Amount of 50 mL of 0.05 wt.% of SWCNT was sonicated in 1.00 wt.% of the aqueous solution of dispersant, giving the stable inks. The SWCNT ink was deposited on the polyethylene terephthalate (PET) by bar coating method (Kobayashi Engineering Works). The coatings were deposited at the diameter of bar wire of 0.2 mm and speed of 100 mm/s. After deposition, the dispersant was removed from the film by washing with 1M HNO_3 for 10 min. Then the films were dried in the air for 30 min at room temperature prior to the sheet resistance and optical transmittance measurements.

4.2.2. Characterization of the SWCNT films

The sheet resistance was measured using four point probe method (LORESTA-GP, MCP-T610) and optical transmittance was measured using an optical spectrometer (JASCO V-670) at 550 nm. The standard deviation of the mean or standard error[42] of sheet resistance and transmittance were used for the quantitative evaluation of the film homogeneity. The scheme of the film with the positions at which the sheet resistance and optical transmittance were measured is shown in ***Figure 4-1***.

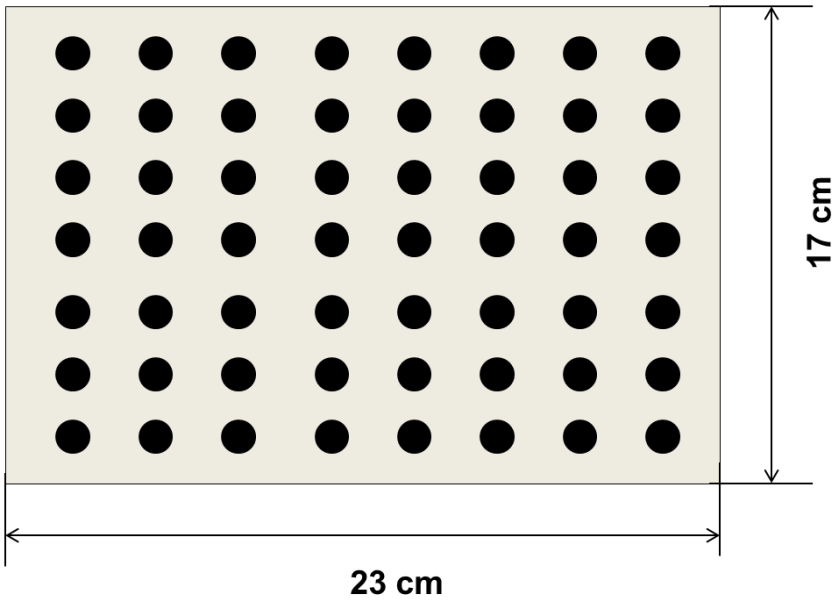

Figure 4-1. The sketch of SWCNT film of 23 cm x 17 cm^2 in size for the quantitative evaluation of the film homogeneity. The sheet resistance and optical transmittance of the black points are measured.

The standard deviation of the mean sheet resistance ($\sigma_{\bar{R}}$) indicates the homogeneity of SWCNT film in terms of the sheet resistance:[42]

$$\sigma_{\bar{R}} = \frac{\sigma_R}{\sqrt{N}}, \tag{4.1}$$

where are:

$\sigma_{\bar{R}}$: The standard deviation of the mean sheet resistance (ohm/sq);

σ_R: The standard deviation of sheet resistance (ohm/sq);

N: Number of points (*i)* at which the sheet resistance was measured;

The standard deviation of sheet resistance can be calculated as follows:[42]

$$\sigma_R = \sqrt{\frac{1}{N}\sum_{i=1}^{N}(R_i - R)^2}, \tag{4.2}$$

where are:

R_i: Sheet resistance measured at position *i* (ohm/sq);

$\bar{R}$: Mean value of the sheet resistance (ohm/sq).

In this case, the R_i was measured at 56 different positions on the film of 23 cm x 17 cm^2 in size as shown in Fig. S1; the N is 56. The $\bar{R}$ value was calculated as an arithmetic average of R_i values as follow:[42]

$$\overline{\mathrm{R}} = \sum_{i=1}^{N} R_i/N \tag{4.3}$$

The standard deviation of the mean optical transmittance ($\sigma_{\bar{T}}$) indicates the homogeneity of SWCNT films in terms of the optical transmittance. It is defined analogously to $\sigma_{\overline{\mathrm{R}}}$ as expressed as follow:

$$\sigma_{\overline{\mathrm{T}}} = \frac{\sigma_{\mathrm{T}}}{\sqrt{\mathrm{N}}}, \tag{4.4}$$

where are:

$\sigma_{\bar{T}}$: The standard deviation of the mean transmittance (%);

σ_T: The standard deviation of transmittance (%);

N: Number of points (*i)* at which the transmittance was measured;

The standard deviation of transmittance is defined as follows:

$$\sigma_T = \sqrt{\frac{1}{N}\sum_{i=1}^{N}(T_i - \bar{T})^2} \tag{4.5}$$

T_i: The transmittance measured at position *i* (%);

$\bar{T}$: Mean value of the transmittance (%).

The T_i was measured at the same points as the R_i on the size of 23 x 17 cm^2; N is equal 56. The $\overline{T}$ value is determined analogously to $\bar{R}$ as follow:[42]

$$\overline{\mathrm{T}} = \sum_{i=1}^{N} T_i / N \tag{4.6}$$

The $\sigma_{\bar{R}}$ and $\sigma_{\bar{T}}$ values express quantitatively the homogeneity of SWCNT films. The SWCNT films with low $\sigma_{\bar{R}}$ and $\sigma_{\bar{T}}$ values indicate the homogeneous films. On the other hand, large values of $\sigma_{\bar{R}}$ and $\sigma_{\bar{T}}$ indicates inhomogeneous films.

4.2.3. Characterization of the SWCNT inks

Surface tension of the ink was measured using Wilhelmy plate method (CBVP-A3, KYOWA). Contact angle of the ink on the PET substrate was recorded by a contact angle meter (DMC-MC3). Viscosity of the ink was determined using an Ostwald viscometer at room temperature, referring to viscosity of water. Observation of the film homogeneity was conducted using an optical microscope (Olympus DP73). The optical microscopy was also employed for the study of drying process of the SWCNT film on the substrate upon coating with SWCNT ink. The videos of drying process were recorded using Microscope digital camera DP73. The micrographs of the film were recorded using Atomic Force Microscopy (5500 SU1 AFM/SPM, Agilent technologies). The roughness parameters were evaluated from AFM images using WSxM software.[43,44] Dispersed SWCNT was observed with a high resolution transmission electron microscope (HR-TEM, JEOL, JEM 2100).

4.3. Results and discussion

4.3.1. Effect of the dispersant on film homogeneity

The homogeneity of SWCNT films depends on the SWCNT inks. ***Figure 4-2*** shows $\sigma_{\bar{R}}$ and $\sigma_{\bar{T}}$ values of the SWCNT films obtained using different dispersants after acid treatment, respectively. The SDS and SDBS based SWCNT films have large $\sigma_{\bar{R}}$ and $\sigma_{\bar{T}}$ values, indicating that the distribution of SWCNT on the substrate is not homogeneous. The regions with the thick and thin layers of SWCNTs are alternately distributed on the film. The parts with thick layers of SWCNT give the low value of the sheet resistance and transmittance and vice versa. Thus, the SDS based SWCNT ink gives the film with the minimum and maximum value of $\sigma_{\bar{R}}$ of 1300 ohm/sq and 3400 ohm/sq, respectively. In case of SDBS based SWCNT film, the distribution of $\sigma_{\bar{R}}$ values is narrower; it varies in the range of 670-1200 ohm/sq. The $\sigma_{\bar{T}}$ shows similar tendency of the SDS and SDBS based SWCNT films; it has a wide range of $\sigma_{\bar{T}}$ distribution of 42-85 %, approximately. On the other hand, the Zn/Al complex and silica based SWCNT films have $\sigma_{\bar{R}}$ values in the range of 170-190 ohm/sq and 260-300 ohm/sq, respectively; $\sigma_{\bar{T}}$ are in the range of 90-91 %. The $\sigma_{\bar{R}}$ and $\sigma_{\bar{T}}$ values do not vary significantly, suggesting the uniform distribution of SWCNT in the network. Therefore, the Zn/Al complex and silica based films are more homogeneous in comparison with SDS and SDBS based SWCNT films.

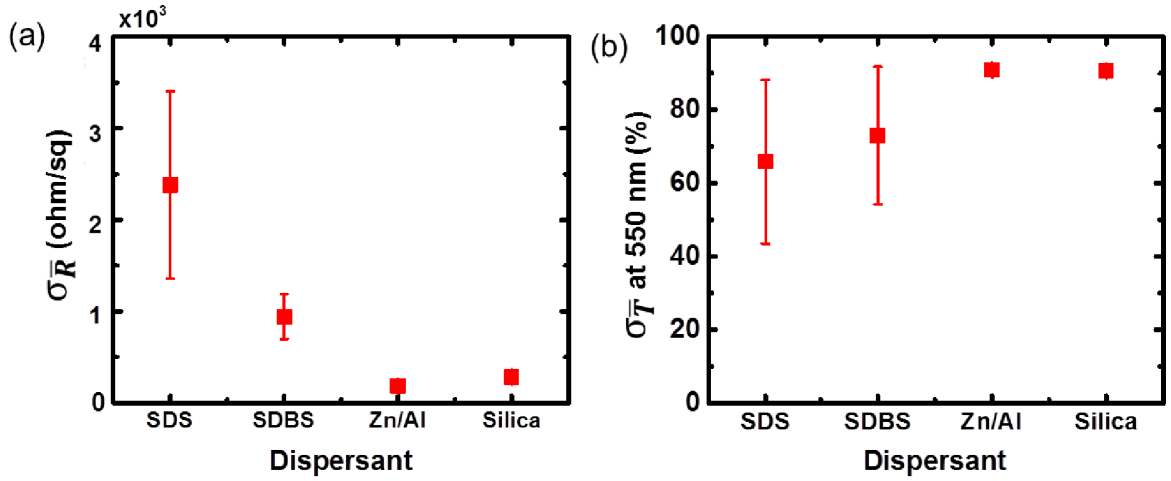

Figure 4-2. (a) The $\sigma_{\bar{R}}$ and (b) $\sigma_{\bar{T}}$ values of SWCNT films prepared by use of different dispersants. The sheet resistance and optical transmittance were recorded after HNO_3 treatment.

The film homogeneity/inhomogeneity can be easily confirmed in the centimeter scale images, as shown in ***Figure 4-3***. The films obtained from the SDS and SDBS-SWCNT inks have many stains of the ink on PET substrate as shown in ***Figures 4-3a and b***. On the other hand, the films obtained from the Zn/Al complex and silica based SWCNT inks have no such stains, being quite homogeneous, as shown in ***Figures 4-3c and 2d***.

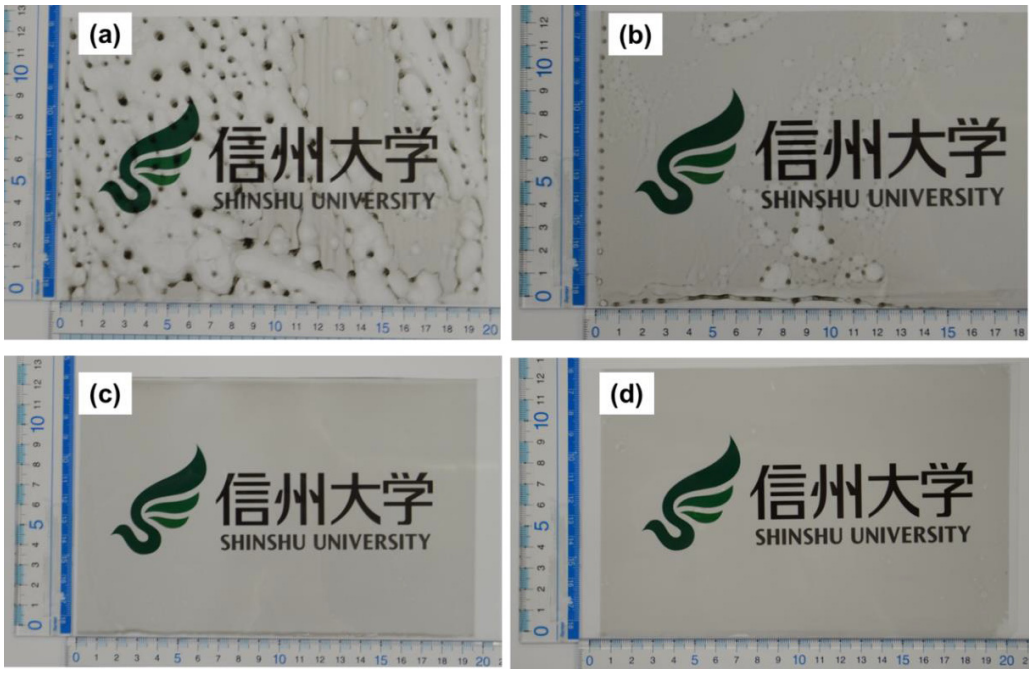

Figure 4-3. Images of the SWCNT films of 20 x 13 cm in size. The films are prepared of SWCNT inks aided with (a) SDS, (b) SDBS, (c) Zn/Al complex and (d) silica dispersants.

The optical microscopy images of SWCNT inks dispersed with the aid of SDS, SDBS, Zn/Al complex, and silica dispersants with the corresponding films are shown in ***Figure 4-4***. The droplets of SWCNT inks show the homogeneous dispersion as shown in ***Figures 4-4a_1-d_1***. However, after spreading and drying on the substrate, the SDS and SDBS based inks form the stains of SWCNT as shown in ***Figures 4-4a_2 and b_2***. On the other hand, the Zn/Al complex and silica based SWCNT inks give the homogeneous films as shown in ***Figures 4-4c_2 and d_2***. The inhomogeneity can be ascribed to the drying process of inks on substrate. The SDS and SDBS based SWCNT inks are more fluidic than Zn/Al complex and silica based inks, leading to the non-uniform drying of the ink on PET substrate.

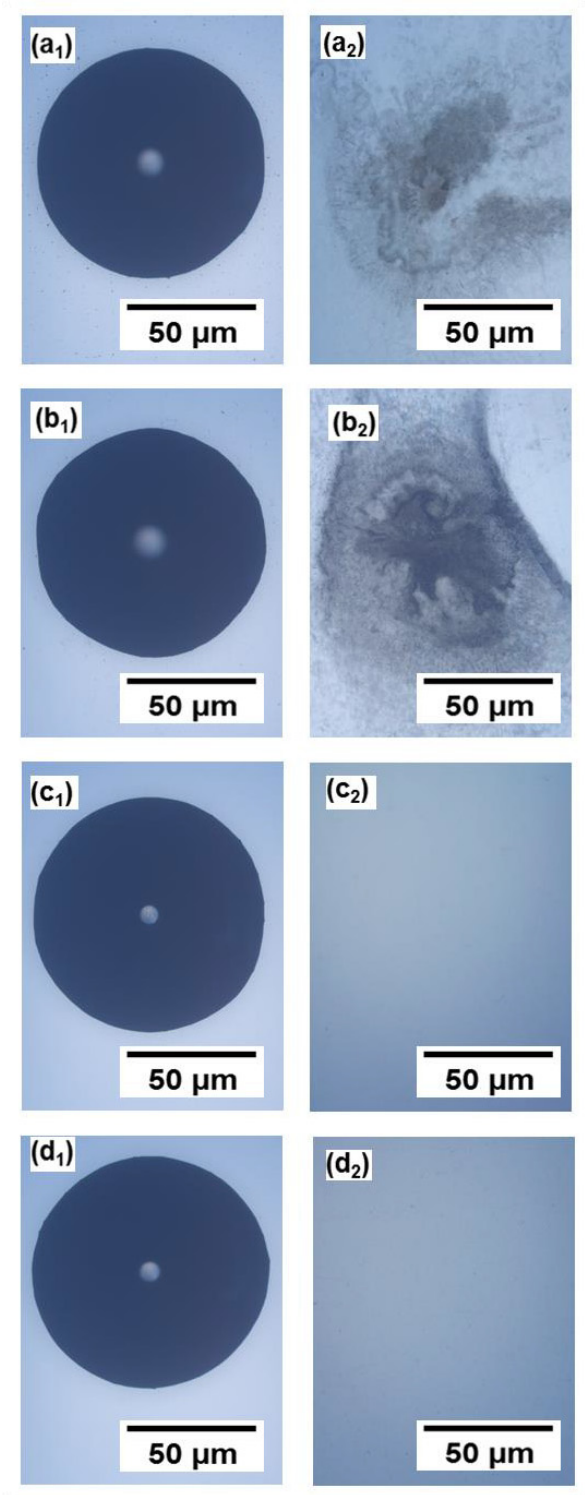

Figure 4-4. The droplets of SDS, SDBS, Zn/Al complex, and Silica based SWCNT inks (a_1, b_1, c_1, and d_1, respectively) with the corresponding films after bar coating (a_2, b_2, c_2, and d_2) on the PET substrate.

4.3.2. Effect of the SWCNT ink properties on uniformity of SWCNT film

The film formation has two steps: Coating and drying processes. The coating process includes wetting and spreading processes of the ink on the substrate. The drying process occurs between the film coating and solidification of SWCNT on the substrate. The contact angle and surface tension are the key factors of the wettability and spreadability of the ink on the substrate, while the viscosity plays a primary role at drying process.

Figure 4-5 and Figure 4-6 show the contact angle and surface tension of Zn/Al complex, silica, SDS, and SDBS-SWCNT based inks together with reference data of water. The contact angle and surface tension of the Zn/Al complex and silica dispersant-based inks are close to those of water (71.5^{o} and 72 mNm^{-1}). This can be explained by the structure of dispersants. The Zn/Al complex has a molecular structure, consisting of the Al-acetate and ionic structure of the hydrated Zn-nitrate, which are weakly interacted.[37] The silica dispersant has a polymeric structure, consisting of the chains of -Si-O-Si- with hydroxyl groups.[38,45] Therefore, both dispersants are mostly hydrophilic. Thus, the dispersants have water like polar structures, suggesting that the ink-substrate interaction is similar to that of water; the contact angle and surface tension are very close to that of the pure water. On the other hand, SDS and SDBS-SWCNT-based inks have significantly lower contact angle and surface tension than water. The surfactants are amphiphilic molecules with long hydrophobic chains that are adhered onto the hydrophobic surface of SWCNT. Also, the long hydrophobic chains interact strongly with the PET substrate which possesses hydrophobicity, lowering the contact angle and surface tension. Here, SDBS-based ink reduces the surface tension and contact angle more than SDS-based ink through the π-π interactions of the benzene ring.[23,46] Hence, the wettability and spreadability of those inks on the PET substrate are enough to give the uniform liquid film coating.

Figure 4-5. Contact angle of SWCNT inks and water on the PET substrate. Here Zn/Al, silica, SDS, and SDBS denote SWCNT inks dispersed with Zn/Al complex, silica, SDS, and SDBS, respectively.

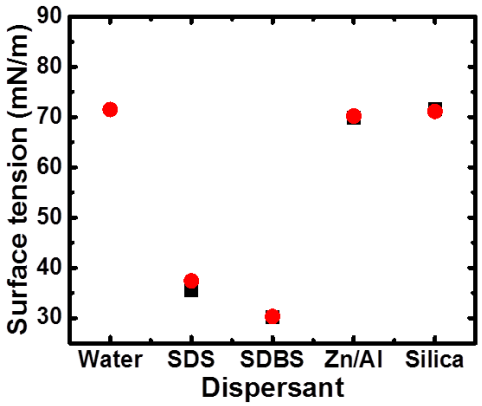

Figure 4-6. Surface tension of SWCNT inks, dispersant solution, and water as a solvent. ■ SWCNT ink and● dispersant solution.

The film has a wavy pattern on bar coating, being followed by the flow of the ink, flattening the film. Then the film is exposed to the further processes such as de-wetting and non-uniform solvent evaporation, which are the driving forces for the local flow of the ink on the substrate.[2] The dominant local flow produces stains where SWCNTs are aggregated. Hence, the film homogeneity requests an optimum viscosity of the SWCNT ink to avoid the local flow.

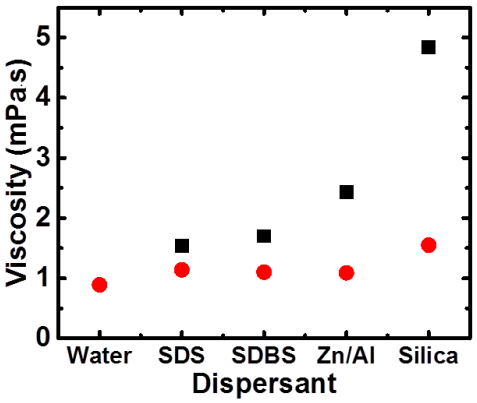

Figure 4-7. (a). Viscosity of SWCNT inks, dispersant solution, and water as a solvent. ■ SWCNT ink and● dispersant solution.

The viscosities of SDS, SDBS, Zn/Al complex, and silica dispersant-based inks, and water as a reference are shown in ***Figure 4-7.*** The SDS and SDBS based-inks have smaller viscosities than Zn/Al complex and silica dispersant. The surfactants SDS and SDBS are adsorbed on the SWCNT surface, yielding stable dispersion.[47,48] However, the viscosities of those inks are rather

close to that of water of 0.90 mPa·s. Thus, the flow of the surfactant based SWCNT-inks on the substrate induces stains after drying. On the other hand, the Zn/Al complex and silica based SWCNT-inks have the jelly structures[37,38] in which SWCNTs are entangled, as shown in ***Figures 4-8a and b***.

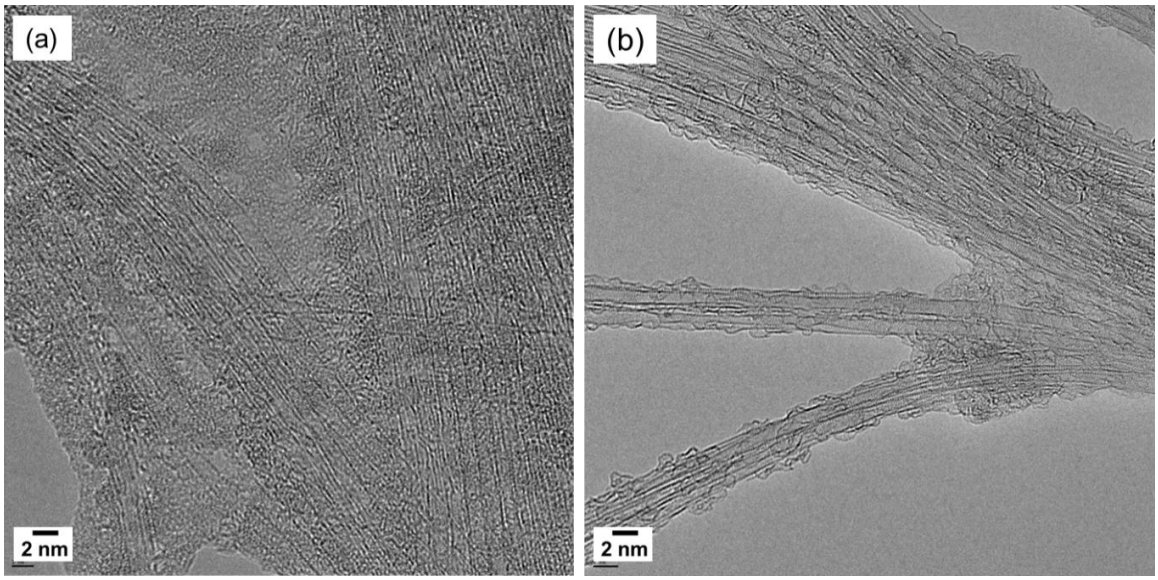

Figure 4-8. HR-TEM images of SWCNT dispersed with (a) Zn/Al complex dispersant and (b) silica dispersant.

The viscosity of Zn/Al complex and silica based SWCNT inks of 2.80 and 4.80 mPa·s, respectively is slightly higher than that of SDS and SDBS. However, this small viscosity is enough to minimize the local flow due to the presence of jelly like network, giving the homogeneous film.

4.3.3. The texture structure of SWCNT film

The texture structure is associated with the orientation of SWCNT on the substrate.[49] Normally SWCNTs are randomly distributed, indicating the presence of a random texture.[50] The texture structure determines the properties of the SWCNT films such as electrical conductivity and optical transmittance. Thus, we need to understand the texture structure of the SWCNT film on the substrate. The texture structure of SWCNT films is analyzed from AFM micrographs. AFM micrographs with the corresponding X-Z cross-sectional profiles of the SWCNT films

prepared using SDS, SDBS, Zn/Al complex, and silica based-SWCNT inks before and after acid treatment are shown in ***Figure 4-9***. The films obtained from SWCNT inks using SDS, SDBS, and silica dispersants are completely covered with the dispersants before acid treatment. Only the film produced from Zn/Al complex-SWCNT ink is partially covered with the Zn/Al complex, providing visible SWCNT networks. In case of silica based SWCNT ink, there are so many aggregates on the substrate, giving the AFM image different from the others. The film treatment with 1M HNO_3 for 10 minutes does not completely remove the SDS and SDBS, while the Zn/Al complex and silica dispersants can be removed from the film as observed in Figs. $8a_2$-d_2. Removal of the SDS and SDBS requires the treatment with 12M HNO_3 for 1 hour.[51,52] The SWCNT bundles of SDS and SDBS based films are hardly visible due to the non-efficient removal with 1M HNO_3. On the other hand, this treatment reveals the SWCNT bundles of Zn/Al complex based film; the SWCNT bundles of silica based films are revealed partially. The Zn/Al complex can be completely removed from the film after the treatment.[18] The SWCNT bundles of silica based film are partially covered with the aggregated silica particles; the sheet resistance of silica based film decreases from 10^7 to 10^2 ohm/sq due to the removal of silica particles.

The AFM image can be associated with the interaction between the dispersant coated SWCNT and PET substrate. The surfactant molecules, possessing long hydrophobic chains have a strong affinity to the PET substrate, giving rise to the highly dense coating. The silica particles have a strong tendency for mutual aggregation layers on the SWCNT,[38,53] giving the film coated with the large aggregates. The hydrophobic moieties of Zn/Al complex mostly used for the interaction with SWCNT provide relatively sparse layers of SWCNT-dispersant.

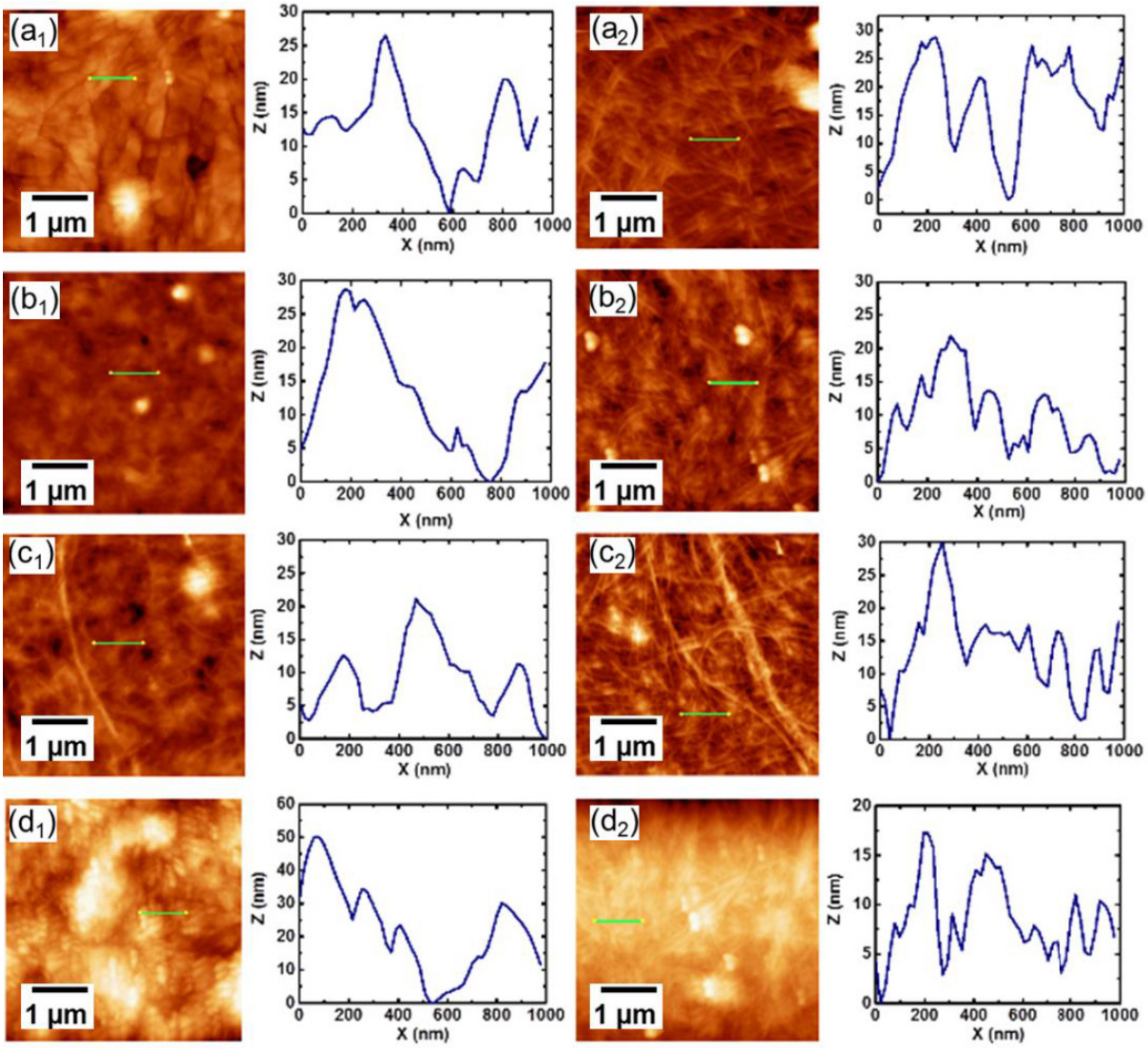

Figure 4-9. AFM micrographs with the corresponding X-Z profiles of the films, prepared from different SWCNT inks before and after acid treatment. X axis refers to the distance, while Z axis refers to the height of the SWCNT bundles. (a_1), (a_2) SDS-SWCNT films. (b_1), (b_2) SDBS-SWCNT films. (c_1), (c_2) Zn/Al complex-SWCNT films. (d_1) and (d_2) silica-SWCNT films. (1) and (2) indicate „before and after" acid treatment.

The texture structure of SWCNT on the substrate before and after acid treatment can be evaluated by use of the roughness parameters from the AFM micrograph, which are roughness average, skewness, and kurtosis, as shown in ***Table 4-1.*** Roughness average is a commonly used parameter, which describes the surface roughness of the materials. It is an average absolute deviation from the X-Z profile mean line;[54] a small roughness average shows a smooth surface.

Skewness gives the information about the symmetry of the roughness peaks observed in X-Z profile.[55] The positive skewness value indicates that the X-Z profile peaks are skew to the right and vice versa. The absolute value of skewness distribution greater than 1 means that the X-Z profile peaks are highly skew, the distribution between ½ and 1 means moderately skew, and the lower than ½ means fairly skew symmetrical distribution.[55] Kurtosis is a measure of the degree of peakedness of the X-Z profile peaks. Kurtosis value greater than 3 means that the X-Z profile peaks are thin, while kurtosis smaller than 3 indicates the broad X-Z profile peaks.[55]

Table 4-1. Surface roughness parameters of the films prepared from different SWCNT inks before and after the acid treatment (B and A denote the roughness parameters before and after acid treatment, respectively).

Parameter	Estimated roughness parameters							
	SDS		SDBS		Zn/Al-complex		Silica	
	B	A	B	A	B	A	B	A
Roughness average	8	14	7	8	10	11	33	15
Skewness	1	3	2	2	1	3	1	-0.5
Kurtosis	7	18	10	21	8	16	3	4

The roughness average increases after acid treatment due to removal of the dispersants from the film. The roughness peaks are shown in the X-Z profiles. The shape of each peak before acid treatment corresponds to the shape of aggregates of SWCNT bundles covered with dispersants. On the other hand, the shape of the peaks after acid treatment represents the shape of SWCNT bundles and dispersant residuals on the surface. The SWCNT films except for silica based film have the low positive skewness values, indicating that the cross-sectional peaks are skew to the right. The silica based SWCNT film has the skewness of -0.5, indicating that those peaks are negligible skew to the left with fairly symmetrical distribution. This symmetrical distribution can be assigned to the round shape of silica particles[38] on the film surface. Kurtosis indicates the presence of the thin X-Z profile peaks. This value increases after acid treatment, indicating the presence of the thin bundles of SWCNT on the substrate.

The texture structure of SWCNT films obtained by bar coating method is relatively smooth, being promising for the fabrication of light emitting diodes[15] and solar cells.[9]

Literature

(1) Geng, H.Z.;Lee, Y. H. *Nanoscale phenomena: basic science to device applications*; Springer: New York, 2008; pp. 15–28.

(2) Dan, B.; Irvin, G. C.; Pasquali, M. *ACS Nano* **2009**, *4*, 835.

(3) Maillaud, L.; Poulin, P.; Pasquali, M.; Zakri, C. *Langmuir* **2015**, *31*, 5928.

(4) Meng, Y.; Xu, X. B.; Li, H.; Wang, Y.; Ding, E. X.; Zhang, Z. C.; Geng, H. Z. *Carbon* **2014**, *70*, 103.

(5) Biswas, C.; Lee, Y. H. *Adv. Funct. Mater.* **2011**, *21*, 3806.

(6) Hecht, D. S.; Thomas, D.; Hu, L.; Ladous, C.; Lam, T.; Park, Y.; Irvin, G.; Drzaic, P. *J. SID* **2009**, *17*, 941.

(7) Peltola, J.; Weeks, C.; Levitsky, I. A.; Britz, D. a.; Glatkowski, P.; Trottier, M.; Huang, T. *Inf. Disp. (1975).* **2007**, *23*, 20.

(8) Schindler, A.; Schau, P.; Fruehauf, N. *J. Soc. Inf. Disp.* **2009**, *17*, 853.

(9) Rowell, M. W.; Topinka, M. a.; McGehee, M. D.; Prall, H.J.; Dennler, G.; Sariciftci, N. S.; Hu, L.; Gruner, G. *Appl. Phys. Lett.* **2006**, *88*, 233506.

(10) Wang, S.; Zeng, Q.; Yang, L.; Zhang, Z.; Wang, Z.; Pei, T.; Ding, L.; Liang, X.; Gao, M.; Li, Y.; Peng, L. M. *Nano Lett.* **2011**, *11*, 23.

(11) Kim, S.; Yim, J.; Wang, X.; Bradley, D. D. C.; Lee, S.; DeMello, J. C. *Adv. Funct. Mater.* **2010**, *20*, 2310.

(12) Jo, J. W.; Jung, J. W.; Lee, J. U.; Jo, W. H. *ACS Nano* **2010**, *4*, 5382.

(13) Kim, Y.; Minami, N.; Zhu, W.; Kazaoui, S.; Azumi, R.; Matsumoto, M. *Jpn. J. Appl. Phys.* **2003**, *42*, 7629.

(14) Eda, G.; Lin, Y.-Y.; Miller, S.; Chen, C.-W.; Su, W.-F.; Chhowalla, M. *Appl. Phys. Lett.* **2008**, *92*, 233305.

(15) Zhang, D.; Ryu, K.; Liu, X.; Polikarpov, E.; Ly, J.; Tompson, M. E.; Zhou, C. *Nano Lett.* **2006**, *6*, 1880.

(16) Wang, J.; Liang, M.; Fang, Y.; Qiu, T.; Zhang, J.; Zhi, L. *Adv. Mater.* **2012**, *24*, 2874.

(17) Hu, L.; Kim, H. S.; Lee, J.; Peumans, P.; Cui, Y. *ACS Nano* **2010**, *4*, 2955.
(18) Kukobat, R.; Hayashi, T.; Matsuda, T.; Sunaga, M.; Sakai, T.; Futamura, R.; Kaneko, K. *Chem. Phys. Lett.* **2016**, *650*, 113.
(19) Moore, V. C.; Strano, M. S.; Haroz, E. H.; Hauge, R. H.; Smalley, R. E.; Schmidt, J.; Talmon, Y. *Nano Lett.* **2003**, *3*, 1379.
(20) Wang, H. *Curr. Opin. Colloid Interface Sci.* **2009**, *14*, 364.
(21) Islam, M. F.; Rojas, E.; Bergey, D. M.; Johnson, A. T.; Yodh, A. G. *Nano Lett.* **2003**, *3*, 269.
(22) Jiang, L.; Gao, L.; Sun, J. *J. Colloid Interface Sci.* **2003**, *260*, 89.
(23) Vaisman, L.; Wagner, H. D.; Marom, G. *Adv. Colloid Interface Sci.* **2006**, *128-130*, 37.
(24) Wang, H.; Zhou, W.; Ho, D. L.; Winey, K. I.; Fischer, J. E.; Glinka, C. J.; Hobbie, E. K. *Nano Lett.* **2004**, *4*, 1789.
(25) Nativ-Roth, E.; Yerushalmi-Rozen, R.; Regev, O. *Small* **2008**, *4*, 1459.
(26) Strano, M.S.; Moore, V.C.; Moller, M.K.; Allen, M.J.; Haroz, E.H.; Kittell, C.; Hauge, R. H.; Smalley, R. E. *J. Nanosci. Nanotechnol.* **2003**, *3*, 81.
(27) Shvartzman-Cohen, R.; Nativ-Roth, E.; Baskaran, E.; Levi-Kalisman, Y.; Szleifer, I.; Yerushalmi-Rozen, R. *J. Am. Chem. Soc.* **2004**, *126*, 14850.
(28) Liu, C.X.; Choi, J.W. *Nanomaterials* **2012**, *2*, 329.
(29) Hasan, T.; Scardaci, V.; Tan, P. H.; Rozhin, A. G.; Milne, W. I.; Ferrari, A. C. *Phys. E* **2008**, *40*, 2414.
(30) Cheng, Q.; Debnath, S.; O'Neill, L.; Hedderman, T. G.; Gregan, E.; Byrne, H. J. *J. Phys. Chem. C* **2010**, *114*, 4857.
(31) Bahr, J. L.; Mickelson, E. T.; Bronikowski, M. J.; Smalley, R. E.; Tour, J. M. *Chem. Commun.* **2001**, 193.
(32) Ramesh, S.; Ericson, L. M.; Davis, V. a.; Saini, R. K.; Kittrell, C.; Pasquali, M.; Billups, W. E.; Adams, W. W.; Hauge, R. H.; Smalley, R. E. *J. Phys. Chem. B* **2004**, *108*, 8794.
(33) Hecht, D. S.; Heintz, A. M.; Lee, R.; Hu, L.; Moore, B.; Cucksey, C.; Risser, S. *Nanotechnology* **2011**, *22*, 075201.
(34) Quintana, M.; Traboulsi, H.; Llanes-Pallas, A.; Marega, R.; Bonifazi, D.; Prato, M. *ACS Nano* **2012**, *6*, 23.
(35) Maggini, L.; Liu, M.; Ishida, Y.; Bonifazi, D. *Adv. Mater.* **2013**, *25*, 2462.
(36) Wang, S.; Guo, H.; Wang, X.; Wang, Q.; Li, J.; Wang, X. *Langmuir* **2014**, *30*, 12923.

(37) Kukobat, R.; Minami, D.; Hayashi, T.; Hattori, Y.; Matsuda, T.; Sunaga, M.; Bharti, B.; Asakura, K.; Kaneko, K. *Carbon* **2015**, *94*, 518.
(38) Matsuda, T.;Minami, D.;Khoerunnisa, F.;Sunaga, M.;Nakamura, M.;Utsumi, S.;Itoh, T.;Fujimori, T.;Hayashi, T.;Hattori, Y.;Endo, M.;Isobe, H.;Onodera, H.;Kaneko, K. *Langmuir* **2015**, *31*, 3194.
(39) Sun, Z.; Nicolosi, V.; Rickard, D.; Bergin, S. D.; Aherne, D.; Coleman, J. N. *J. Phys. Chem. C* **2008**, *112*, 10692.
(40) Hecht, D. S.; Hu, L.; Irvin, G. *Adv. Mater.* **2011**, *23*, 1482.
(41) Saito, T;Ohshima, S.;Okazaki, T.; Ohmori, S.;Yumura, M.;Ijima, S. *J. Nanosci. Nanotechnol.* **2008**, *8*, 6153.
(42) Taylor, J. *An introduction to error analysis*; 2nd ed.; University Science Books: California, 1997; p. 327.
(43) Horcas, I.; Fernández, R.; Gómez-Rodríguez, J. M.; Colchero, J.; Gómez-Herrero, J.; Baro, a. M. *Rev. Sci. Instrum.* **2007**, *78*.
(44) Giacomelli, L.; Derchi, G.; Frustaci, A.; Bruno, O.; Covani, U.; Barone, A.; De Santis, D.; Chiappelli, F. *Open Dent. J.* **2010**, *4*, 191.
(45) Iler, R. K. *The Chemistry of Silica*; Wiley: New York, Chichester, Brisbane, Toronto, 1979; p. 790.
(46) White, B.; Banerjee, S.; O'Brien, S.; Turro, N. J.; Herman, I. P. *J. Phys. Chem. C* **2007**, *111*, 13684.
(47) Sa, V.; Kornev, K. G. *Langmuir* **2011**, *27*, 13451.
(48) Utsumi, S.; Kanamaru, M.; Honda, H.; Kanoh, H.; Tanaka, H.; Ohkubo, T.; Sakai, H.; Abe, M.; Kaneko, K. *J. Colloid Interface Sci.* **2007**, *308*, 276.
(49) Okotrub, A. V.; Dabagov, S. B.; Kudashov, A. G.; Gusel'nikov, A. V.; Kinloch, I.; Windle, A. H.; Chuvilin, A. L.; Bulusheva, L. G. *J. Exp. Theor. Phys. Lett.* **2005**, *81*, 34.
(50) Detavernier, C.; Ozcan, A. S.; Jordan-Sweet, J.; Stach, E. A.; Tersoff, J.; Ross, F. M.; Lavoie, C. *Nature* **2003**, *426*, 641.
(51) Geng, H.Z.; Kim, K. K.; So, K. P.; Lee, Y. S.; Chang, Y.; Lee, Y. H. *J. Am. Chem. Soc.* **2007**, *129*, 7758.
(52) Gao, J.; Wang, W. Y.; Cui, L. J.; Chen, L. T.; Hu, X. Y.; Li, H.; Geng, H. Z. *Adv. Mater. Res.* **2013**, *658*, 3.

(53) Bharti, B.; Kukobat, R.; Minami, D.; Kaneko, K. *Colloids Interface Sci. Commun.* **2014**, *3*, 13.

(54) Hansson, K. N.; Hansson, S. *ISRN Mater. Sci.* **2011**, *2011*, 1.

(55) Bulmer, M. G. *Principles of Statistics*; Dover: New York, **1965**; Vol. 2, p. 641.

Chapter 5

5. General conclusions

This study was carried out in order to prepare highly conductive and transparent SWCNT films from sol-gel dispersant based SWCNT inks.

Chapter 1 gives a general overview of the TCFs, materials, and methods for their synthesis. The SWCNT inks based on surfactants, polymers, superacids, chemical functionalization methods were described thoroughly. The techniques for the TCF fabrication such as bar coating, spray coating, dip coating, vacuum filtration, and Langmuir-Blodgett were described. The bar coating method was explained more detailed because it was used for the film fabrication in this study; this technique is scalable. Those methods for SWCNT ink preparation have advantages and disadvantages, regarding the properties and ease of the film fabrication on the large scale. The excellent optoelectrical properties of SWCNTs are often suppressed and electrical conductivity and optical transparency are rather modest. Therefore, the study of SWCNT inks for TCF fabrication is highly encouraged.

Chapter 2 deals with the synthesis of sol-gel Zn/Al complex dispersant for SWCNT ink preparation. The dispersibility of SWCNTs by Zn/Al complex dispersant in aqueous media is comparable with that of CTAB and SDS based SWCNT inks. The Zn/Al complex was synthesized from the reaction mixture of $Zn(CH_3COO)_2$ and $Al(NO_3)$ with the molar fraction of Zn of 0.66. The Zn/Al complex is stable and can be preserved in powder form; it can be used to disperse SWCNT in water just after quick dissolution. The complex containing amorphous $Al(CH_3COO)_3$, Zn^{2+}, and NO_3^- ions is strongly adsorbed onto the surfaces of the SWCNTs, leading to their stabilization. Optical absorption suggests a charge transfer interaction between Zn/Al complexes and SWCNTs, causing positive charge of SWCNTs of + 55 mV; the stability of SWCNTs arises from the electrostatic repulsive interactions. The Zn/Al complex is a potential

material for the fabrication of transparent and conducting films as well as hybrid materials based on SWCNT-Zn/Al species.

Chapter 3 deals with the TCFs fabrication by Zn/Al complex-SWCNT based inks. The Zn/Al complex dispersant offers SWCNT inks for the fabrication of TCFs by bar coating method. The Zn/Al complex-based SWCNT ink has sufficient viscosity (> 1.30 mPa·s) to suppress local flows which cause inhomogeneous film formation. Dipping the film in 1M HNO_3 for 10 min completely removes the Zn/Al complex, decreasing the sheet resistance significantly; the sheet resistance and optical transmittance at 550 nm are 150 ohm/sq and 90 %, respectively.

Chapter 4 deals with the homogeneity study of SWCNT films obtained from Zn/Al complex, silica, SDS, and SDBS-based SWCNT inks. The Zn/Al complex and silica-based SWCNT inks are more appropriate than SDS and SDBS-based inks for the scalable fabrication of SWCNT films by bar coating method. Due to the relatively high viscosity of Zn/Al complex and silica-based inks in comparison with SDS and SDBS-based inks, Zn/Al complex and silica are promising for the homogeneous film fabrication. In particular, the Zn/Al complex is highly recommended for production of uniform SWCNT films due to excellent stability. The viscous jelly like Zn/Al complex and silica-SWCNT inks can be applicable to the fabrication of composite and ceramic materials with good mechanical properties.

List of publications

1. R. Kukobat, D. Minami, T. Hayashi, Y. Hattori, T. Matsuda, M. Sunaga, B. Bharti, K. Asakura, and K. Kaneko, "Sol–gel chemistry mediated Zn/Al-based complex dispersant for SWCNT in water without foam formation", *Carbon* 94, **2015**, 518-523
2. R. Kukobat, T. Hayashi, T. Matsuda, M. Sunaga, T. Sakai, R. Futamura, and K. Kaneko, "Zn/Al complex-SWCNT ink for transparent and conducting homogeneous films by scalable bar coating method" *Chem. Phys. Lett.* 650, **2016**, 113-118
3. R. Kukobat, T. Hayashi, T. Matsuda, M. Sunaga, R. Futamura, T. Sakai, and K. Kaneko, "Essential Role of Viscosity of SWCNT Inks in Homogeneous Conducting Film Formation", *Langmuir*, 32, **2016**, 6909-6916.
4. B. Bharti, R. Kukobat, D. Minami, and K. Kaneko, "Modulating SWCNT-silica interactions for enhanced dispersibility and hybrid cryogel formation" *Coll. Interf. Sci. Comm.* 3, **2014**, 13-17.
5. F. Khoerunnisa, A. M. Gomez, H. Tanaka, T. Fujimori, D. Minami, R. Kukobat, T. Hayashi, S. Y. Hong, Y. C. Choi, M. Miyahara, M. Terrones, M. Endo, and K. Kaneko, "Metal semiconductor transition like behavior of naphthalene-doped single wall carbon nanotube bundles" *Faraday Discuss.* 173, **2014**, 145-156.

Conferences

1. R. Kukobat, D. Minami, B. Bharti, T. Fujimori, T. Hayashi, and K. Kaneko, "Development of Zn/Al complex for intensive dispersion of SWCNTs in water". **Oral presentation**. The 95-th CSJ Annual Meeting. Nihon University, Chiba, Japan, March 25-29, 2015.
2. R. Kukobat, D. Minami, T. Hayashi, Y. Hattori, B. Bharti, T. Fujimori, K. Asakura, K. Kaneko, "Highly transparent and conducting SWCNT film prepared by easy removable Zn/Al complex dispersant". **Poster presentation**. The Sixteenth International Conference on Science and Application of Nanotubes. Nagoya University, Nagoya, Japan, June 29-July 3, 2015.
3. R. Kukobat, D. Minami, T. Hayashi, Y. Hattori, B. Bharti, K. Asakura, and K. Kaneko, "Development of Zn/Al complex for intensive dispersion of SWCNTs in water". **Oral presentation**. The 66-th Divisional Meeting on Colloid and Interface Chemistry. Kagoshima University, Kagoshima, Japan, September 10-12, 2015.
4. R. Kukobat, T. Hayashi, T. Matsuda, M. Sunaga, and K. Kaneko, "Transparent and conductive film fabrication with the Zn/Al complex-aided SWCNT inks". **Oral presentation**. The World Conference on Carbon: Common fundamentals, remarkably versatile applications. The Penn Stater Conference Center Hotel, State College, Pennsylvania, USA, July 10-15, 2016.
5. R. Kukobat, T. Hayashi, N. Ohashi, Y. Watanabe, and K. Kaneko, "Sol-gel dispersant-derived transparent and conductive films". **Oral presentation**. The 77-th JSAP Autumn Meeting. Toki Messe, Niigata city, September 13-16, 2016.
6. R. Kukobat, T. Hayashi, and K. Kaneko, "Interfacial and rheological properties of SWCNT inks with relevance to the transparent and conductive film fabrication". **Oral presentation**. The 43-rd annual meeting of Carbon Society of Japan. Chiba University, December 07-09, 2016.